Differential Inhibition of adenylylated and deadenylylated *Mycobacteriun tuberculosis* glutamine synthetase by ATP scaffold-based inhibitors

Anjo Theron (née. Steyn)

Dissertation presented for the degree of Doctor of Philosophy in Science (Molecular Biology) in the Faculty of Health Sciences at Stellenbosch University

Promoter: Prof Ian Wiid
Co-promotor: Prof Colin Kenyon

December 2015

Declaration

By submitting this dissertation electronically, I declare that the entirety of the work contained therein is my own, original work, that I am sole author thereof (save to the extent explicitly otherwise stated), that the reproduction and publication thereof by Stellenbosch University will not infringe any third party rights and that I have not previously in its entirety or in part submitted it for obtaining any qualification.

Signature..................................... Date..

i

Summary

Mycobacterium tuberculosis (M.tb) glutamine synthetase (GS) is a potentially valuable therapeutic target for tackling the problem of tuberculosis disease. Its regulation via the adenylylation of a tyrosine residue on each subunit makes it distinct from the human form of the enzyme. Previous reports of heterologous expression of *M.tb* GS in *Escherichia coli* (*E. coli)* have shown that the endogenous adenylyl transferase (ATase) activity of *E. coli* does not adenylylate *M.tb* GS sufficiently, with only 25% of the *M.tb* GS subunits produced displaying adenylylation (Mehta *et al.,* 2004). The use of this expression system was therefore not considered optimal for the expression of adenylylated *M.tb* GS for further study.

Here we have described an *E. coli* production system lacking endogenous GS and ATase activity, which utilises the co-expression of the *M.tb* ATase with *M.tb* GS. By co-expressing *M.tb* ATase and *M.tb* GS we improved the percentage of subunits modified (or adenylylated) with ± 60-70% to ± 85-94%. In this way, we have produced recombinant *M.tb* GS that has a better adenylylation state than any previously reported.

Three methods were used to assess the degree of adenylylation of adenylylated and deadenylylated *M.tb* GS, and *E. coli* GS.   The first assay used, termed the γ-glutamyl transferase enzyme assay, is a variation of the reverse of the reaction that GS catalyses:

$$\text{Glutamate} + NH_4^+ + ATP \rightarrow \quad \text{glutamine} + ADP + P_i + H^+$$
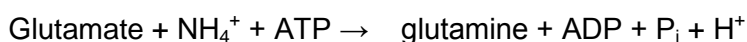
In this reverse reaction; hydroxylamine and glutamine react to form γ-glutamylhydroxamate and free ammonia in the presence of ADP, arsenate and manganese or magnesium. This forms the basis of an assay for GS activity. Based on the data from the γ-glutamyl transferase assay, the adenylylation state of adenylylated *M.tb* GS expressed in this novel system is at least 68% compared to the 25% obtained from Mehta and co-workers.

The second assay used is the determination of the inorganic phosphate concentration after the hydrolysis of both adenylylated and deadenylylated *Mtb* GS. In the case of the deadenylylated enzyme, there is no formation of phosphate after the hydrolysis. For the adenylylated *Mtb* GS, each adenyl moiety contains 1 phosphate, and 1 µM of GS (containing 12 subunits) should contain 12 µM of phosphate, if each subunit is adenylylated. The result obtained for the adenylylated *M.tb* GS enzyme was the formation of 0.93 µM phosphate produced per µM GS active site, *i.e.* 94% adenylylated compared to the 25% obtained from Mehta and co-workers.

The third method used to assess the adenylylation is mass spectrometry. MS spectra showed distinct peaks for adenylylated and deadenylylated enzymes, with calculated masses agreeing with the theoretical values. Based on this data, it can be concluded that the adenylylation state of adenylylated *M.tb* GS expressed in this novel system is at least 85% from the MS spectra obtained.

In addition, the rate of conversion of ATP, glutamate and ammonia to glutamine and ADP was assessed using HPLC. This is termed the 'forward' or 'biosynthetic" reaction and is assayed by HPLC to determine the conversion of ATP to ADP.

The primary invention of this project relates to a biochemical pathway that yielded a new drug target that can be exploited to develop new therapies against *M.tb*. GS catalyses the conversion of glutamate to glutamine via a glutamyl phosphate intermediate, utilising ATP. ATP is utilized as either Mg-ATP or Mn-ATP, depending on the adenylylation state of the enzyme. The enzyme is regulated via adenylylation in bacteria containing the GS-I form of the enzyme, a mechanism not found in the GS-II in humans.

213 compounds were tested against the adenylylated and deadenylylated forms of both *M.tb* GS and *E. coli* GS at a concentration of 10 µM. The rational design and selection of these inhibitors were based on the typical ATP binding site. It has been shown that GS in the adenylylated form uses a novel histidine kinase-like reaction mechanism in the phosphorylation of the carboxyl of glutamate. The primary outcome of the project was the demonstration of the selective inhibition of adenylylated GS and the identification of specific compounds capable of inhibiting adenylylated GS. These compounds could be considered for further hit-to-lead and lead optimisation campaigns for the development of novel candidates for the treatment of TB. Based on the dose-response assays, two compounds have emerged as the most promising anti-*M.tb* GS inhibitors with IC_{50} (µM) values of 9.6 µM and 17.4 µM respectively. They have regularly produced the most potent inhibitory activity against *M.tb* adenylylated GS enzyme in fixed concentration screens with 87% and 81% inhibition, respectively. These compounds, 10057 and 10059, are structurally very similar. These two compounds that have been found to be inhibitory to *M.tb* GS may now be used as templates to synthesize additional target specific compounds as part of a lead optimisation programme and further optimised to yield a suitable drug candidate for clinical evaluation.

In the study we also looked at the utilization of ATP by looking at the enzyme kinetics of both *M.tb* GS and *E. coli* GS as well as the kinetic isotope effect of these enzymes. It is proposed that for enzymes such as *M.tb* GS and *E. coli* GS, the enzyme kinetics follow the classical Michaelis-Menton kinetics where an equilibrium is set up between the enzyme concentration [E] and the substrate concentration [S] and binding of the second ATP is dependent on the conversion of the second active site into an ATP binding form by the release of ATP from the first active site, as defined by the coordinated half-sites mechanism.

As the regulation of the enzyme activity and ligand binding in these enzymes function in a coordinated half-the-sites manner, and binding in the second site only occurs on release of the ADP from the first site, it is therefore proposed that deuteration of the ATP improves the binding characteristics but does not impact on the catalysis of phosphoryl transfer. As the equilibrium shifts towards the binding of ATP with increasing ATP concentration, the deuterated ATP effectively binds twice as efficiently as the non-deuterated ATP, thereby negating the impact of the deuteration on the apparent enzyme activity at high ATP concentrations, yielding a KIE of 1.

Opsomming

Mikobakterium tuberkulosis (*M.tb*) glutamien sintetase (GS) is 'n potensieel waardevolle terapeutiese teiken vir die aanpak van die probleem van tuberkulose siekte. Die regulering deur die adenylylation van 'n tyrosine groep op elke subeenheid laat dit verskil van die menslike vorm van die ensiem. Vorige verslae van heteroloë uitdrukking van *M.tb* GS in *Escherichia coli* (*E. coli*) het getoon dat die endogene adeniel transferase (ATase) aktiwiteit van *E. coli* nie *M.tb* GS optimaal adenylylate nie, met slegs 25% adenylylation van die *M.tb* GS subeenhede (Mehta et al., 2004). Die gebruik van hierdie uitdrukking stelsel is dus nie oorweeg as die optimale stelsel vir die uitdrukking van adenylylated *M.tb* GS vir verdere studie.

Hier beskryf ons 'n *E. coli* produksie stelsel wat ontbreek in endogene GS en ATase aktiwiteit asook die mede-uitdrukking van *M.tb* ATase met *M.tb* GS. Deur mede-uitdrukking van *M.tb* ATase en *M.tb* GS het ons die persentasie van die subeenhede wat gemodifiseerd is (of adenylylated is) verbeter van ± 60-70% na ± 85-94%. Op hierdie manier, het ons rekombinante *M.tb* GS wat 'n beter adenylylation is as ooit van te vore berig.

Drie metodes is gebruik om die graad van adenileering te evalueer by adenileerde en d-adenileerde *M.tb* GS en *E. coli* GS. Die eerste toets wat gebruik was, staan bekend as die γ-glutamiel transferase ensiem toets, is 'n variasie van die omgekeurede reaksie wat GS kataliseer:

$$\text{Glutamaat} + NH_4 + + ATP \rightarrow \text{glutamine} + ADP + P_i + H^+$$
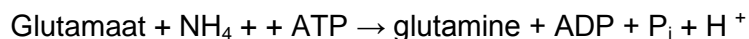
In hierdie omgekeerde reaksie; hidroksielamien en glutamine reageer om γ-glutamylhydroxamate en vry ammoniak in die teenwoordigheid van ADP, arsenaat en mangaan of magnesium te vorm. Hierdie reaksie vorm die basis van 'n toets vir GS aktiwiteit. Op grond van die data uit die γ-glutamiel transferase toets, die adenileering toestand van adenileerde *M.tb* GS wat in hierdie unieke stelsel uitgedruk word is ten minste 68% adenileerd in vergelyking met die 25% wat deur Mehta en mede-werkers gekry is.

Die tweede toets wat gebruik was, is die bepaling van die anorganiese fosfaat konsentrasie na die hidrolise van beide adenileerde en d-adenileerde *M.tb* GS. In die geval van die d-adenileerde ensiem, is daar geen vorming van fosfaat na hidrolise nie. In die geval van die adenileerde *M.tb* GS sal elke adeniel moietie 1 fosfaat bevat dus sal 1 µM van GS (wat 12 subeenhede bevat) 12 µM fosfaat moet bevat, as elke subeenheid geadenileerd is. Die resultaat wat verkry word vir die adenileerde *M.tb* GS ensiem was die vorming van 0,94 µM fosfaat geproduseer per µM GS aktiewe setel, naamlik 94% adenileering in vergelyking met die 25% adenileerde GS wat deur Mehta en mede-werkers gepubliseer is.

Die derde metode wat gebruik was is massaspektrometrie. Die MS-spektra toon duidelike die pieke vir die adenileerde en d-adenileerde ensieme aan, die berekende massas het ooreengestem met die teoretiese massa. Die afleiding kan gemaak word dat die adenileering toestand van *M.tb* GS wat in hierdie unieke stelsel uitgedruk is 85% is.

Daarbenewens is die tempo van omskakeling van ATP, glutamaat en ammoniak na glutamien en ADP deur HPLC bepaal. Dit word die "vorentoe" of "biosintetiese" reaksie

genoem en word deur HPLC geanaliseer die omskakeling van ATP na ADP te bepaal.

Die primêre uitvinding van hierdie projek hou verband met 'n biochemiese pad wat 'n nuwe dwelm teiken kan oplewer wat aangewend kan word om nuwe behandelings teen *M.tb* te ontwikkel. GS kataliseer die omskakeling van glutamaat na glutamine deurmiddel van 'n glutamiel fosfaat intermediêre deur gebruik te maak van ATP. ATP word gebruik as of Mg-ATP of Mn-ATP, afhangende van die adenileerde toestand van die ensiem. Die ensiem word gereguleer deur adenileering in bakterieë en is die GS-I vorm van die ensiem, 'n meganisme wat nie by die GS-II ensiem wat by die mens voorkom bestaan nie.

213 verbindings is teen die adenileerde en d-adenileerde vorme van beide *M.tb* GS en *E. coli* GS getoets teen 'n konsentrasie van 10 µM. Die rasionele ontwerp en seleksie van hierdie inhibeerders is gebaseer op die tipiese ATP bindings setel. Dit het getoon dat GS in die adenileerde vorm 'n unieke histidien kinase-agtige reaksie meganisme gebruik in die fosforilering van die karboksielgroep van glutamaat. Die primêre uitkoms van die projek was die demonstrasie van die selektiewe inhibisie van adenileerde GS en die identifisering van spesifieke verbindings wat in staat is om adenileerde GS te inhibeer. Hierdie verbindings kan oorweeg word vir verdere tref-tot-teiken en teiken optimalisering veldtogte vir die ontwikkeling van nuwe kandidate vir die behandeling van TB. Op grond van die dosis-reaksie toetse, het twee verbindings na vore gekom as die mees belowende anti-*M.tb* GS inhibitore met IC_{50} (µM) waardes van 9.6 µM en 17.4 µM onderskeidelik. Hulle het gereeld die mees kragtige inhiberende aktiwiteit getoon teen *M.tb* adenileerde GS ensiem in vaste konsentrasie toetse met 87% en 81% inhibisie, onderskeidelik. Hierdie verbindings, 10057 en 10059, is struktureel baie soortgelyk. Hierdie twee verbindings wat gevind is om inhiberend te wees vir *M.tb* GS kan nou gebruik word as template om bykomende teiken spesifieke verbindings te sintetiseer as deel van 'n teiken optimalisering program en verdere identifikasie van nuwe geskikte kandidate vir kliniese evaluering.

In die studie het ons ook gekyk na die gebruik van ATP deur te kyk na die ensiemkinetika van *M.tb* GS en *E. coli* GS asook die kinetiese isotoop effek van hierdie ensieme. Daar word voorgestel dat ensieme soos *M.tb* GS en *E. coli* GS, die ensiemkinetika volg van die klassieke Michaelis-Menton kinetika waar 'n balans gehandhaf word tussen die ensiem konsentrasie [E] en die substraatkonsentrasie [S] en waar die binding van die tweede ATP afhanklik is van die sukses van die tweede aktiewe setel om in 'n ATP bindend vorm verander te word deur die vrystelling van 'n ATP uit die eerste aktiewe setel, soos gedefinieer deur die gekoördineerde half-setel meganisme.

As die regulering van die ensiemaktiwiteit en ligand binding in hierdie ensieme funksioneer in 'n gekoördineerde half-die-setel wyse en binding in die tweede plek kom slegs op die vrylating van die ADP uit die eerste plek, word dit dus voorgestel dat deuterasie van die ATP die binding eienskappe verbeter, maar nie 'n impak het op die katalise van die fosforielgroep oordrag nie. As die ewewig skuif na die binding van ATP met toenemende ATP konsentrasie, die deuterated ATP effektief bind twee keer so doeltreffend as die nie-deuterated ATP, wat dan die impak van die deuterasie op die skynbare ensiemaktiwiteit teen hoë konsentrasies aan ATP, die opbrengs van 'n KIE van 1.

Presentations and Publications

The author has made the following oral and poster presentations, as well as publications, of work containing in this dissertation:

1. Poster Presentations

    1.1   A. Theron (née. Steyn), R.L. Roth, H. Hoppe, C. Parkinson, C.W. van der Westhuyzen, S. Stoychev and C.P. Kenyon. Differential inhibition of adenylylated and deadenylylated *M. tuberculosis* glutamine synthetase in *E. coli.* **SASBMB, Drakensberg, 2012**

2. Oral Presentations

    2.1   A. Steyn, R.L. Roth, C.P. Kenyon; Differential inhibition of adenylylated and deadenylylated *M. tuberculosis* glutamine synthetase in *E. coli.* CSIR **Biosciences Student Day, 2011**

    2.2   Oral presentations were made at various research meetings at **CSIR Biosciences, Structural Biology group, Pretoria, 2011-2013**

3. Publications

    3.1   C.P. Kenyon, A. Steyn, R.L. Roth, P.A. Steenkamp, T.C. Nkosi and L.C. Oldfield (2011). The role of the C8 proton of ATP in the regulation of phosphoryl transfer within kinases and synthetases. ***BMC Biochemistry***, 12:36.

Acknowledgements

Ian, my husband and the love of my life: this has not been an easy road for you to walk, but without you this would not have been possible. It has been a road full of sacrifices and many frustrations. However, I would never have undertaken this journey and completing it if it was not for you. I thank you from the bottom of my heart for motivation, endless support, lots of love, wiping of tears and understanding me and giving me the room to achieve what I needed to. Love you endlessly.

To my incredible family on both sides: your love, understanding and support carried me through to the bitter end. Mom and Dad thank you for all the love and the manner you brought me up. Delna, thank you for always managing to look interested in my work! Your love and support means more than you know.

To Robyn, my friend and mentor: thank you for teaching me to be the scientist I am today. Your support gave me the courage to think on my own and work towards my gaols. Your input has been invaluable.

A very special thanks to Prof Colin Kenyon. Thank you for the support and your inputs. You became my mentor and friend during this journey. Thank you for always making me feel counted and cared for.

Prof Ian Wiid, my supervisor: thank you for always answering my emails in minutes and the valuable inputs through out this journey. Thank you for understanding the delay when Mieke was born. I was realy privilege to have you as my supervisor.

Dr Chris Parkinson and Dr Chris van der Westhuysen both chemists at CSIR for the synthesis of the ATP scaffold inhibitors.

CSIR Biosciences for the PhD studentship.

Table of Content

Detailed Content

List of Abbreviations

ADP	Adenosine diphosphate
AIDS	Acquired Immune Deficiency Syndrome
Amp	Ampicillin
Amp^R	Ampicilin resistance
AMP	Adenosine monophosphate
ATase	Adenylyltransferase
ATP	Adenosine triphosphate
bp	Base pairs
^{o} C	Degrees Celsius
CV	Coefficients of variation
DMSO	Dimethyl sulfoxide
DNA	Deoxyribonucleic acid
dNTP	Deoxynucleotide triphosphate
dH$_2$O	Double distilled water
E. coli	*Escherichia coli*
EMB	Ethambutol
EMEM	Eagle's minimal essential medium
Enz	Enzyme
GI	Growth index
Glu	Glutamate/glutamic acid
Gln	Glutamine
GS	Glutamine synthetase
HIV	Human immunodefiency virus
HPLC	High Performance Liquid Chromatography
hr(s)	Hour(s)

INH	Isoniazid
IPTG	Isopropyl-β-D-thiogalactopyranoside
Kan	Kanamycin
LB	Luria-Bertani medium
M	Molar
MCS	Multiple cloning site
MDR	Multidrug resistant
mM	Milli Molar
$MgCl_2$	Magnesium chloride
min	Minute
$MnCl_2$	Manganese chloride
MOI	Multiplicity of infection
MSO	L-methionine-*S, R*-sulphoxamine
Mtb	*Mycobacterium tuberculosis*
*Mtb*GS	*Mycobacterium tuberculosis* glutamine synthetase
nM	Nano Molar
µM	Micro Molar
µl	Microliter
NH_4^+	Ammonium
OD	Optical density
PAGE	Poly-acrylamide gel electrophoresis
PBS	Phosphate buffered saline
PCR	Polymerase chain reaction
PhosT	Phosphinothricin
PZA	Pyrazinamide
RIF	Rifampicin
rpm	revolutions per minute

SD   Standard deviation

SDS   Sodium dodecyl sulphate

sec   Second

SRB   Sulforhodamine B

TB   Tuberculosis

TCA   Trichloroacetic acid

Tm   Annealing temperature

TraSH   Transposon site hybridization

V   Volts

WHO   World Health Organisation

XDR   Extensively drug-resistant

ZN   Ziehl-Neelsen stain

Chapter 1

Literature Review

1.1 Mycobacteria

Mycobacteria are non-motile, unicellular, aerobic, Gram-positive rod shaped bacilli. The complete genome sequence of the best-characterized strain of *Mycobacterium tuberculosis* (*M.tb*), H37Rv, has been determined and analysed in order to improve the understanding of the biology of this slow-growing pathogen and to help the conception of new prophylactic and therapeutic interventions. The genome comprises of 4,411,529 base pairs and contains around 4,000 genes. It has a very high guanine and cytosine content which is reflected in the biased amino-acid content of the proteins. *M.tb* differs radically from other bacteria in that a very large portion of its coding capacity is devoted to the production of enzymes involved in lipogenesis and lipolysis, and to two new families of glycine-rich proteins with a repetitive structure that may represent a source of antigenic variation. *M.tb* can be characterised by the following parameters: (1) the presence of mycolic acids in their cell walls, (2) 61-71% rich guanine and cytosine content of the genome and (3) being acid-fast (Shinnick and Good, 1994).

M.tb, the aetiological agent of the disease tuberculosis (TB), has returned to become one of the leading causes of preventable deaths in 200 countries and territories, including South Africa.

1.2 Tuberculosis Epidemic

The first reported study of TB dates back to the "Canon of Medicine" written by Ibn Sina (Avicenna) almost 1000 years ago. He was the first physician to identify pulmonary TB as a contagious disease and suggest that it could spread through contact with soil and water. Avicenna also developed the method of quarantine in order to limit the spread of TB. Regardless of this early characterisation of TB as a disease and the pioneering work leading to the identification in the nineteenth century of *M.tb* as the causative agent by Robert Koch, TB remains today one of the world's major health problems and the leading cause of death from a single infectious agent (Saleem and Azher, 2013).

According to the World Health Organisation (WHO), it is estimated that 1.77 million deaths resulted from TB in 2007, including 456,000 people with HIV (WHO, 2010). There were 9.4 million new TB cases in 2008 (WHO, 2010). The estimated tuberculosis incidence rates by country are indicated in Figure 1.1. Although current treatment can be effective, existing frontline drugs must be taken for at least six months to prevent relapse. Poor treatment compliance contributes directly to the emergence of multidrug- and extensively drug-resistant (MDR and XDR) strains of *M.tb.*
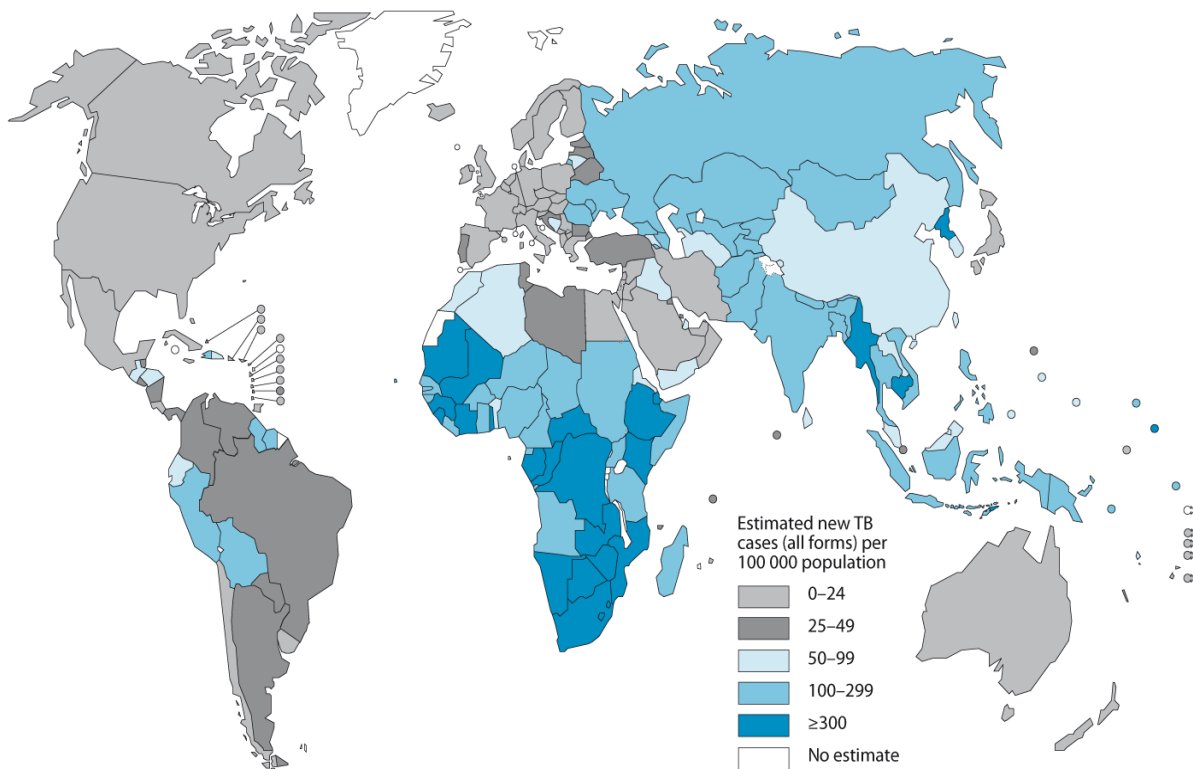
Figure 1.1: Estimated tuberculosis incidence rates, by country, in 2009 (WHO, 2010)

1.3 Transmission of *M.tb*

TB is spread through the air by droplet nuclei, these particles are 1 to 5 mm in diameter. These droplet nuclei which are spread from person to person (which are produced by persons with pulmonary or laryngeal TB cough, sneeze or speak) do contain the *M.tb* complex (Edwards and Kirkpatrick, 1986). They also may be produced by aerosol treatments, sputum induction, aerosolization during bronchoscopy, and through manipulation of lesions or processing of tissue or

secretions in the hospital or laboratory. Due to the small size of the droplet nuclei air currents normally present in any indoor space can keep them airborne for long periods of time (Riley, 1993). These small droplet nuclei are able to reach the alveoli within the lungs, and replication of the bacilli can then start (Murray, 1986). There are four factors which will determine the likelihood of the transmission of *M.tb*: (1) the number of organisms being expelled into the air, (2) the concentration of organisms in the air determined by the volume of the space and its ventilation, (3) the length of time an exposed person breathes the contaminated air, and (4) presumably the immune status of the exposed individual. HIV-infected persons and others with impaired cell mediated immunity are thought to be more likely to become infected with *M.tb* after exposure than persons with normal immunity; also, HIV-infected persons and others with impaired cell-mediated immunity are much more likely to develop disease if they are infected. However, they are no more likely to transmit *M.tb* (Horsburgh, 1996). There are a number of measures which can be put into place to reduce the spread of TB namely: (1) Ventilation with fresh air is especially important, particularly in health care settings, (2) the number of viable airborne tubercle bacilli can be reduced by ultraviolet irradiation of air in the upper part of the room and (3) the most important means to reduce the number of bacilli released into the air is by treating the patient with effective anti-tuberculosis chemotherapy (Riley, 1993; Centers for Disease Control and Prevention , 1994; Jindani *et al.,* 1980).

1.4 Multidrug-resistant and extensively drug-resistant TB in South Africa

The serious threat of TB, especially multidrug- and extensively drug-resistant (MDR and XDR) TB, is a great concern in Southern Africa particularly to individuals with HIV/AIDS. XDR-TB comes about when resistance to isoniazid (INH) and rifampicin (RIF) is compounded by an additional resistance to the second line drugs, including any fluoroquinolones and at least one of the three injectables (kanamycin, amikacin or capreomycin) (Andrews *et al.*, 2007).

The concern about XDR-TB was emphasized following a clinical study in 2006 at the Church of Scotland Hospital in KwaZulu-Natal, South Africa. Of the 536 TB patients hospitalized at the time, 221 were found to have MDR-TB, of which 53 were diagnosed with XDR-TB. Of these, 52 died within 25 days. At the time, it was thought

that the co-infection of 44 of these patients with HIV was reason behind their development of XDR-TB (Wise, 2006). However, evidence presented by Dr. Tony Moll at the 2nd TB conference, 1-4 June 2010 in Durban South Africa, indicated that the XDR-TB primarily originated in the hospital through inadequate infection control. XDR-TB development in patients that never had TB or HIV infection before, but were hospitalized for other ailments in wards that held one or two undiagnosed XDR-TB patients. In another study done in a HIV co-infected population at a South African gold mine, it was found that existing TB control measures were insufficient to control the spread of drug resistant TB. Furthermore inappropriate therapy as well as a delay in diagnosis contributed to drug resistance and transmission of the disease. Poor treatment compliance contributes directly to the emergence of multidrug- and extensively drug-resistant (MDR and XDR) strains of *M.tb* (Calver *et al.,* 2010)*.*

1.5 TB treatment
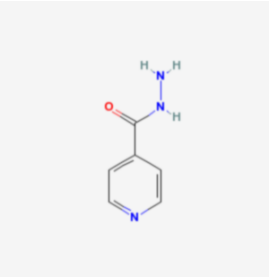
The discovery of streptomycin in 1946 followed by the successful testing of INH in 1952, which was shown to be the most important antibiotic in the standard treatment regime against TB, started the era of antibiotics for TB. Other drugs were developed in the following years: pyrazinamide in 1954, ethambutol in 1962 and rifampicin in 1963 (Tuberculosis, In Encyclopaedia Britannica, 2010).
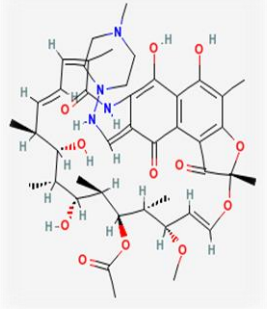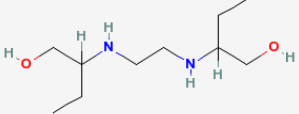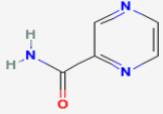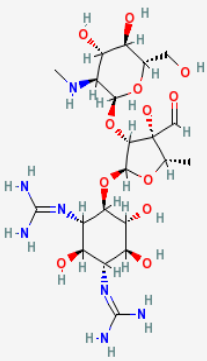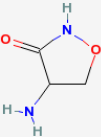
The treatment of TB differs from that of other infectious diseases due to the long treatment time needed to cure the patient (Cole and Riccardi, 2011). A characteristic difficulty of TB is the persistence of the pathogenic mycobacteria, regardless of prolonged antibiotic treatment. The micro-environment containing dormant bacteria could change over a period of time causing the bacteria to recommence growth, at which stage they are vulnerable to standard drugs (Parrish *et al.,* 1998). Because some of the subpopulations of *M.tb* may not be eliminated effectively with standard antibiotics, prolonged periods of the treatments are required (Barry *et al.,* 2009). These heterogeneous subpopulations of the bacteria are able to survive within granulomatous lesions surrounded by foamy macrophages in a persistent or latent state, without clinical symptoms (Korf *et al.,* 2005). Most bactericidal drugs are only effective against actively growing bacilli and the extended treatment times are needed to then inhibit the regrowth of the bacteria (Cardona, 2006). The length of treatment depends on the presence of non-replicating bacteria and pathogens in a
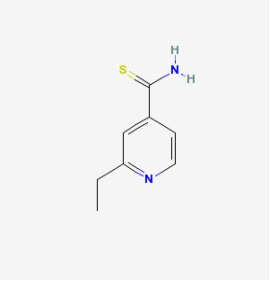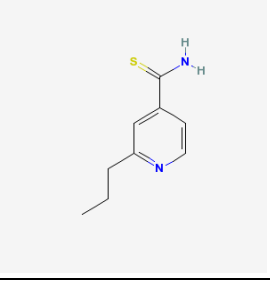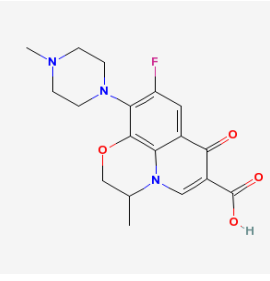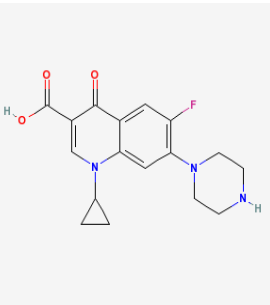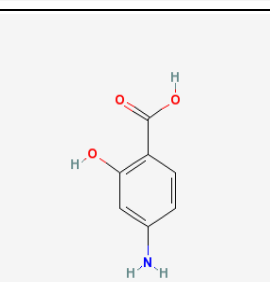
stationary phase present in old lesions of fibrotic tissue (Sosnik *et al.,* 2009). The implementation of a 6 month or longer treatment regime with antibiotics for cases of susceptible TB resulted in a remarkable reduction in the number of deaths of TB cases per 100 000 population in the 1960s, such that TB was thought to be a curable disease that was easy to manage.

Antibiotics against TB can be classified into two lines of combination treatment, of which application of the more expensive and less efficient second line is dictated by the development of drug resistance to the first. The decision to commence with a treatment regime for TB is not taken lightly, due to the severe side effects that can occur. For example, first line drugs can cause, drug induced hepatitis, nausea, deafness and progressive loss of vision (Department of Health, 2004). The first line of drugs includes INH, rifampicin, ethambutol, pyrazinamide and streptomycin used for the treatment of drug sensitive TB (See table 1.1). There is currently 6 second line drugs used for the treatment of MDR-TB. However these drugs have more toxic side effects (e.g. cycloserine). Second line drugs are difficult to come by in developing countries (e.g. flouroquinolones) or are less effective than first line drugs (e.g. p-aminosalicylic acid). XDR-TB brought the concept of 'third line' drugs that are not listed by the WHO as second line drugs or of which the efficacies are not yet proven (Nardell, 2009).

Table 1.1: First and second-line drugs used in the treatment of TB, with their structures, targets and cellular processes (Handbook of Anti-Tuberculosis Agents, www. thomson-pharma.com, www. drugbank.ca and http://pubchem.ncbi.nlm.gov).

First line TB drugs		Target	Cellular process
Isoniazid		Cell wall	Mycolic acid synthesis

Rifampicin		RNA synthesis	Binds to RNA polymerase to prevent mRNA synthesis and consequent protein production.
Ethambutol		Cell wall	Prevents arabinogalactan synthesis
Pyrazinamide		Cell wall	Fatty acid biosynthesis
Streptomycin		Translation	Binding of the drug to ribosomes inhibits protein synthesis
Second line TB drugs		**Target**	**Cellular process**
Cycloserine		Cell wall	Inhibits cell wall synthesis

Ethionamide		Cell wall	Pro-drug which when activated inhibits mycolic acid biosynthesis
Prothionamide		Cell wall	Pro-drug which when activated inhibits mycolic acid biosynthesis
Ofloxacin		DNA structure replication	Prevent DNA supercoiling and replication
Ciprofloxacin		DNA structure replication	Prevent DNA supercoiling and replication
p-aminosalicylic acid		Folate metabolism	Disrupt intracellular folate levels

The current standard first line treatment regimen according to the South African tuberculosis control programme of 2004 consist out of an initial (or intensive) phase of 2 months consisting of 4 drugs INH, rifampicin, pyrazinamide and ethambutol. Streptomycin is added to the regime when the person is re-treated for TB. A continuation phase of 4 months with INH and rifampicin follows after the intensive

phase to effect sterilization, i.e. the complete elimination of the infecting mycobateria (Cole and Riccardi 2011). Due to the duration of the treatment and the increased probability of non-compliance that this holds for the patient, drug resistance to any one drug can develop.

Most of the standard chemotherapy is not effective for individuals that have MDR-TB and there is practically no cure for XDR-TB. Drug resistant mycobacterial pathogens are increasingly detected in persons who have been previously treated for TB where a possible cause could be the failure to complete lengthy drug regimens and the pathogens becoming resistant to especially the two first line drugs, INH and rifampicin through mutations in genes such as the InhA and RpoB genes (Sosnik *et al.,* 2009). The approach to control this disease now is either to discover new chemotherapies effective against *M.tb* and with different targets as well as to enhance the potential of existing drugs to treat MDR-TB (Rastogi *et al.,* 1998)

Treating TB patients who are co-infected with HIV poses some major challenges. This includes drug-drug interactions between antiretroviral drugs (protease inhibitors and non-nucleoside reverse transcriptase inhibitors) and rifamycins, which could result in subtherapeutic concentrations of anti-retroviral drugs. When overlapping toxicities of the anti-retroviral and anti-tuberculosis drugs increase, discontinuation of the treatment may be required. Another complication is immunupathological reactions and clinical deterioration due to immune reconstitution inflammatory syndrome where a worsening or recurrence of TB occurs when anti-retroviral treatment is commenced. It is suggested that anti-retroviral therapy should be delayed until the intensive phase of anti-tuberculosis treatment is completed, but delayed anti-retroviral therapy on the other hand also increases the risk of morbidity and mortality in patients in the advanced stages of HIV infection (McIlleron *et al.,* 2007).

If a new TB treatment is going to replace the already existing therapy then it should at least shorten the duration of the treatment or reduce the number of dosages to be taken. Furthermore the new drug should improve the treatment of MDR-TB or provide effective treatment against latent TB infection (Barry, 1997). The identification and investigation of new drug targets is also an approach to follow.

Drug discovery programmes are normally focussed on pathogen proteins whose function is known to be essential to the bacterial cell, combined with a lack of mammalian homologues. The solution lies in a combined effort to improvements of current drug regimes by shortening the treatment period, supply treatment for multidrug resistant TB and to discover an effective treatment for persistent or latent tuberculosis infection.

1.5.1 Drugs in late stage development for the treatment of TB

Seven candidate TB drugs (Table 1.2) representing five different chemical classes are currently known to be undergoing clinical evaluation (Thomson Pharma, August 2013, Cole and Riccardi, 2011). These will be described by chemical class, in order according to stage of clinical development.

Fluoroquinolones:

Gatifloxacin and Moxifloxacin: The furthest advanced of these seven are two drugs belonging to the family of C8-methoxy fluoroquinolones: gatifloxacin and moxifloxacin. Both gatifloxacin and moxifloxacin are approved drugs for other indications (gatifloxacin from Bristol-Myers Squibb in the United States and moxifloxacin from Bayer Healthcare Pharmaceuticals). Both are now in phase III clinical evaluation for treatment of newly diagnosed, drug sensitive, adult, pulmonary TB.

Diarylquinolines: TMC-207

TMC-207: This novel compound, also referred to in the literature as R207910, is a diarylquinoline, owned by Johnson & Johnson and being developed by its subsidiary, Tibotec. It was originally discovered by whole-cell phenotypic screening and acts by inhibiting the *M.tb* adenosine triphosphate (ATP) synthase.

Nitroimidazoles: PA-824 and OPC-67683

The nitroimidazoles represent a novel class of drugs for TB treatment. Two members of this chemical class are presently in phase II of clinical development: PA-824, a nitroimidazo-oxazine, being evaluated currently for drug sensitive TB, and OPC-67683, a nitroimidazo- oxazole, currently being studied in MDR-TB patients.
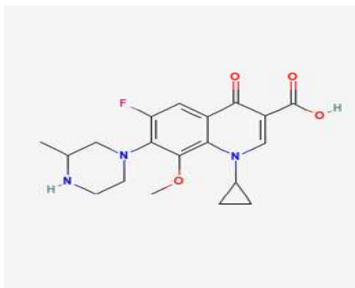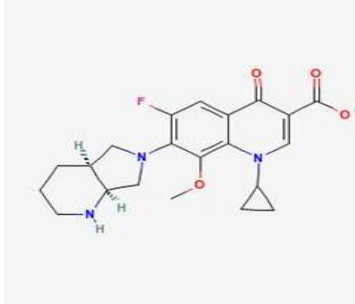
Ethylenediamine: SQ109
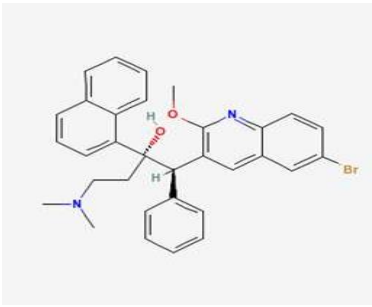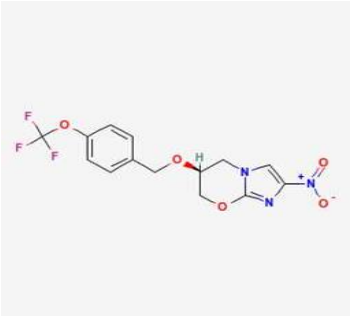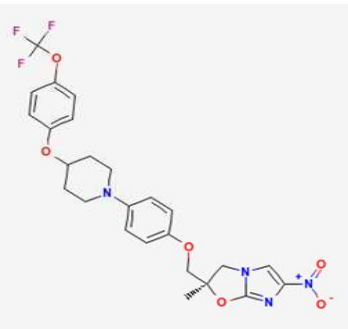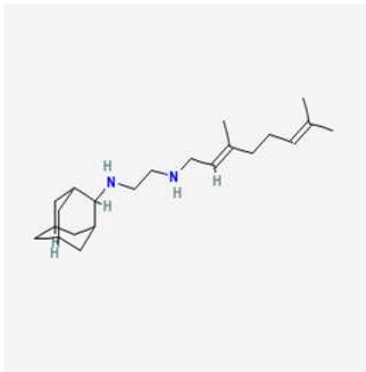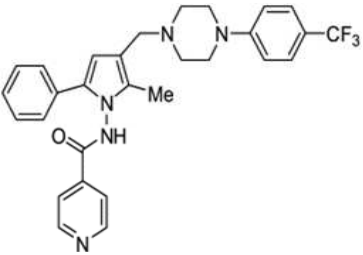
SQ109 is a novel 1,2-ethylenediamine. It was originally identified as part of collaboration between the biotech company Sequella, Inc., and the National Institute of Allergy and Infectious Diseases of the U.S. National Institutes of Health to synthesize via combinatorial chemistry and screen ethambutol analogs for killing *M.tb* in vitro under aerobic conditions using a high-throughput bioluminescence-based assay.

Pyrrole: LL-3858

LL-3858 is a pyrrole derivative being developed by Lupin, Ltd. Little published information is available about this compound. Its mechanism of action is unknown. Its MIC in vitro against *M.tb* has been reported to be 0.12 to 0.25 µg/mL, and it demonstrated synergistic activity with rifampicin in vitro. As of the last public report, this compound is in phase I of clinical development in India.

Table 1.2: Selected drugs in late stage development for the treatment of Tuberculosis, with their structures, clinical phase, class and mechanism of action (www. thomson-pharma.com, www. drugbank.ca and http://pubchem.ncbi.nlm.gov).

Selected drug in development	Structure	Clinical Phase	Class: Mechanism of action
Gatifloxacin		Phase III	Fluoroquinolone: Inhibition of DNA gyrase and topoisomerase II
Moxifloxacin		Phase III	Fluoroquinolone: Inhibition of DNA gyrase and topoisomerase II

TMC-207		Phase II	Diarylquinoline: Inhibition of ATP synthase
PA-824		Phase II	Nitroimidazol: Oxidative stress
OPC-67683		Phase II	Nitroimidazol: Oxidative stress
SQ-109		Phase I	Ethylenediamine: Inhibition of cell-wall synthesis
LL-3858		Phase I	Pyrrole derivative: Unknown

1.6 Drug targets

1.6.1 *M.tb* drug targets

The quest for better, faster and cheaper drugs will require innovative approaches to novel drug target identification. The increase in data available and the improved understanding of the physiology and metabolism of *M.tb* are making the task of target identification easier. There are certain criteria a protein must meet in order to progress to the next stage of being identified as a new drug target. Important factors include low or no homology between the target and host (to minimize the host-drug interaction), an unambiguously proven role the target plays in the diseased state and the importance of the target to the pathogen's growth and survival (like metabolic choke points) (Hasan *et al.*, 2006). In TB, identification of targets that play a role in the maintenance of the dormant phase of the bacteria is receiving the most attention. Genes and gene products that are involved in dormancy or persistence should make good drug targets, considering the extended periods of time for which the latent infection can persist. An example is isocitrate lyase, a key enzyme of the glyoxylate shunt. Important tuberculosis drugs like INH and ethambutol target cell wall synthesis, so enzymes involved in this pathway will always be favoured targets for drug development. Organisms related to *M.tb* exhibit different degrees of pathogenicity or virulence, and by comparing pathogenic with non-pathogenic organisms, a few virulence factors have been identified and marked as drug targets. Rifampicin targets RNA polymerase, and other essential transcription factors like the sigma factors (SigH, SigF and SigA) can also be potential drug targets. Transporter proteins and other proteins needed for maintaining the important nutrient environment can also serve as possible targets for drug development. Serine/threonine protein kinases, tyrosine phosphatase and histidine kinase two component systems are vital to the signal transduction system in a number of organisms during the stress responses, developmental processes and the pathogenicity (Chopra et al., 2003).

New targets for drugs are therefore required. These new drugs should also simplify and shorten the treatment period, as well as reduce drug-drug interactions in patients co-infected with HIV. Drug discovery programmes are normally focussed on pathogen proteins whose function is known to be essential to the bacterial cell,

combined with a lack of mammalian homologues. One such potential drug target for TB is glutamine synthetase (GS).

1.6.2 Glutamine synthetase (GS)

GS (EC 6.3.1.2) is a complex dodecameric oligomer (Figure 1.2) which is the ubiquitous central enzyme in nitrogen metabolism (Metha *et al.,* 2004). GS catalyzes the reversible conversion of L-glutamic acid, ATP and ammonia to L-glutamine, ADP and inorganic phosphate via a γ-glutamyl phosphate intermediate (Shapiro and Stadman, 1970). It is a central enzyme in nitrogen metabolism, and can be regulated by at least four different mechanisms: (a) adenylylation and deadenylylation of a conserved tyrosine residue, (b) conversion between a relaxed (inactive) and taut (active) state depending on the divalent metal cation present, (c) cumulative feedback inhibition by multiple end products of glutamine metabolism, and (d) repression and derepression of GS biosynthesis in response to nitrogen availability (Shapiro and Stadman, 1970).
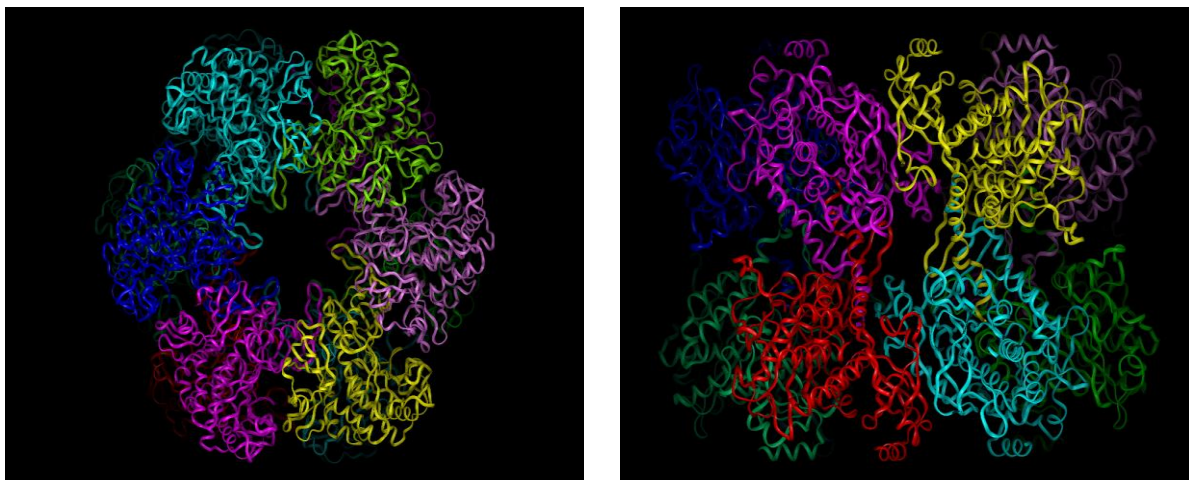
Figure 1.2: The dodecameric structure of GS (Kenyon *et al.,* 2011).

Three distinct forms of GS occur, with GS-I found only in bacteria (eubacteria) and archaea (archaebacteria) (Kumada *et al*., 1993). GS-II occurs only in eukaryotes, and soil-dwelling bacteria, while GS-III genes have been found only in a few bacterial species. Two significant prokaryotic GS-I sub-divisions exist: GS-Iα and GS-Iβ (Brown *et al*., 1994). The GS-Iβ enzyme is regulated via the adenylylation/deadenylylation cascade, which does not occur in the GS-Iα or GS-II

sub-divisions. *M.tb* and *Escherichia coli* (*E.coli*) GS are regulated in this manner, while the human homologue belongs to GS-II and is not subject to adenylylation, a difference that can be exploited by developing drugs that are only active against the adenylylated form of the enzyme.

The extent of adenylylation of *E.coli* GS is regulated in response to the intracellular concentrations of α-ketoglutarate and glutamine, via the reversible adenylylation of a tyrosine residue (Tyr-406) in each subunit of GS (Tyler, 1978; Gaillardin and Magasanik, 1978; Floor *et al.,* 1975; Janssen and Magasanik, 1977 and Senior, 1975). The presence of adenylylated GS predominates in a nitrogen-rich, carbon-limited media, while the deadenylylated form tends to predominate under conditions of nitrogen limitation (Tyler, 1978; Gaillardin and Magasanik, 1978; Floor *et al.,* 1975; Janssen and Magasanik, 1977 and Senior, 1975). This regulation of the adenylylation state of GS is accomplished by three proteins: (1) uridylyltransferase/uridylyl-removing enzyme, (2) the signal transduction protein P_{II}, and (3) adenylyl transferase or ATase. High intracellular concentrations of glutamine activate the uridylyl-removing enzyme, which causes the deuridylylation of P_{II}. This interacts with ATase, which then catalyses the adenylylation of GS. A high intracellular α-ketoglutarate concentration activates uridylyltransferase, which transfers UMP to each subunit of P_{II}, forming P_{II}-UMP. The P_{II}-UMP interacts with the ATase, which in turn catalyses the removal of AMP from the GS. Research on the effect of glucose, ammonia and glutamic acid concentrations has shown that the adenylylation state of GS is a function of metabolic flux rather than absolute concentration only (Wolhueter *et al.,* 1973). The activity of GS is therefore regulated by both the nature and the availability of the ammonia source (Merrick and Edwards, 1995; Senior, 1975). The level of GS activity is inversely related to the degree of adenylylation (Kenyon *et al.,* 2011; Okano *et al.,* 2010, reviewed in Shapiro and Stadtman, 1970; Ginsberg and Stadtman, 1973 and Wolhueter *et al.,* 1973) and that adenylylated residues may be present on any number of subunits from zero to twelve, depending on carbon and nitrogen availability (Harper *et al.,* 2010 Holzer *et al.,* 1968; Shapiro *et al.,* 1967; Shapiro and Stadtman 1968; Kingdon *et al.,* 1967; Mecke *et al.,* 1966 and Reitzer and Magasanik, 1987). GS is therefore responsible for the assimilation of ammonia when the available ammonia in the environment is restricted, as well as for the formation of glutamine for the synthesis of protein and

other nitrogen compounds. In ammonia-rich medium, the level of GS is low and GS functions primarily for the synthesis of glutamine.

The identification of genes which are required for mycobacterial growth by means of transposon site hybridization (TraSH) studies done by Sassetti indicated that the glutamate degradation pathway is essential for growth in which GS plays an essential role (Sassetti *et al.,* 2003). In another study done by Chandra and co-workers they shown that GS is necessary for cell wall resistance and pathogenicity (Chandra *et al.,* 2010). GS can therefore be offered as a potential new drug target.

1.7 Study design and objectives of this thesis

Hypothesis

Glutamine synthetase has emerged as a potentially viable drug target for tuberculosis, and is also hypothesised that the adenylylation cascade may provide additional pharmacological targets for tuberculosis therapy.

Aims

- To demonstrate the production of soluble adenylylated *M.tb* GS in *E.coli* by co-expression with *M.tb* adenylyl transferase.

- To demonstrate the production of soluble deadenylylated *M.tb* GS in *E.coli.*

- To examine the inhibitory effect of a library of ATP scaffold-based inhibitors.

- To demonstrate differential inhibition of adenylylated and deadenylylated *M.tb* GS.

- To demonstrate the effect of deuterated ATP on *M.tb* and *E.coli* GS regulation*.*

Methodology

- Previously published reports shown that, when *M.tb* GS is expressed in *E.coli*, the *E.coli* adenylyl transferase does not optimally adenylylate the *M.tb* GS.

Here, we will demonstrate the production of soluble adenylylated *M.tb* GS in *E.coli* by co-expression with *M.tb* adenylyl transferase.

- Isolation of soluble adenylylated and deadenylylated *M.tb* GS using anion exchange, followed by affinity purification.

- The functionality of both adenylylated and deadenylylated *M.tb* GS will be determined using the γ-glutamyl transferase assay, an HPLC-based assay to determine ADP formation, and determination of inorganic phosphate formation.

- The assessment of the degree of adenylylation of *M.tb* GS will be determined by enzyme hydrolysis and Mass spectrometry.

- The inhibitory effect of 214 ATP scaffold-based inhibitors against both adenylylated and deadenylylated *M.tb* GS activity will be measured by the HPLC-based assay for ADP formation, and the determination of inorganic phosphate. Dose-response assays will be carried out for IC_{50} determination.

- Compounds showing promising inhibition will be incubated with the *H. sapiens* HeLa cell line and their effect on cell numbers will be determined.

- Compounds identified in inhibitor screens will be tested for antibacterial activity using BACTEC assay with H37Rv reference strain at the University of Stellenbosch.

- Intracellular survival of *M.tb* (H37Rv/Beijing220) in mouse bone-marrow derived macrophages will be monitored in response to identified compounds at the University of Stellenbosch.

Chapter 2

PCR-mediated synthesis of *Mycobacterium tuberculosis* glutamine synthetase and functional expression in *Escherichia coli*

2.1 Introduction

2.1.1 Importance of glutamine synthetase

Glutamine synthetase (GS, EC 6.3.1.2) catalyzes the reversible conversion of L-glutamic acid, ATP and ammonia to L-glutamine, ADP and inorganic phosphate via a γ-glutamyl phosphate intermediate (Kenyon *et al.,* 2011; Shapiro and Stadman, 1970). It is a central enzyme in nitrogen metabolism, and can be regulated by at least four different mechanisms: (a) adenylylation and deadenylylation of a conserved tyrosine residue (Figure 2.1), (b) conversion between a relaxed (inactive) and taut (active) state depending on the divalent metal cation present, (c) cumulative feedback inhibition by multiple end products of glutamine metabolism, and (d) repression and derepression of GS biosynthesis in response to nitrogen availability (Shapiro and Stadman, 1970).

GS enzymes are classified into four forms according to the number of subunits present and whether or not the enzyme is post-translationally regulated. Two significant prokaryotic GS-I sub-divisions exist: GS-Iα and GS-Iβ (Hayward *et al.,* 2009; Brown *et al.,* 1994). The GS-Iβ enzyme is regulated via the adenylylation/deadenylylation cascade, which does not occur in the GS-Iα or GS-II sub-divisions. *Mycobacterium tuberculosis* (*M.tb*) and *Escherichia coli* (*E.coli)* GS are regulated in this manner, while the human homologue belongs to GS-II and is not subject to adenylylation, a difference that can be exploited by developing drugs that are only active against the adenylylated form of the enzyme.
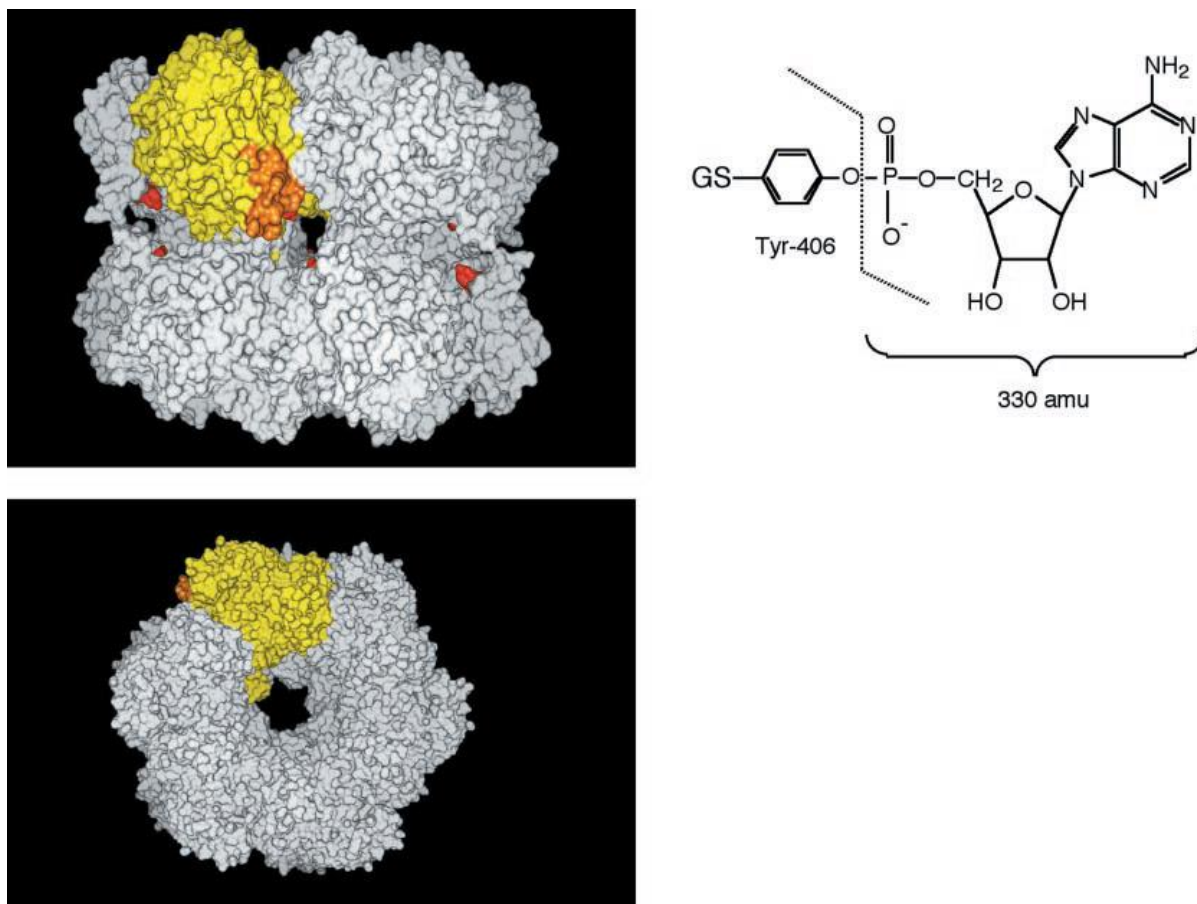
Figure 2.1: Space-filling model of the x-ray structure of *M.tb* GS (Protein Data Bank number 1HTQ) and the chemical structure of the adenylyl group that regulates GS activity. The enzyme is a dodecamer of identical subunits forming face-to-face hexagonal rings. Top left, edge-on view with the 6-fold axis of symmetry running vertically in the plane of the page. A single subunit is coloured yellow, with the adenylylation loop in orange and the Tyr-406 in each subunit coloured red. The adenylylation loop includes residues 398–410. Bottom left, a top view of the enzyme with the 6-fold axis perpendicular to the page. Top right, the chemical structure of the adenylyl group (330 atomic mass unit) which attached to Tyr-406 (Metha *et al.,* 2004).

The extent of adenylylation of *E.coli* GS is regulated in response to the intracellular concentrations of α-ketoglutarate and glutamine, via the reversible adenylylation of a tyrosine residue (Tyr-406) in each subunit of GS (Tyler, 1978; Gaillardin and Magasanik, 1978; Floor *et al.,* 1975; Janssen and Magasanik, 1977 and Senior, 1975). The presence of adenylylated GS predominates in a nitrogen-rich, carbon-limited media, while the deadenylylated form tends to predominate under conditions of nitrogen limitation (Tyler, 1978; Gaillardin and Magasanik, 1978; Floor *et al.,* 1975; Janssen and Magasanik, 1977 and Senior, 1975). This regulation of the adenylylation state of GS is accomplished by three proteins: (1) uridylyltransferase/

uridylyl-removing enzyme, (2) the signal transduction protein P_{II}, and (3) adenylyl transferase or ATase. High intracellular concentrations of glutamine activate the uridylyl-removing enzyme, which causes the deuridylylation of P_{II}. This interacts with ATase, which then catalyses the adenylylation of GS. A high intracellular α-ketoglutarate concentration activates uridylyltransferase, which transfers UMP to each subunit of P_{II}, forming P_{II}-UMP. The P_{II}-UMP interacts with the ATase, which in turn catalyses the removal of AMP from the GS. Research on the effect of glucose, ammonia and glutamic acid concentrations has shown that the adenylylation state of GS is a function of metabolic flux rather than absolute concentration only (Wolhueter *et al.,* 1973). The activity of GS is therefore regulated by both the nature and the availability of the ammonia source (Merrick and Edwards, 1995; Senior, 1975). The level of GS activity is inversely related to the degree of adenylylation (Kenyon *et al.,* 2011; Okano *et al.,* 2010, reviewed in Shapiro and Stadtman, 1970; Ginsberg and Stadtman, 1973 and Wolhueter *et al.,* 1973) and that adenylylated residues may be present on any number of subunits from zero to twelve, depending on carbon and nitrogen availability (Harper *et al.,* 2010 Holzer *et al.,* 1968; Shapiro *et al.,* 1967; Shapiro and Stadtman 1968; Kingdon *et al.,* 1967; Mecke *et al.,* 1966 and Reitzer and Magasanik, 1987). GS is therefore responsible for the assimilation of ammonia when the available ammonia in the environment is restricted, as well as for the formation of glutamine for the synthesis of protein and other nitrogen compounds. In ammonia-rich medium, the level of GS is low and GS functions primarily for the synthesis of glutamine.

A number of factors make GS a potential drug target in the fight against TB, including being considered essential for the survival of *M.tb* (Reynaud *et al.,* 1998; Harth and Horwitz, 1999 and 2003 and Tullius *et al.,* 2003). The GS inhibitor L-methionine-*S,R*-sulphoxamine (MSO) inhibits growth of *M.tb* both *in vitro* and *in vivo* (Reynaud *et al.,* 1998 and Harth and Horwitz, 1999). The extracellular location of GS is a characteristic that is only found in the pathogenic mycobacteria's such as *M.tb* and *M.bovis*, and not with the non-pathogenic strains of *M.smegmatis* and *M.phlei* (Shapiro and Ginsburg, 1968 and Reynaud *et al.,* 1998). It appears to play an important role in cell wall biosynthesis, in the form of a cell wall component found only in pathogenic mycobacteria: poly-L-glutamate / glutamine (Wietzerbin *et al.,* 1975 and Hirschfield *et al.,* 1990). *M.tb* GS has previously been successfully

expressed in heterologous systems, including *E.coli* and the non-pathogenic mycobacterial strain *M. smegmatis* (Mehta *et al.,* 2004 and Singh *et al.,* 2004). Mehta and co-workers expressed *M.tb* GS in *E.coli* host strains that were deficient in either chromosomal GS (*glnA*), or both chromosomal GS and ATase (*glnE*). They found that the *E.coli* ATase was inefficient in adenylylating the heterologous *M.tb* GS, with only ~25% of subunits being modified. A lack of *E.coli* ATase yielded completely deadenylylated *M.tb* GS. From the literature it was evident that this is not the optimal road to follow for the production of adenylylated *M.tb* GS, therefore a different approach will be followed here for the production of adenylylated *M.tb* GS production. We will demonstrate the production of soluble adenylylated *M. tuberculosis* glutamine synthetase in *E.coli* by the co-expression of *M.tb* glutamine synthetase and *M.tb* adenylyl transferase.

Here, we describe the production of both the deadenylylated and adenylylated forms of *M.tb* GS in *E.coli.* Deadenylylated *M.tb* GS is produced by constitutive expression in an *E.coli* strain deficient in both *E.coli* GS and ATase activities, while adenylylated *M.tb* GS is produced in the same host when co-expressed with an inducible *M. tuberculosis* ATase. For comparison purposes, *E.coli* GS was also produced in the adenylylated and deadenylylated forms. Adenylylated *E.coli* GS was produced in a host lacking chromosomal GS and uridylyltransferase, while the deadenylylated *E.coli* GS host strain lacked chromosomal GS and ATase. Adenylylation was measured using the γ-glutamyl transferase assay, mass spectrometry and determination of phosphate content by enzyme hydrolysis.

2.1.2 Study Objectives

- Objective 1: To demonstrate the production of soluble adenylylated *M.tb* GS in *E.coli* by co-expression with *M.tb* adenylyl transferase, as well as the production of soluble deadenylylated *M.tb* GS in *E.coli.*

- Objective 2: To demonstrate the production of soluble adenylylated and deadenylylated *E.coli* GS in *E.coli.*

- Objective 3: To determine the functionality of both adenylylated and deadenylylated *M.tb* and *E.coli* GS by making use of (1) the γ-glutamyl transferase assay, (2) an HPLC-based assay for ADP formation determination, and (3) determination of inorganic phosphate formation.

- Objective 4: To assess the degree of adenylylation of *M.tb* and *E.coli* GS, using enzyme hydrolysis and mass spectrometry.

2.2 Methods

2.2.1 Production of *glnD* and *glnE* knockout strains of *E.coli* YMC11 (CGSC)

The Quick & Easy *E.coli* Gene Deletion Kit (Gene Bridges GmbH) was used to knock out the *glnD* (uridylyltransferase/uridylyl-removing enzyme) or *glnE* (adenylyl transferase) genes on the *E.coli* chromosome of YMC11, a strain already lacking *glnA* (Backman *et al.*, 1981). Primers were designed to the *glnD* and *glnE* genes (Genbank database, http://www.ncbi.nlm.nih.gov/genbank/), each containing a region specific to the relevant gene adjoining a sequence specific to the kit-supplied FRT cassette (underlined in Table 2.1). A diagrammatic sketch showing gene orientation and primer position for both *glnD* and *glnE* are shown in Figure 2.2 and Figure 2.3 respectively.

Table 2.1: Sense and antisense oligonucleotides used for the production of *glnD* and *glnE* knockout strains of *E.coli* YMC11

Primer name	Primer sequence (5' to 3')
glnD sense primer	Ga**ggatcc**cagaaccagcgccatcagcgttaccatggcaccagctacaac cttgaacc<u>aattaaccctcactaaagggcg</u>*
glnD antisense primer	Gt**ggatcc**gcgatatcgtgaaacagcgcggcgatgaaaatcagctcagttga cggcag<u>taatacgactcactatagggctc</u>*
glnE sense primer	Ga**ggatcc**tgcgcctgtttgaactgacgcagcgcctcaagctgttgctcttcgtc atc<u>aattaaccctcactaaagggcg</u>*
glnE antisense primer	Gt**ggatcc**aggtgttccagctcattcgcggcggacgcgaaccgtcgctgcaat cgcgc<u>taatacgactcactatagggctc</u>*

* The region specific to the relevant gene adjoining a sequence specific to the kit-supplied FRT cassette.

```
  1      ATGAATACCCTTCCAGAACAGTACGCAAACACCGCTCTCCCCACCCTGCC
 51      CGGTCAACCGCAAAATCCATGCGTCTGGCCCCGTGATGAATTAACCGTCG
101      GTGGGATAAAAGCCCATATCGATACTTTCCAGCGTTGGCTGGGTGATGCC
151      TTTGACAATGGGATCTCTGCAGAACAGTTGATTGAGGCGCGCACCGAGTT
201      TATCGACCAGCTCCTGCAACGATTATGGATTGAAGCGGGATTCAGCCAGA
251      TTGCCGACCTGGCATTGGTCGCCGTCGGTGGCTACGGTCGTGGCGAGCTG
301      CATCCACTTTCAGACGTCGATTTACTGATTTTAAGCCGTAAAAAGCTCCC
351      GGACGATCAGGCGCAAAAGTGGGCGAGCTGTTAACGCTGCTCTGGGATG
401      TAAAGCTGGAAGTCGGTCATAGCGTGCGCACGCTTGAAGAGTGCATGCTG
451      GAAGGGTTATCGGATTTAACCGTCGCCACCAATTTAATCGAATCCCGCTT
501      ATTAATTGGCGATGTTGCGCTGTTCCTCGAACTGCAAAAACATATTTTCA
551      GCGAAGGATTCTGGCCTTCCGACAAGTTCTACGCGGCGAAAGTTGAAGAA
```

<u>***glnD* sense primer**</u>
*Bam*HI
5'-ga**<u>ggatcc</u>**cagaaccagcgccatcagcgttaccatggcaccagctacaaccttgaacc**<u>aattaaccctcactaaagggcg</u>**-3'

```
601      CAGAACCAGCGCCATCAGCGTTACCATGGCACCAGCTACAACCTTGAACC
651      AGACATCAAAAGCAGCCCTGGCGGCTTGCGCGATATCCACACTCTGCAAT
701      GGGTGGCCCGCCGTCATTTTGGCGCAACATCGCTGGATGAAATGGTCGGG
751      TTTGGCTTCTTAACCTCAGCGGAGCGGGCGGAATTAAACGAATGTCTGCA
801      TATATTGTGGCGTATTCGCTTTGCCCTGCATCTGGTCGTCAGCCGTTACG
851      ATAATCGCCTGTTATTCGATCGCCAGCTTAGCGTCGCCCAGCGTCTGAAT
901      TACAGTGGTGAAGGTAACGAACCGGTCGAGCGGATGATGAAGGATTACTT
951      CCGCGTTACACGCCGCGTCAGTGAACTCAACCAGATGCTGCTGCAACTGT
1001     TCGATGAAGCCATCCTCGCCCTTCCCGCCGACGAAAAACCACGTCCAGTG
1051     GACGATGAGTTTCAGCTACGCGGTACGCTAATCGACCTGCGTGATGAAAC
1101     ACTATTTATGCGCCAGCCGGAAGCCATCTTGCGTATGTTCTACACCATGG
1151     TGCACAACAGTGCGATCACCGGCATTTACTCCACCACGCTGCGCCAGTTA
1201     CGCCATGCCCGTCGCCATCTGCAACAACCGCTGTGTAATATTCCGGAAGC
1251     ACGAAAACTGTTTTTGAGCATTCTGCGTCACCCCGGAGCGGTGCGGCGCG
1301     GGCTATTGCCAATGCATCGCCATAGCGTGCTCGGCGCGTARATGCCGCAA
1351     TGGTCGCATATCGTCGGGCAGATGCAGTTTGATCTGTTCCACGCCTACAC
1401     GGTGGATGAACATACTATCCGCGTGATGCTGAAACTGGAGAGTTTTGCCA
1451     GTGAAGAAACGCGCCAGCGCCATCCGTTGTGTGTGGACGTCTGGCCGCGC
1501     CTGCCGTCAACTGAGCTGATTTTCATCGCCGCGCTGTTTCACGATATCGC
```

3'-**<u>ctcgggatatcactcagcataat</u>**gacggcagttgactcgactaaaagtagcggcgcgacaaagtgctatagcg**<u>cctagg</u>**tg-5'
*Bam*HI
glnD antisense primer

```
1551     CAAAGGACGCGGCGGCGACCACTCCATTCTCGGTGCTCAGGATGTAGTGC
1601     ATTTTGCCGAACTCCACGGGCTGAACTCACGCGAAACACAGCTGGTCGCC
1651     TGGCTGGTTCGCCAGCACCTGTTGATGTCGGTGACCGCCCAACGCCGCGA
1701     TATTCAGGACCCGGAAGTCATCAAGCAGTTTGCCGAAGAAGTGCAAACGG
1751     AAAATCGTCTGCGCTATCTGGTATGCCTGACTGTGGCTGACATTTGCGCC
1801     ACCAACGAAACGCTGTGGAATAGCTGGAAGCAAAGTCTGTTGCGTGAGCT
1851     CTACTTTGCCACCGAAAAGCAGCTACGACGCGGAATGCAAAACACGCCGG
1901     ATATGCGAACGGGTTCGCCATCACCAACTCCAGGCACTGGCACTACTG
1951     CGCATGGATAACATCGACGAAGAGGCGCTGCACCAAATTTGGTCACGCTG
2001     TCGTGCTAACTATTTTGTCCGCCATAGCCCAAATCAACTGGCCTGGCATG
2051     CCCGCCATTTATTACAGCATGATTTAAGCAAACCGCTGGTATTGCTTAGC
2101     CCGCAGCGTACGCGTGGAGGCACCGAGATTTTTATCTGGTATTGCTTAGC
2151     CCCTTATCTGTTTGCCGCCGTCTGTGCCGAATTAGACCGCCGCAATTTAA
2201     GTGTTCACGACGCACAAATTTTCACCACTCGCGACGGTATGGCGATGGAT
2251     ACCTTTATCGTGCTGGAACCCGATGGCAACCCGCTGTCCGCAGATCGTCA
2301     TGAGGTTATTCGGTTTGGTCTGGAGCAAGTACTGACGCAAAGTAGCTGGC
2351     AGCCACCGCAGCCCCGTCGCCAACCCGCCAAATTACGCCATTTTACTGTT
2401     GAAACCGAAGTAACGTTTTTGCCGACCCATACCGACCGCAAATCGTTCCT
2451     CGAACTGATCGCCCTCGACCAACCTGGACTGCTGGCGCGAGTCGGGAAAA
2501     TTTTTGCCGATCTGGGAATTTCGCTTCATGGTGCCCGAATTACAACCATT
2551     GGCGAGCGAGTAGAAGATTTATTCATAATTGCCACCGCTGACCGGCGTGC
2601     GCTTAATAACGAGTTGCAGCAGGAAGTGCATCAGCGGTTGACAGAGGCCC
2651     TCAATCCAAACGATAAAGGGTGA
```

Figure 2.2: DNA sequence of *E.coli glnD* showing gene orientation and primer positions. The *glnD* sequences were obtained from the Genbank database. The *glnD* sense primer is indicated in red. Th*e BamHI* enzyme restriction site is on the 5' site of the primer and is coloured blue. The primer also contains a region specific to the relevant gene adjoining a sequence specific to the kit-supplied FRT cassette and this region is bold and underlined on the 3' side of the primer. The *glnD* antisense primer is indicated in green. Th*e Bam*HI enzyme restriction site is on the 5' site of the primer and is coloured blue. The primer also contains a region specific to the relevant gene adjoining a sequence specific to the kit-supplied FRT cassette and this region is bold and underlined located on the 3' side.

```
1      TCATTCTTCCACCAGCCACTTCTGCCAGCTTGCCCGCACCAGTTCACGCT
51     CTGCGGTGAAGCAATCCTCCGACACATGGCCCGGCAATTCCTGTAATGCC
101    AGATGATGAAGTTCATCGCGAAGCGTAGTGTAAGCACGGGTCAGCGCCAT
151    CGCTTCCTGCTCTTCCATAATGTCGTTTTGCGCCAGTAGTTCCAGAATAC
201    GCACGTTGTCTGACCAGCGCGTTAACTTCGGTTTTTCATGAGCGTAGCGC
251    AACACCAGATATTGGGTAATAAATTCGATATCGGTAATTCCCCCTTCATC
301    AGCTTTGATATCAAAGCGATCGCGATGTTTATTGCCGAGATGAGCGCGCA
351    TTTTCTCGCGCATTTCCCGCACTTCCGTTTGCAGAGTTTTACCTTCACGC
401    GGCAGCGTCATAATCTCGCGACGCACTGCGTCAAAGTGCGCGGTGAGCTG
451    CGGATCGCCGTACACTACACGCGCACGCACCAGCGCCTGATGTTCCCACG
501    TCCAGGCCTCGTTTTTCTGATAATCGGCAAATGCTTCTGCGGATGTCACC
551    AGCATTCCCGCCGCCCCGGACGGACGCAGTCGAGCATCCACTTCATACAA
601    AATGCCGGAAGAGGTACGCGTACTGAACAGATGCATAATGCGTTGCGCCA
651    GACGCAGATAAAACTGCCGCCCGTCGATTTCCCGCTCACCGTCAGTCATC
701    GCATCCATTGGGCAATCATGGAGGAAGATAAGGTCAAGATCGGAACTGTA
751    GCCTAACTCCCAGCCGCCCAGCTTGCCGTAGCCGACCACCGCAAAACCAC
801    GCCCTTCGCGTTCGTTCAGGTGATTCGGCTTACCGTAGCGGGCAACCATT
851    TGAACCCACGCCTGCTGAACGACGGCATCTATCATGGCTTCCGCCAGCCA
901    GGTTAAGTGATCGCTCACTTCATCACCGGTAGCGTACCGGCGATATCCGC
```

glnE sense primer   *Bam*HI
            5'-ga**ggatcc**tgcgcctgtttgaactgacgcagcgcctcaagctgttgctcttcgtcatc**aattaaccctcactaaagggcg**-3'
```
951    TGCGCCTGTTTGAACTGACGCAGCGCCTCAAGCTGTTGCTCTTCGTCATC
1001   TTCCGGCACGCGCAGCAAATACTGGCGCAACTCATCGCGGTAGGCATCGG
1051   TCGCCGTCGGCTGGTAAAGGGTGTTTGGATCGAGCAATTCATCCAGCAAT
1101   AATGGATAACGCGCCAGCTGGCTGGCAATCATCGGCGACGCGGCACACAG
1151   AGAAATCAAATGTTTAAGCGCCGCGGGGAATTCACTGAGCAATTCTAAAT
1201   AGGTGGTGCGGGTAACAATCCCCACCAGCAAGGCGGTAATGCGCGACAGC
1251   GTAACGGCAGCGTCTTCACGCGCACAGACATCACTTAGCAGATGCGGCAT
1301   CAGATGGTCGAGCACCTGACGTCCTCGCGGCCCGATGGTGCGCTTATCCA
1351   GCTCTTTGCGGAAATCGGCAATCAGCGTTAGCACCTGTTTGCGATCATCC
1401   TCGCTAAGATGCGCCAGCACTGGCGTAGTGTCATCTTCCTGCAACGCATC
1451   CTGCCACAGCTCACGCCACTGTTCCGACAGCGACTCTTCCTGAGTTTCAC
1501   TTTCATCGTCGCCAATCAATTCATTAAACACCCGGCGCACATTGGTCATA
1551   TGTGCGGTCAGCGCCCCGGTCAGTTGCGGCCAGTCAGCAAAGTCCATCGC
1601   CCACGCCAGCCGCGCACGATTAAGCTCATCAGAAGGAAGCGTCTGGGTTT
1651   GTTCGTCGTTAATGCTTTGCAGCAGGTTTTCCAGACGCCGCAGGAACAGA
1701   TACGCCACTCGCAATTGTTCAGCATCGTTTTCAGAAAGCAGATGCAGCTC
1751   GGCAATGGCGCTGAGCGTTGGCAGTAAAGATACCCATGCCTAAGGATCAG
1801   GCGCGATTGCAGCGACGGTTCGCGTCCGCCGCGAATGAGCTGGAACACCT
```
3'-**ctcgggatatcactcagcataat**cgcgctaacgtcgctgccaagcgcaggcggcgcttactcgaccttgtggac**ctagg**tg-5'
                                                                          *Bam*HI
```
1851   GAACGATAAATTCAATTTCGCGAATGCCGCCTGCGCCGAGTTTGATATTG
```
glnE antisense primer
```
1901   CCTTTCATGTTGCGCAGCGACTGAATCACGCTGAAATCGATGTAACGACG
1951   GAAAACAAACGGGCGCAGCATCGCACGCAACTCGTTAGCATAGACGCCTT
2001   CGCTATCGCCCATAATCCGCGCCTTGACCATCGCGTAACGCTCCCAGTCG
2051   CGCCCCTGCTCCTGGTAATAATCTTCCAACGCGGCAAAGCTCAGCACCAG
2101   CGGGCCACTTTCGCCAAACGGACGCAGCCGCATATCCACGCGATAGACGA
2151   AGCCATCCTGCGTTGGTTGATCCAGCACTTTAATCAGCCGCTGCCCCATG
2201   CGGGTAAAAAACTGCGCGTTATCCAGTTCCCGGCGTCCACCCTGCGTACA
2251   ACCATGTTCCGGCCAGGCAAAAATCAGATCGATATCAGAGGAGAAATTCA
2301   GCTCCCCACCGCCCAGCTTACCCATGCCTAAAATCAGCAGCGGTTGCGCT
2351   TCGCCCTGCGCATTGCACGGCGTTCCCCACTCGCGGCAGCAGGCGTCATA
2401   CAGCCAGTCACGCGCCGCAACAATCAGCGTCTCCGCCAGATAGCTGAGCT
2451   GCTGCAATATGCTCTCTTCAGTAACCAGTGCCAGCGTTTGCGCCCAGGCG
2501   ATGCGCACCATAATGCGCCGCCGGAATAGCCGCAGCTCGCGCATTAACCC
2551   GGCTTCGTCACTCACATTACAGAGCGCCTCCTGCAACCATGCCGCGTAAT
2601   GCTGCCATTCGTCGGCCTGCGGCGGTTGGCTTTCCAGTTCCGTCAGCCAC
2651   TCTGGATGCGCAATCACGCTGTCCTGCACAAAATCACTAAAAGTAAGTAC
2701   TGACTTCGCCTGTGCGCTAAGTGATTCCTCGGCTAAAGGCTCTGGCAGCC
2751   GCTCAACAACGGTCTGCCAGTACTGCTGTAACGGTGAAGAGAGCGGCTTC
2801   AT
```

Figure 2.3: DNA sequence of *E.coli glnE* showing gene orientation and primer positions. The *glnE* sense primer is indicated in red. Th*e Bam*HI enzyme restriction site is on the 5' site of the primer and is coloured blue. The primer also contains a region specific to the relevant gene adjoining a sequence specific to the kit-supplied FRT cassette and this region is bold and underlined on the 3' side of the primer. The *glnE* antisense primer is indicated in green. Th*e Bam*HI enzyme restriction site is on the 5' site of the primer and is coloured blue. The primer also contains a region specific to the relevant gene adjoining a sequence specific to the kit-supplied FRT cassette and this region is bold and underlined located on the 3' side.

The knockout strains were produced using these primers as described in the kit protocol. The only deviation from the protocol was the incorporation of *Bam*HI restriction sites at the ends of the primers (shown in bold in Table 2.1). This enabled the PCR products to be cloned into pGEM T-Easy (Promega Corporation), and the cassette was then cut out of the pGEM construct as a *Bam*HI fragment. Further preparation of the knock-out strains was as described in the protocol.

The kanamycin (Kan) resistance marker was subsequently removed using the 706-FLP plasmid carrying the site-specific recombinase, as described in the protocol. Integrations were confirmed by sequencing.

The strain with the *glnD* deletion was designated YMC11D, while the strain with the *glnE* deletion was designated YMC11E.

2.2.2 Cloning

Molecular cloning of target DNA sequences into various vectors was done essentially as described by Sambrook *et al.,* (1989). Target DNA sequences were cloned into vectors by simple T/A cloning or ligated into vectors after restriction enzyme digestion.

2.2.2.1 Ligation and plasmid isolation

All ligations were done with T4 DNA Ligase (Promega, T4 DNA Ligase) as per the manufacturer's instructions. Ligation reactions were prepared by die addition of 1 µl T4 DNA ligase and 1 µl 10 x ligation buffer (Promega, T4 DNA Ligase) to the specific insert to vector ratio (20:1 or 3:1) and made up to a final volume of 10 µl with nuclease free water. The reaction was incubated overnight at 4°C. The ligation was cleaned up by using the following method: the reaction mixture was dried *in vacuo* using a speedy vac (Sarvant, Speed Vac SC110) for 20 min and the pellet was dissolved in 1 ml ice cold (-20°C) 70% ethanol. It was centrifuged at 4°C at 10 000g for 30 min and the pellet dried for 10 min under vacuum. The ligation mixture was resuspended in 2 µl dH$_2$O and then transformed into the appropriate *E.coli* cells see sections 2.2.5 and 2.2.6.

Plasmids were isolated using the E.Z.N.A. ®Plasmid Miniprep Kit I (Peqlab Biotechnology GmbH, Germany). The composition of the E.Z.N.A. ®Plasmid Miniprep Kit I is proprietary and the kit was used as per manufacturer's instructions. The concentration of the plasmid DNA were determined by agarose gel electrophoresis making use of MassRuler™ Express DNA Ladder (Fermentas, Germany).

2.2.3 Screening for positive clones
2.2.3.1 Colony screening PCR

Colony screening PCR was used to identify clones with the correct insert in pBSK or CDFDuet-1 vectors (Section 2.3.1, Figure 2.4). In order to identify positive clones, colonies were randomly picked from fresh transformation plates and resusepended in 10 µl dH$_2$O. As template, 1 µl of this bacterial culture was used. The sense oligonucleotide TB1: 5'-GATGGATCCACCCGATAACCAG-3' and the antisense oligonucleotide TB2: 5'-GATGGATCCTCGAAAAACCTCG-3', with both primers containing *Bam*HI restriction site (sites underlined in primer sequences) were used to identify clones with the correct *M.tb* GS insert in pBSK. The sense and antisense oligonucleotide primer set TBglnE-8: 5'-TAGCATATGGTCGTGACCAAAC-3' (*Nde*I restriction site underlined) and TBglnE-9: 5'-CAGGATCCTTAACTCCCGAACAC-3' (*Bam*HI restriction site underlined) were used to identify clones with the correct TBglnE insert in CDFDuet-1. The cycling conditions were as described in section 2.2.8. The PCR products were analyzed by running on a 0.8% w/v agarose/TAE gel and checked for the correctly sized product as described in section 2.2.4.

2.2.3.2 Restriction enzyme digestion

Plasmid isolation (section 2.2.2) was carried out on the clones that gave the correctly sized band with colony screening PCR, followed by restriction enzyme digestion (Sections 2.3.1.1, 2.3.1.2 and 2.3.1.3). The samples were analysed using a 0.8% w/v agarose/TAE gel to verify possible positive clones.

2.2.4 Agarose gel electrophoresis and purification of PCR products

All PCR reactions and restriction digests were analyzed on 0.8% w/v agarose (Promega, USA)/TAE (0.04 M Tris-acetate, 1 mM EDTA, pH 8.0) gels in TAE (0.04 M Tris-acetate, 1 mM EDTA, pH 8.0) running buffer at 4-10 V/cm. Each sample was loaded in 1x loading dye (0.025% w/v bromophenol blue and 30% v/v glycerol).

GeneRuler™ 1kb DNA ladder (Fermentas, USA) was used as molecular marker. The agarose/TAE gels contained ethidium bromide (EtBr), a DNA base intercalator (1.25 ng/ml), for DNA visualization. The DNA bands were visualized at 312 nm on a Bio-Rad Chemidoc Gel Documentation System (Bio-Rad Laboratories, USA), using the QuantityOne software.   PCR products were purified (for removal of primer dimers, template and non-specific contaminants) using a High Pure PCR Purification Kit (Roche diagnostics, Germany).

2.2.5 Preparation of *E.coli* electrocompetent cells and transformation

Electrocompetent cells were prepared by the following method (Sambrook *et al.*, 1989): a single colony of *E.coli* from the purchased *E.coli* strain (Novagen, Madison, Wisconsin, USA) was inoculated into 5 ml Luria-Bertani (LB) liquid media (1% Tryptone, 0.5% yeast extract, 1% NaCl at pH 7) and grown overnight at 37°C with shaking (220 rpm on an orbital shaker). Fresh LB-Broth (50 ml) was inoculated with 1 ml of the overnight culture and grown at 37°C with shaking (220 rpm on an orbital shaker) until the cells reached early to mid-log phase (OD at 600 nm of 0.3-0.6). To harvest the cells, the culture was transferred to two cold 4°C centrifuge tubes and pelleted at 4,000g in a Sorvall RC-5C Plus (Sorvall, UK) for 10 minutes (min) at 4°C. All the subsequent steps were done at 4°C. After the supernatant was discarded, the cells were washed with 250 ml ice-cold water. The suspension was centrifuged at 4,000g in a Sorvall RC-5C Plus (Sorvall, UK) for 10 min. This washing step was repeated twice. After the final centrifugation step, the supernatant was immediately removed from the loose pellets. The pellets were resuspended in 10 ml of ice-cold 10% glycerol in water and incubated on ice for 30 min. Cells were subsequently pelleted (3,000g for 10 min), the supernatant removed and the pellets resuspended in 800 µl of 10% ice-cold glycerol. This was divided into 100 µl aliquots and frozen at -70°C. The prepared electrocompetent cells were thawed from -70°C on ice when required.   After 10-50 ng plasmid was added to 100 µl cells, the mixture was transferred to a pre-chilled 2 mm electroporation cuvette (Hybaid) and a pulse of 2500 V applied for 5 ms in a Bio-Rad MicroPulser electroporator (Bio-Rad Laboratories, Hercules, California) (Dower *et al.*, 1988). LB liquid media (1 ml) was added directly after electroporation and the cells were incubated for 1 hour at 37°C with shaking (180 rpm on an orbital shaker). The transformation mixture was plated at different volumes (50 µl, 100 µl and 250 µl) on LB agar (1.5% w/v Bacto-agar in

LB medium, autoclaved for 20 min at 121°C) plates containing the appropriate antibiotic for the pTBSK construct ampicillin (final concentration of 0.1 mg/ml) was added and for the pTBglnE construct both ampicillin (final concentration of 0.1 mg/ml) and streptomycin (final concentration of 0.05 mg/ml) were added. The LB agar plates were incubated at 37°C for 16 hours in a Sarvall incubator. Colonies on these plates were subsequently screened using PCR as described in section 2.2.3.1 to identify positives colonies.

2.2.6 Preparation of *E.coli* TSB competent cells and transformation

A single colony of *E.coli* was inoculated into 5 ml Luria-Bertani (LB) liquid media (1% Tryptone, 0.5% yeast extract, 1% NaCl at pH 7) and grown overnight at 37°C with shaking (220 rpm). Fresh LB-Broth (50 ml) was inoculated with 1 ml of the overnight culture and grown at 37°C with shaking (220 rpm) until the cells reached early to mid-log phase (OD at 600 nm of 0.3-0.6). The culture was transferred to a pre-chilled sterile centrifuge tube and centrifuged at $4{,}000g$ for 5 min at 4°C. After the supernatant was discarded, the cells were resuspended in 5 ml ice-cold Transformation and Storage Buffer (TSB, 1% Tryptone, 0.5% yeast extract, 1% NaCl, 2% PEG 4000, 10mM $MgCl_2$ and 10mM $MgSO_4$)) and incubated on ice for approximately 10 min. This step was followed by transformation. The freshly prepared competent cells were used. 100 µl of the cells were mixed with 10-100 ng of DNA (as prepared in section 2.2.2 and 2.2.4) in a chilled Eppendorf tube. The transformation mix was placed on ice for 15 min. After the 15 min incubation, 900 µl of ice-cold TSB was added and incubated at 37°C for 60 min to allow expression of the antibiotic resistance gene present on the plasmid. The transformation mixture was plated on LB agar plates containing the appropriate antibiotic.

2.2.7 Creating YMC11E(DE3) from YMC11E

The Novagen λDE3 Lysogenization Kit was used to create YMC11E(DE3). This kit is designed for the site specific integration of λDE3 prophage into *E.coli* chromosome, such that the lysogenized host can be used to express target genes cloned in the vectors under the control of the T7 promoter. Lysogenization is accomplished in a three-way infection with λDE3, a helper phage (B10) and a selection phage (B482). The kit also contains a tester phage (4107) for verification of λDE3 lysogeny on most host strains, and a positive control lysogen. All phage are provided as clarified

lysates, and the positive control lysogen is provided as a glycerol stock. Lysogenization of YMC11E was done according to the manufactures manual.

2.2.8 Cloning of *M.tb* GS and ATase

The complete coding region of *M.tb* GS *glnA* gene was PCR amplified and cloned into expression vector pBluescript SKII$^+$ (Agilent Technologies, Germany) plasmid map available in Appendix A. In short, genomic DNA from *M.tb* H37Rv (ATCC 25618) from Professor Paul van Helden at the University of Stellenboch was used as template during the amplification reaction using Taq DNA polymerase (Strategene, USA), together with the sense oligonucleotide TB1: 5'-GAT<u>GGATCC</u>ACCCGATAACCAG-3' and the antisense oligonucleotide TB2: 5'-GAT<u>GGATCC</u>TCGAAAAACCTCG-3', with both primers containing *Bam*HI restriction site (sites underlined in primer sequences). Ex-*Taq* DNA polymerase (Bioline) was routinely used for DNA amplification of up to 2000 base pairs (bp). A typical PCR reaction contained 250 nM of each oligonucleotide (forward and reverse primer), 200 µM of each deoxynucleotide triphosphate (dNTP, Bioline), 1 x reaction buffer (supplied), 1 U Ex-*Taq* polymerase, approximately 80-100 ng DNA template and dH$_2$O to a final volume of 25 µl. The following cycling conditions were used for the PCR reaction: 95°C for 5 min which was followed by 30 cycles of 95°C for 1 min, 50°C for 1 min and 72°C for 1 min, followed by 72°C for 5 min. Both the PCR product and vector were digested with the restriction enzyme *Bam*HI since both the oligos were designed with this restriction enzyme site and ligated into pBSK to form the final construct, hereafter referred to as pTBSK with the *glnA* gene under control of the constitutive T3 promotor. The final construct was sent for sequencing at Inqaba biotec for verification.

The complete coding region of *M.tb* adenylyl transferase *glnE* gene was PCR amplified from genomic H37Rv DNA using the sense and antisense oligonucleotide primer set TBglnE-8: 5'-TAG<u>CATATG</u>GTCGTGACCAAAC-3' (*Nde*I restriction site underlined) and TBglnE-9: 5'-CA<u>GGATCC</u>TTAACTCCCGAACAC-3' (*Bam*HI restriction site underlined). The same PCR reaction mix was used as described in section 2.2.8. The following cycling conditions were used for the PCR reaction: 95°C for 5 min which was followed by 30 cycles of 95°C for 1 min, 56°C for 1 min and 72°C for 3 min, followed by 72°C for 5 min. The amplified DNA was then co-digested

with *Nde*I and *Bam*HI and ligated into pGEM-T Easy (Novagen, United Kingdom). A ligation mixture was set up at a picomole insert:vector ratio of 20:1 using T4 DNA Ligase (Promega Corporation, USA) as per the manufacturer's instructions. The TBglnE insert was ligated into pGem T-easy vector. The ligation was cleaned up by using the following method: the reaction mixture was dried *in vacuo* using a speedy vac (Sarvant, Speed Vac SC110) for 20 min and the pellet was dissolved in 1 ml ice cold (-20°C) 70% ethanol. It was centrifuged at 4°C at 10 000*g* for 30 min and the pellet dried for 10 min under vacuum. The ligation mixture was resuspended in 2 µl dH$_2$O and then transformed into electrocompetent XL10 Gold as per section 2.2.5. The transformation mixture was plated on LB agar plates (1.5% w/v Bacto-agar in LB media, autoclaved for 20 min at 121°C) containing 100 µg/mL ampicillin, 80 µg/mL 5-bromo-4-chloro-indolyl-β-D-galactopyranoside (X-Gal) and 0.1 mM isopropyl-β-D-thiogalactopyranoside (IPTG). The plates were incubated at 37°C in a Sarvall incubator for 16 hours. White colonies on these plates were subsequently screened using PCR (section 2.2.3.1) to identify positives containing the TBglnE gene. The plasmid was isolated described in section 2.2.2, digested with *Nde*I and *Bam*HI and the TBglnE fragment purified from agarose gel see section 2.2.4. The purified DNA fragment was ligated (see section 2.2.2) with a *Nde*I and *Bgl*II digested expression vector CDFDuet-1 (Novagen, United Kingdom) to construct pTBglnE the plasmid maps are available in Appendix A, with *glnE* downstream of the IPTG-inducible T7*lac* promoter.

2.2.9 Recombinant protein expression of adenylylated and deadenylylated *M.tb* GS and *E.coli* GS in *E.coli*

For comparison of the production of *M.tb* GS in *E.coli,* adenylylated and deadenylylated *E.coli* GS were heterologously expressed and purified. Recombinant deadenylylated *E.coli* GS was produced in an *E.coli* strain lacking chromosomal *glnA* (GS) and *glnE* (ATase) genes. Adenylylated *E.coli* GS was produced in a strain lacking chromosomal *glnA* (GS) and *glnD* (uridylyl transferase) genes (Kenyon *et al.,* 2011).

2.2.9.1 Production of deadenylylated *E.coli* GS

The *E.coli* YMC11 strain in which the endogenous GS gene is knocked out was used as the basic expression host. To enhance the expression of fully deadenylylated

E.coli GS, the endogenous chromosomal *E.coli glnE* adenylyl transferase gene was deleted using the Quick and Easy *E.coli* Gene Deletion Kit (Gene Bridges, GmbH) to create the strain YMC11E as per section 2.2.1. A pBSK plasmid vector containing the *glnA* gene encoding *E.coli* GS under the transcriptional control of a constitutive T3 promoter was used to transform YMC11E by electroporation as described in section 2.2.5. The resultant recombinant *E.coli* strain was named pBSK-ECgln (YMC11E). This work is published by Kenyon *et al.,* 2011.

pBSK-ECgln (YMC11E) was inoculated into 50 ml LM medium (1% tryptone, 0.5% yeast extract, 1% NaCl) supplemented with 50 µl Ampicillin (100 µg/ml). The inoculum was grown at 37ºC for 16 hours with shaking at 220 rpm. Subsequently, 1ml of the culture was transferred to 50 ml LM medium supplemented with 50 µl Amp_{100}. This second inoculum was again grown at 37ºC for 6 hours with shaking at 220 rpm. Subsequently, 8 ml of the culture was transferred to a modified M9 medium (6 g/l Na_2HPO_4, 3 g/l KH_2PO_4, 0.5 g/l NaCl pH 6.3) supplemented with 70 mM L-glutamate, trace salts (1,000x stock: 4.5 mM $CaCl_2.2H_2O$, 6.2 mM $FeCl_3.6H_2O$, 0.63 mM $ZnCl_2$, 0.64 mM $CuSO_4.5H_2O$, 0.76 mM $CoCl_2.6H_2O$, 2.4 mM $MnCl_2.4H_2O$), 4% glucose, 1 mM $MgSO_4$, 0.1 mM $CaCl_2$ and 1 mM thiamine. The culture was grown at 37ºC for 16 hours with shaking at 220 rpm. The cells were harvested by centrifugation for 10 min at 16,300*g* and the bacterial pellet used for deadenylylated *E.coli* GS purification.

2.2.9.2 Production of adenylylated *E.coli* GS

The *E.coli* YMC11 strain, lacking the endogenous *glnA* gene was used. However, to enhance the expression of fully adenylated *E.coli* GS, the endogenous *E.coli* uridylyl transferase gene (*glnD*) was deleted using the Quick and Easy *E.coli* Gene Deletion Kit (Gene Bridges, GmbH) to create the strain YMC11D as per section 2.2.1. The same vector as in 2.2.9.1 was introduced into YMC11D by electroporation. The resultant *E.coli* strain was named pBSK-ECgln (YMC11D).

pBSK-ECgln (YMC11D) was used for the expression of adenylylated GS using a similar method to that described above for deadenylylated GS. The only difference is the addition of 5 mM L-glutamine to the M9 medium. The cells were harvested by

centrifugation for 10 min at 16,300*g* and the bacterial pellet used for adenylylated *E.coli* GS purification.

2.2.9.3 Production of deadenylylated *M.tb* GS

The *E.coli* YMC11 strain in which the endogenous GS gene is knocked out was used as the basic expression host see section 2.2.9.2. To enhance the expression of fully deadenylylated *M.tb* GS, the endogenous *E.coli* adenylyl transferase *glnE* gene was also knocked out by homologous recombination to produce the YMC11E strain as per section 2.2.1. The pTBSK plasmid vector containing the *glnA* gene encoding *M.tb* GS under the transcriptional control of a constitutive T3 promoter was used to transform YMC11E by electroporation. The resultant recombinant *E.coli* was named pTBSK (YMC11E).

pTBSK (YMC11E) was inoculated in 50 ml M9ZB medium (1% w/v N-Z-Amine A; 85 mM NaCl) containing M9 Salts (22 mM Na_2HPO_4; 22 mM KH_2PO_4; 18 mM NH_4Cl; 8.5 mM NaCl) and supplemented with 100 µg/ml ampicillin, 1mM $MgSO_4$ and 4% (w/v) glucose. The inoculum was grown at 28ºC (after temperature studies the optimal incubation temperature of 28˚C was selected) for 16 hours with shaking at 220 rpm on an orbital shaker. Subsequently, 5 ml of the culture was transferred to 250 ml of the same medium and the culture grown at 28ºC for 16 hours. The cultures were harvested by centrifugation for 10 min at 16,300*g* (4ºC) and the bacterial pellet used for deadenylylated *M.tb* GS purification.

2.2.9.4 Production of adenylylated *M.tb* GS

Adenylylated *M.tb* GS was produced using YMC11E(DE3) containing both pTBSK and pTBglnE see section 2.2.8. This strain was inoculated into 50 ml of the same medium as in section 2.2.9.3, including 50 µg/ml streptomycin. The cultures were incubated at 33ºC (after temperature studies the optimal incubation temperature of 33˚C was selected) for 16 hours with shaking at 220 rpm. Thereafter, 5 ml was transferred to 250 ml of the same medium and grown at 33ºC for a further 8 hours. *M.tb* adenylyl transferase expression was then induced by the addition 1 mM IPTG. After a further incubation at 33ºC for 16 hours with shaking at 220 rpm on an orbital shaker, the cultures were harvested by centrifugation for 10 min at 16,300*g* (4ºC) and the bacterial pellet used for adenylylated *M.tb* GS purification.

2.2.10 Quality control of isolated *M.tb* GS and *E.coli* GS

2.2.10.1 Protein concentration

Protein concentrations were determined by using the Quant-IT™ Protein Assay Kit (Invitrogen, USA) that is used in conjunction with the QUBIT™ fluorometer. The protein-containing sample is made up to 10 µl, to which 190 µl of the Quant-IT™ working solution (1 µl Quant-IT™ reagent and 199 µl Quant-IT™ buffer) is added. After 15 minutes incubation at room temperature, the fluorescence is quantified by using the QUBIT™ fluorometer. The following protein standards 0 ng/µl, 200 ng/µl and 400 ng/µl were included in the Quant-IT™ Protein Assay Kit and used in conjunction with the QUBIT™ fluorometer as per supplier's manual.

2.2.10.2 SDS-PAGE analysis

Sodium dodecyl-sulphate polyacrylamide gel electrophoresis (SDS-PAGE) was used to analyse the molecular mass and purity of the isolated enzymes. Gels consisted of a 4% stacking gel (4% Bio-Rad Acrylamide-Bisacrylamide mix, 0.1% SDS, 0.05% ammonium persulphate, 0.1% TEMED, 0.05 M Tris- HCl, pH 6.8) and a 12% separating gel (12% Bio-Rad Acrylamide-Bisacrylamide mix, 0.1% SDS, 0.05% ammonium persulphate, 0.1% TEMED, 0.375 M Tris-HCl, pH 8.8). An aliquot of protein sample (±60 µg) was transferred to a clean microcentrifuge tube. Subsequently, an equal volume of denaturing buffer (1.2% SDS, 30% glycerol, 15% ß-mercaptoethanol, 0.18 mg/ml bromophenol blue, 0.15 M Tris, pH 6.8) was added. The protein samples were denatured at 90°C for 5 minutes. Ten µl of each sample was loaded onto the gel. Electrophoresis was performed in a 0.025 M Tris, 0.2 M Glycine, 0.1% SDS buffer (pH 8.3) at 200 V in a Bio-Rad Mini Protean 3 Electrophoresis system. Protein bands were visualized with Coomassie Blue G250 staining solution (0.1 g Coomassie Blue G250 in 40% methanol, 10% acetic acid), followed by destaining (40% methanol, 10% acetic acid).

2.2.10.3 γ-glutamyl transferase assay for enzyme activity

This functional assay was carried out to: i) confirm the functionality of the purified GS enzyme; and ii) assess the degree of adenylylation of the purified enzymes. Both the adenylylated and deadenylylated forms of the enzymes were found to be active in this assay in the presence of Mn^{2+}. When the same assay is further supplemented

with Mg^{2+}, only the deadenylylated enzyme is active. The activities of the two forms of the enzyme are therefore differentiated on the basis of the difference in activity in the presence of Mn^{2+} or Mg^{2+}. The assay protocol was adapted from Shapiro and Stadtman (1970). The composition of the Mn^{2+} reaction mix was 15 mM L-glutamine, 0.4 mM Na.ADP, 30 mM sodium arsenate, 0.3 mM $MnCl_2$, 60 mM hydroxylamine in 50 mM imidazole buffer (pH 7.0). The composition of the Mn^{2+} + Mg^{2+} reaction mix was the same, except that an additional 60 mM $MgCl_2$ was added. A blank reaction mix was prepared in the same manner as the Mn^{2+} reaction, but the ADP and arsenate components were absent. Both assays were carried out in a total volume of 600 µl. The assay mix was equilibrated for 5 min at 37°C, and then initiated by the addition of 50 µl of purified enzyme preparation. The reaction was allowed to proceed for 30 min and then terminated by the addition of 900 µl Stop Mix (1 M $FeCl_3$, 0.2 M trichloroacetic acid, 7.1% v/v HCl). The samples were centrifuged at 10,361g for 2 min to remove any precipitate, and the absorbance measured at 540 nm in a Perkin Elmer precisely lambda 35 UV/VIS spectrometer. The degree of adenylylation was calculated from the ratio of the deadenylylated γ-glutamyl transferase activity (Mn^{2+} + Mg^{2+} reaction) to the total γ-glutamyl transferase activity (Mn^{2+} reaction), taking the number of subunits into account (Shapiro and Stadtman, 1970).

2.2.11 Purification of adenylylated and deadenylylated *M.tb* GS and *E.coli* GS
2.2.11.1 Purification of adenylylated and deadenylylated *M.tb* GS

Step 1 (streptomycin sulphate precipitation): The bacterial pellet (prepared in section 2.2.9.3 and 2.2.9.4) was resuspended in 10 ml of RBA (10 mM imidazole pH 7, 10 mM $MnCl_2$) buffer and sonicated for 20 min on a 50% on/off cycle with a Vibracell sonicator (Sonics and materials Inc, USA) with a 40% dutycycle and a 5 output controle, followed by centrifugation for 10 min at 12,100g (4ºC) to collect the soluble *E.coli* lysate. A precipitation step was carried out to eliminate nucleic acids by adding streptomycin sulphate to a final concentration of 1% w/v and stirring at 4ºC for 10 min. After centrifugation for 10 min at 12,100g (4ºC), the supernatant was retained and the pH was adjusted to pH 4.4 with 8% HCl. The supernatant was slowly stirred at 4ºC overnight, followed by centrifugation at 12,100g (4ºC) for 10 min and aspiration of the supernatant.

Step 2 (anion-exchange chromatography): A column containing 5 ml bed volume DEAE Sepharose CL-6B (Pharmacia Biotech) was prepared and equilibrated with 5 column volumes of Buffer H (50 mM HEPES pH 7.6, 10 mM $MnCl_2$) containing 100 mM NaCl. The final supernatant from Step 1 was applied and the column washed with 10 column volumes of Buffer H containing 100 mM NaCl. Bound *M.tb* GS was eluted by applying a step gradient of Buffer H containing 0.4 M, 0.5 M, 0.6 M and 0.7 M NaCl. Fractions were collected and assayed for the presence of *M.tb* GS using the γ-glutamyl transferase assay see section 2.2.10.3. The fractions with GS activity were pooled and dialysed in SnakeSkin^{TM} dialysis tubing (Thermo Scientific, USA) with a 10,000 molecular weight cut off overnight against Buffer H containing 100 mM NaCl as per supplier's manual.

Step 3 (AMP affinity chromatography): A column containing 5 ml bed volume AMP Sepharose (Sigma A1271 adenosine-5'-monophosphate-agarose, cross-linked 4% beaded agarose) was prepared and equilibrated with 5 column volumes of Buffer A (10 mM imidazole pH 7.0, 10 mM $MnCl_2$, 150 mM NaCl). The pooled *M.tb* GS fractions from Step 2 were applied and allowed to bind for 1 ½ hours with gentle shaking at 4ºC. The column was washed with 10 column volumes Buffer A. *M.tb* GS was eluted with 10 ml of Buffer B (10 mM imidazole pH 7.0, 10 mM $MnCl_2$, 450 mM NaCl, and 2.5 mM ADP). Fractions were collected and the fractions with γ-glutamyl transferase (see section 2.2.10.3) activity were pooled and dialysed in SnakeSkin^{TM} dialysis tubing (Thermo Scientific, USA) with a 10,000 molecular weight cut off overnight against Buffer H containing 100 mM NaCl as per supplier's manual.

Sodium dodecyl-sulphate polyacrylamide gel electrophoresis (SDS-PAGE) described in section 2.2.10.1 was used to analyse the molecular mass and purity of the isolated enzymes. Protein concentrations were determined by using the Quant-IT^{TM} Protein Assay Kit (Invitrogen, USA) which includes the following protein standards 0 ng/µl, 200 ng/µl and 400 ng/µl in conjunction with the QUBIT^{TM} fluorometer as per supplier's manual.

2.2.11.2 Purification of adenylylated and deadenylylated *E.coli* GS

Step 1 (streptomycin sulphate precipitation): The bacterial pellet (prepared in section 2.2.9.1 and 2.2.9.2) was resuspended in 10 ml of RBA (10 mM imidazole pH 7, 10 mM $MnCl_2$) and sonicated for 20 min on a 50% on/off cycle (as described in section 2.2.11.1), followed by centrifugation for 10 min at 12,100g (4°C) to collect the soluble *E.coli* lysate.   A precipitation step to eliminate nucleic acids was carried out by adding streptomycin sulphate to a final concentration of 1% and stirring at 4°C for 10 min.   After centrifugation for 10 min at 12,100g (4°C) the supernatant was retained and the pH was adjusted to pH 5.15 with dilute HCl (8%).   The supernatant was stirred at 4°C for 15 min, followed by centrifugation at 12,100g for 10min (4°C).   The supernatant was retained, and 30% by volume of ice cold (4°C) saturated $(NH_4)_2SO_4$ solution was added.   The pH was adjusted to pH 4.6, and the solution stirred at 4°C for 15 min, followed by centrifugation at 12,100g for 10 min (4°C).   The precipitate was resuspended in 5 ml RBA and stirred at 4°C for 3 hours, before the pH was adjusted to pH 5.7.   Stirring continued at 4°C overnight, followed by centrifugation at 12,100g for 10 min (4°C).

Step 2 (AMP affinity chromatography): A 5 ml Bed volume AMP Sepharose column (Sigma A1271 adenosine-5'-monophosphate-agarose, cross-linked 4% beaded agarose) was prepared and equilibrated with 5 column volumes of Buffer A (10 mM imidazole pH7, 10 mM $MnCl_2$, 150 mM NaCl).   The *E.coli* GS supernatant from Step 1 was applied and allowed to bind for 1 hour with gentle shaking at 4°C.   The column was washed with 10 column volumes of Buffer A.   The *E.coli* GS was eluted with 12 ml of Buffer B (10 mM imidazole pH7, 10 mM $MnCl_2$, 450 mM NaCl, 2.5 mM ADP).   Fractions were collected and assayed using the γ-glutamyl transferase assay (see section2.2.10.3).   The fractions with *E.coli* GS activity were pooled and dialysed in SnakeSkin^{TM} dialysis tubing (Thermo Scientific, USA) with a 10,000 molecular weight cut off overnight against RBA as per supplier's manual.

2.2.12 Mass Spectrometry

An ABI QSTRA-ELITE (QTOF) Mass Spectrometer was used. A 40 µl aliquot of purified GS in 10 mM imidazole pH 7.0 was loaded on an OPTI-LYNX C4 trap cartridge at 100 µl/min using 2% acetonitrile and 0.1% formic acid.   Samples were

eluted using linear acetonitrile gradient (2-90% acetonitrile and 5% formic acid) in 5min and TOF-MS spectra, in the range 700-1700 mz, collected using an ABI QSTRA-Elite mass spectrometer with TurboIon source installed. The multiply charged series of TBGS was deconvoluted by the Bayesina Protein Recostruct tool of Bioanalyst QS 2.0 using a mass range of 40-70 kD and signal to noise threshold of three.

2.2.13 Hydrolysis of GS for determination of phosphate content

The relative phosphate content of the purified GS proteins was determined by hydrolysis to release the phosphate (Ludden and Burris, 1978). Purified GS (4 to 8 nmol in 1 ml) was digested by the addition of 4 M HCl (1 ml), the mixture was mixed carefully by inverting the tubes and then evaporated to dryness in air. The residue was resuspended in 2 M HCl (1 ml) plus 20 µl of H_2O_2 (30% v/v), and the mixture was again evaporated to dryness. Five sequential additions of H_2O_2 (200 µl) with evaporation to dryness were used to complete the hydrolysis. The residue was resuspended in Milli-Q water (1 ml), and phosphate content was determined by using the *BioVision* Phosphate colorimetric assay kit as per supplier's manual.

2.2.14 HPLC analysis

Samples were analysed on a Agilent series 1100 HPLC fitted with a Phenomenex 5µ LUNA C_{18} column. Each sample was automatically injected (2 µl) and separated with a mobile phase containing 51 mM KH_2PO_4, PIC A Low UV Reagent (Waters Coorperation), 25% (v/v) acetonitrile. The flow rate of the mobile phase was 1 ml/min with UV detection. An AMP, ADP and ATP standard was used to calibrate the HPLC and the concentration of ADP in each sample was determined by the area under the curve, using Agilent ChemStation (Revision B.02.01) software. The ADP values in the blank wells were subtracted from enzyme-containing wells, and percentage enzyme activity in each well calculated relative to the average net ADP values of the control wells.

2.3 Results

2.3.1 Construction of pTBSK and *M.tb* glnE-CDFDuet for the expression of adenylylated and deadenylylated *M.tb* GS

The *M.tb glnE* gene, encoding adenylyl transferase (ATase), was inserted into the second multiple cloning site (MCS) of the Novegen vector CDFDuet-1. The MCS is preceded by a T7*lac* promoter and ribosome binding site. The vector carries the CloDF13-derived CDF replicon, the *lac*I gene and the streptomycin resistance gene, and was designated pTBglnE. This CloDF13 replicon is compatible with a number of replicons, including the ColE1 replicon found in pBluescript vectors. pBluescript vectors carry the ampicillin resistance gene*.* The *M.tb* glutamine synthetase *glnA* gene is contained in pBluescript SKII⁺, in a construct named pTBSK. The compatible replicons and different antibiotic resistance markers enable the plasmids to be used in combination for co-expression in a single host strain. The expression of *glnA* is constitutive, under control of the T3 promoter, while the expression of *glnE* is under the regulation of the T7*lac* promoter and is induced by the addition of IPTG. Both plasmids are indicated in Figure 2.4.

These two vectors were introduced into the *E.coli* GS auxotrophic strain containing a deletion in the *E.coli glnE* gene (YMC11E). To allow IPTG-inducible expression of the *M.tb* adenylyl transferase from the T7*lac* promoter in pTBglnE, the strain was a lysogen of bacteriophage DE3.
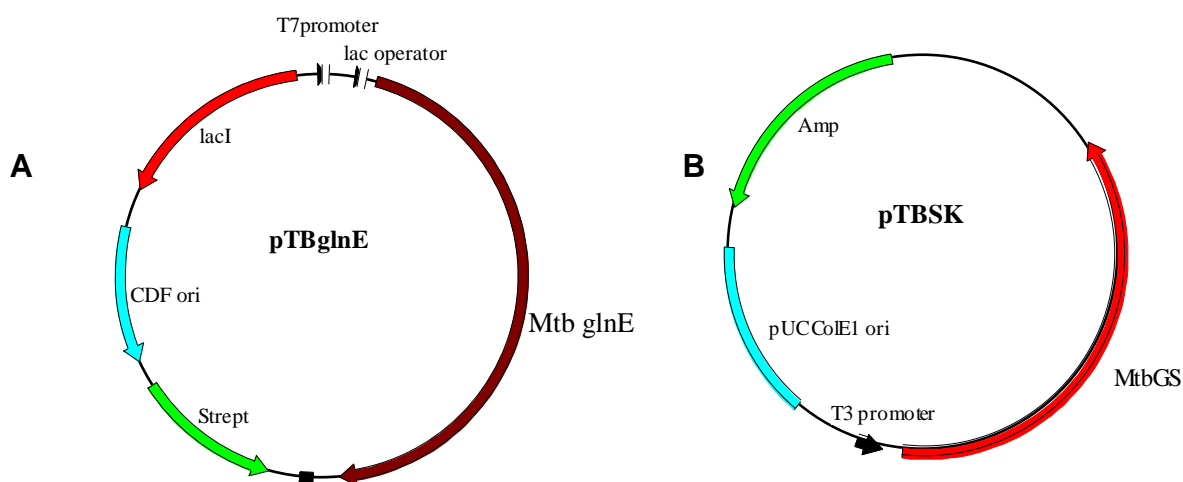

Figure 2.4: (A) Vector map of pTBglnE for IPTG-inducible expression of *M.tb glnE*. (B) Vector map of pTBSK for constitutive expression of *M.tb glnA*.

2.3.1.1 Construction of pTBSK expression vector

Both the PCR product and expression vector were digested with the restriction enzyme *Bam*HI and ligated to form the final construct, hereafter referred to as pTBSK, with the *glnA* gene under control of the constitutive T3 promotor. After plasmid isolation pTBSK was digested with *Bam*HI and the resulting fragments at 2,961 bp (vector backbone) and 1,703 bp (*glnA* insert) are indicated in Figure 2.5 lane 2.
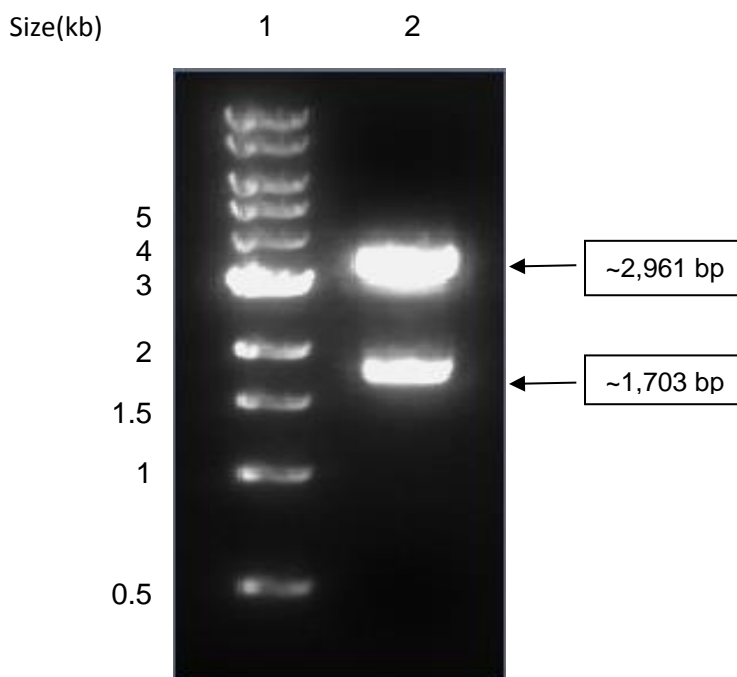

Figure 2.5: Restriction enzyme digest of pTBSK to verify the correct insert and vector size. Lane 1: NEB 1kb marker, with the sizes indicated in kb on the left. Lane 2: *Bam*HI digest of pTBSK with the vector at 2,961 bp and the *glnA* insert at 1,703 bp.

2.3.1.2 Construction of *M.tb* glnE-CDFDuet expression vector

The complete coding region of *M.tb glnE* was amplified and cloned into the pGEM-T Easy vector (Novagen). Genomic DNA from *M.tb* H37Rv cultures was used as template during the amplification reaction and the fragments cloned as described in section 2.2.8. The plasmid was isolated and a digest was set up with *Nde*I, *Bam*HI and *Xmn*I. As can seen from Figure 2.6, *Nde*I/*Bam*HI/*Xmn*I digestion of *M.tb* glnE:pGEM-T should give fragments of ~3 kb, ~2 kb and ~1 kb. *Xmn*I was included to fragment the ~ 3 kb backbone into ~2 kb and ~1 kb, in order to separate it from the ~3 kb desired   *M.tb glnE* fragment. The digest was analyzed on a 0.8% agarose/TAE gel and the *Nde*I/*Bam*HI fragment was cut out and purified.
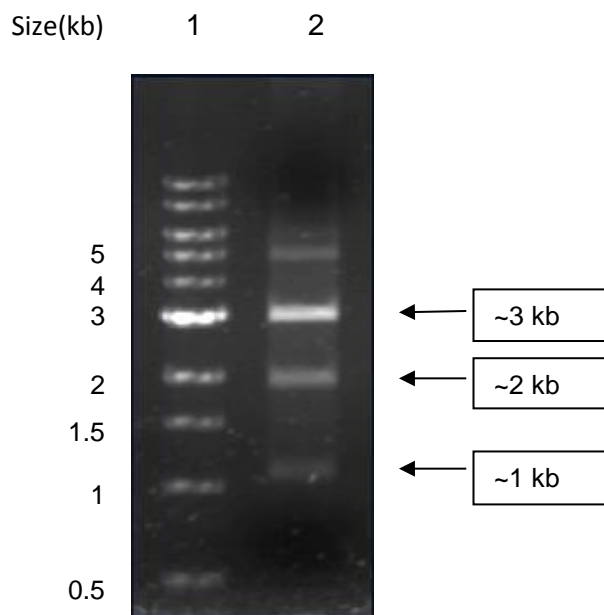
Figure 2.6: Restriction enzyme digest of *M.tb* glnE:pGEM-T to verify the correct insert and vector size. Lane 1: NEB 1kb marker, with the sizes indicated in kb on the left. Lane 2: *Nde*I, *Bam*HI and *Xmn*I enzyme digest of *M.tb* glnE:pGEM-T with the vector at ~1 kb and ~2 kb and the *M.tb glnE* insert at ~3 kb.

Agarose gel elecrophoresis of the purified *M.tb glnE* fragment determined the concentration at ~17 ng by the Mass ruler as indicated in Figure 2.7 A. The purified *M.tb glnE* fragment was used as insert and ligated into the *Nde*I/*Bgl*II enzyme sites of the CDF-Duet-1 vector. From a positive colony the pTBglnE plasmid was isolated and restriction enzyme digested to confirm the fragments as indicated in Figure 2.7 B. Restriction enzyme digests of pTBglnE with *Kpn*I will give the following fragment sizes: 59 bp, 1,243 bp and 5,459 bp in size. When the expected fragment sizes were compared with the fragment sizes in Figure 2.7 B lane 3 it was concluded that the insert was ligated correctly into the vector. Just to verify the following digest was also set up: Lane 4: *Nco*I digest, with fragments of 2,640 bp and 4,121 bp in size. Lane 5: *Pst*I digest, with fragment of 153 bp, 547 bp, 591 bp, 735 bp, 801 bp and 3,934 bp in size. Lane 6: *Pvu*I digest, did not cut. Lane 7: *Sal*I digest, with fragments of 26 bp, 235 bp, 292 bp, 2,097 bp and 4,111 bp in size. Lane 8: *Xho*I digest, with fragments of 144 bp, 420 bp, 618 bp, 1,018 bp and 4,561 bp in size. All of these correspond with the expected fragments sizes as indicated in Figure 2.7 B.
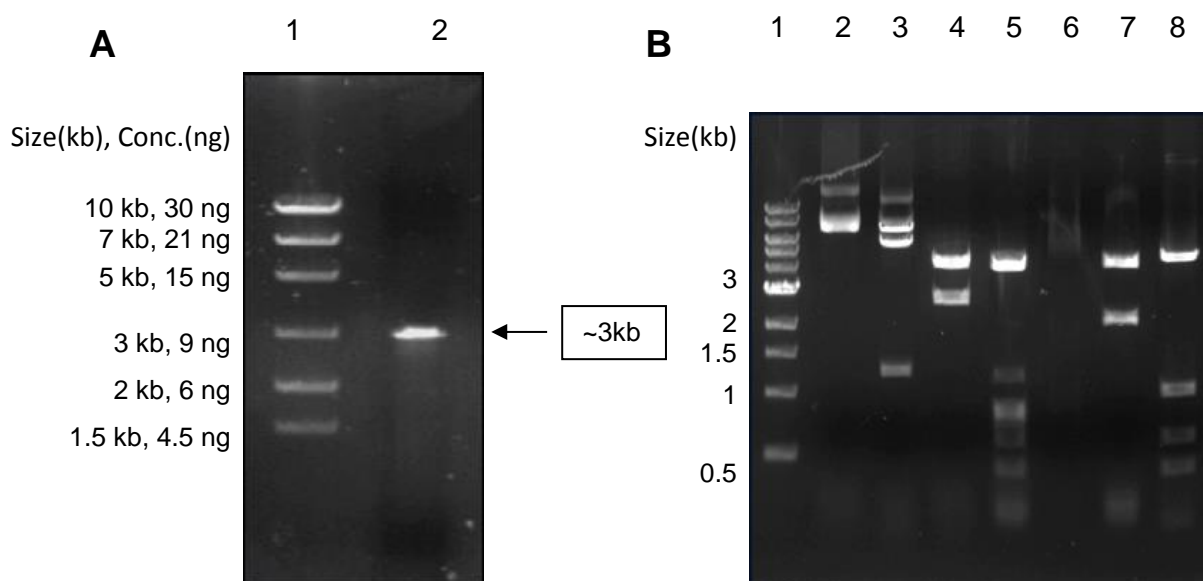
Figure 2.7: (A) Concentration determination of *M.tb*glnE: Lane 1: Mass Ruler Express High range (Fermentas). Lane 2: *M.tb glnE* with an estimate concentration of ~17 ng. **(B)** Restriction enzyme digests of pTBglnE: Lane 1: NEB 1kb marker. Lane 2: *Cla*I digest, did not cut. Lane 3: *Kpn*I digest, with fragments of 59 bp, 1,243 bp and 5,459 bp in size. Lane 4: *Nco*I digest, with fragments of 2,640 bp and 4,121 bp in size. Lane 5: *Pst*I digest, with fragment of 153 bp, 547 bp, 591 bp, 735 bp, 801 bp and 3,934 bp in size. Lane 6: *Pvu*I digest, did not cut. Lane 7: *Sal*I digest, with fragments of 26 bp, 235 bp, 292 bp, 2,097 bp and 4,111 bp in size. Lane 8: *Xho*I digest, with fragments of 144 bp, 420 bp, 618 bp, 1,018 bp and 4,561 bp in size.

2.3.1.3 Co-transformation of pTBSK and TBglnE:CDFDuet-1

Plasmids pTBSK and pTBglnE were transformed into TSB competent YMC11E(DE3), with selection requiring both ampicillin and streptomycin due to the antibiotic resistance gene on pTBSK and pTBSglnE plasmids respectively. Plasmid purification and restriction enzyme digests were done to verify the presence of both plasmids, with the correct fragments indicated in Figure 2.8. On the left hand side of Figure 2.8 the numbers represents the fragment sizes of the 1kb marker. When pTBSK and pTBglnE plasmids were digested with *Sal*I the following fragment sizes were expected 2,097 bp, 3,173 bp and 4,111 bp. This was confirmed with the fragment sizes obtained in Lane 2 of Figure 2.8 for pTBSK and pTBglnE enzyme digest of the plasmids, therefore both the plasmids and the fragment were present and correct. The *Sal*I enzyme digest of pTBglnE should provide two fragments

(2,097 bp and 4,111 bp in size). These sizes were obtained and are indicated in Lane 4 of Figure 2.8.
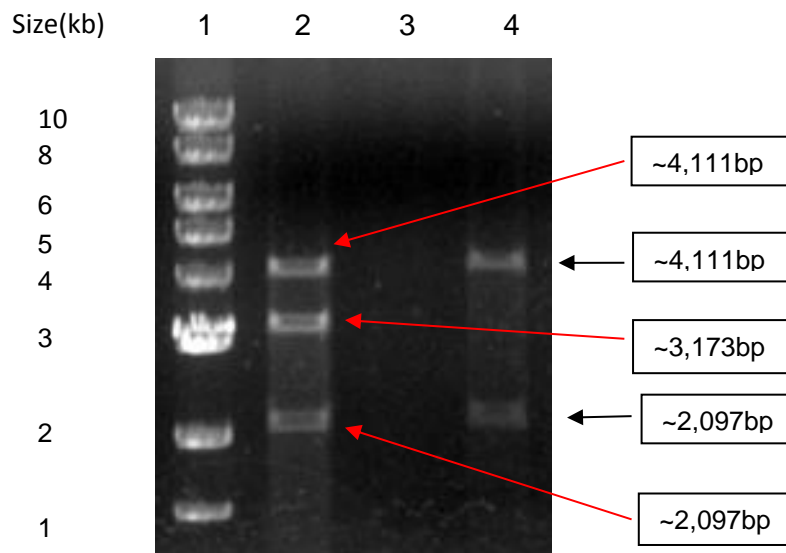

Figure 2.8: Enzyme digests of pTBSK + pTBglnE and pTBglnE alone. Lane 1: NEB 1kb marker. Lane 2: *Sal*I digest of pTBSK + pTBglnE with fragment sizes of 2,097 bp, 3,173 bp and 4,111 bp. Lane 3: Empty lane. Lane 4: *Sal*I digest of pTBglnE with fragment sizes of 2,097 bp and 4,111bp.

2.3.2 Production and purification of adenylylated and deadenylylated *M.tb* GS and *E.coli* GS

Deadenylylated *M.tb* GS was expressed from pTBSK in *E.coli* YMC11E. Adenylylated *M.tb* GS was produced in YMC11E(DE3) via co-expression of *M.tb* GS in pTBSK and *M.tb* ATase in pTBglnE. *M.tb* GS was expressed constitutively, while ATase production was induced by the addition of IPTG. The two plasmids used contain compatible origins of replication and can thus be maintained stably in the same strain. Figure 2.9 illustrates a SDS-PAGE of the cell-free *E.coli* soluble extracts, as well as the purified adenylylated and deadenylylated forms of *M.tb* GS. The average protein concentrations from three purifications of adenylylated and deadenylylated *M.tb* GS are 120 ± 28 and 145 ± 49 µg/ml, respectively. The estimated size is in agreement with the theoretical ~53.4 kDa per subunit of the *M.tb* GS dodecamer.
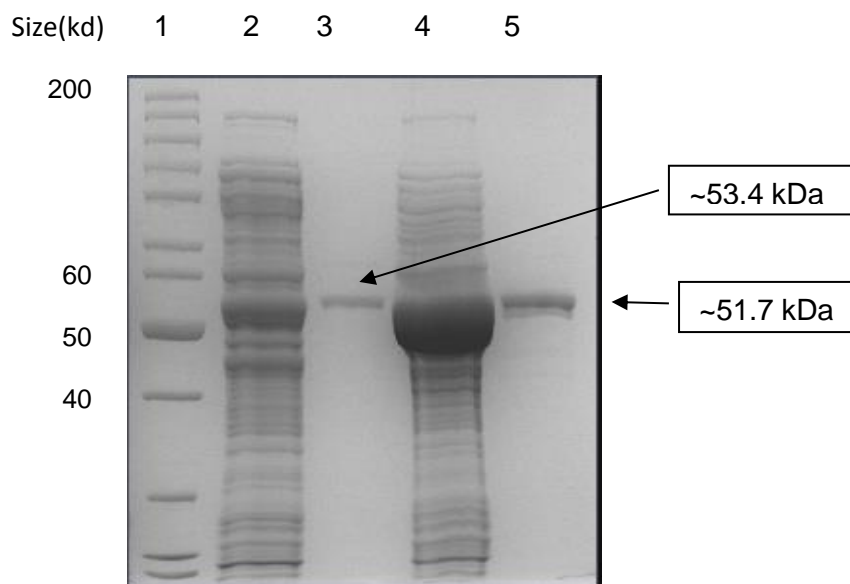
Figure 2.9: 12% SDS-PAGE gel of cell-free *E.coli* extracts, as well as purified adenylylated and deadenylylated *M.tb* GS. Lane 1: molecular weight marker with size in kDa indicated on left (PageRuler Protein ladder, Fermentas). Lane 2: Adenylylated *M.tb* GS cell-free extract. Lane 3: Adenylylated *M.tb* GS purified protein. Lane 4: Deadenylylated *M.tb* GS cell-free extract. Lane 5: Deadenylylated *M.tb* GS purified protein.

Deadenylylated *E.coli* GS was expressed from pBSK in *E.coli* YMC11E. Adenylylated *E.coli* GS was produced in YMC11D. Adenylylated and deadenylylated *E.coli* GS was expressed constitutively. After expression and purification, the purified adenylylated and deadenylylated *E.coli* GS were analysed on 8.5% SDS-PAGE. Figure 2.10 illustrates a SDS-PAGE of the purified adenylylated and deadenylylated forms of *E.coli* GS. The average protein concentrations from three purifications of adenylylated and deadenylylated *E.coli* GS are 118 $\pm$ 28 and 120 $\pm$ 15 µg/ml, respectively. The estimated size is in agreement with the theoretical ~51.7 kDa per subunit of the *E.coli* GS dodecamer.
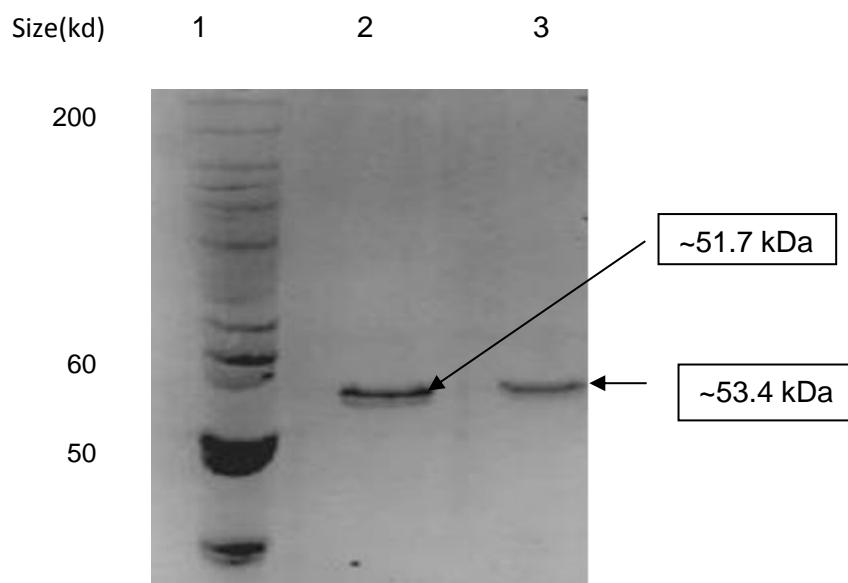
Figure 2.10: 12% SDS-PAGE gel of purified adenylylated and deadenylylated *E.coli* GS. Lane 1: molecular weight marker with size in kDa indicated on left (PageRuler Protein ladder, Fermentas). Lane 2: Purified deadenylylated *E.coli* GS protein. Lane 3: Purified adenylylated *E.coli* GS protein.

2.3.3 Determination of the adenylylation state of *M.tb* GS and *E.coli* GS

2.3.3.1 γ-glutamyl transferase enzyme assay

The γ-glutamyl transferase enzyme assay was carried out with purified GS to: i) confirm the functionality of the purified enzymes, and ii) assess the degree of adenylylation of the purified enzyme. At a specific pH, the total enzyme activity of GS (both adenylylated and deadenylylated) occurs in the presence of Mn^{2+}. At the same pH in the presence of Mn^{2+} and an excess Mg^{2+}, only the deadenylylated component of the enzyme activity is measured. The resultant ratio is then used to calculate the degree of adenylylation of the enzyme. After three purifications, the typical degree of adenylylation for deadenylylated *M.tb* GS is 3% $\pm$ 2%, while the adenylylated form is 70% $\pm$ 4% adenylylated indicated in Table 2.2. For comparison purposes, adenylylated and deadenylylated *E.coli* GS yielded results of 0% and 95% $\pm$ 3% adenylylation respectively, indicated in Table 2.2.

Table 2.2: Average protein concentrations and % adenylylation as determined by γ-glutamyl transferase assays of *M.tb* GS and *E.coli* GS

Enzyme	Protein concentration	% Adenylylation
Adenylylated *M.tb* GS	96.4µg/ml	70% ± 4%
Deadenylylated *M.tb* GS	91.8µg/ml	3% ± 2%
Adenylylated *E.coli* GS	90.5µg/ml	95% ± 3%
Deadenylylated *E.coli* GS	131µg/ml	0%

2.3.3.2 Mass Spectrometry

MS analysis of deadenylylated *M.tb* GS yielded a single peak with a calculated mass of 53,438.00 Da (Figure 2.13), in agreement with the theoretical mass of 53.4 kDa. Deadenylylated *E.coli* GS (Figure 2.11) had a calculated mass of 51,774.00 Da (theoretical mass = 51.7 kDa). Adenylylated *E.coli* GS (Figure 2.12) was calculated to be 52,100.00 Da (theoretical mass = 52.1 kDa), with a single peak indicating 100% adenylylation. The 330 Da adenyl moiety accounts for the mass difference between the adenylylated and deadenylylated forms of each enzyme. Adenylylated *M.tb* GS would not ionise properly, therefore the spectra obtained (Figure 2.14) that shows 85% adenylylation, could therefore be potentially higher than 85%.

Figure 2.11: MS analysis of deadenylylated *E.coli* GS had a calculated mass of 51,774.00 Da (theoretical mass = 51.7 kDa)
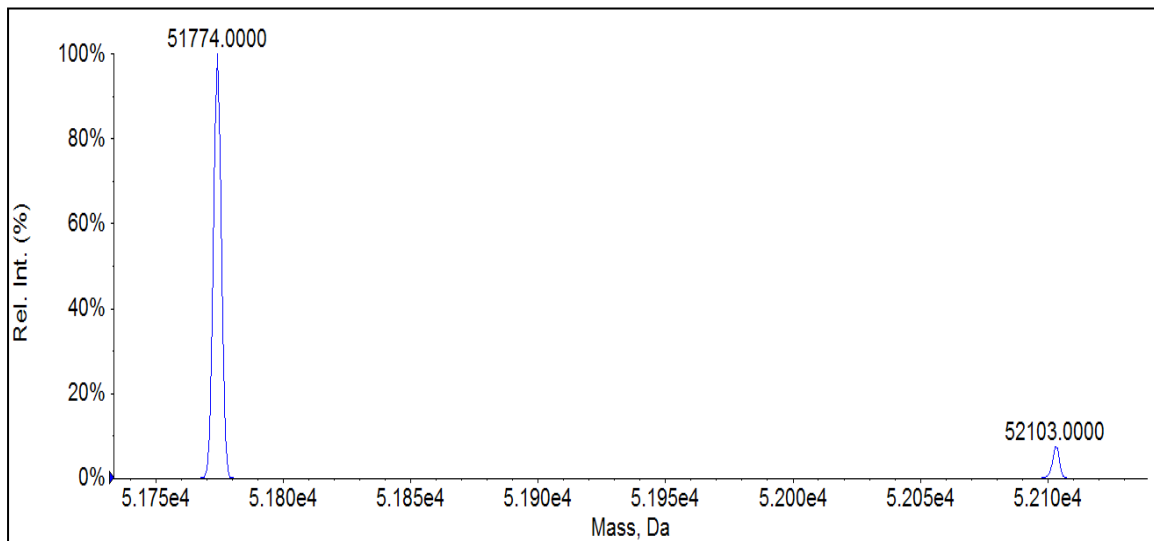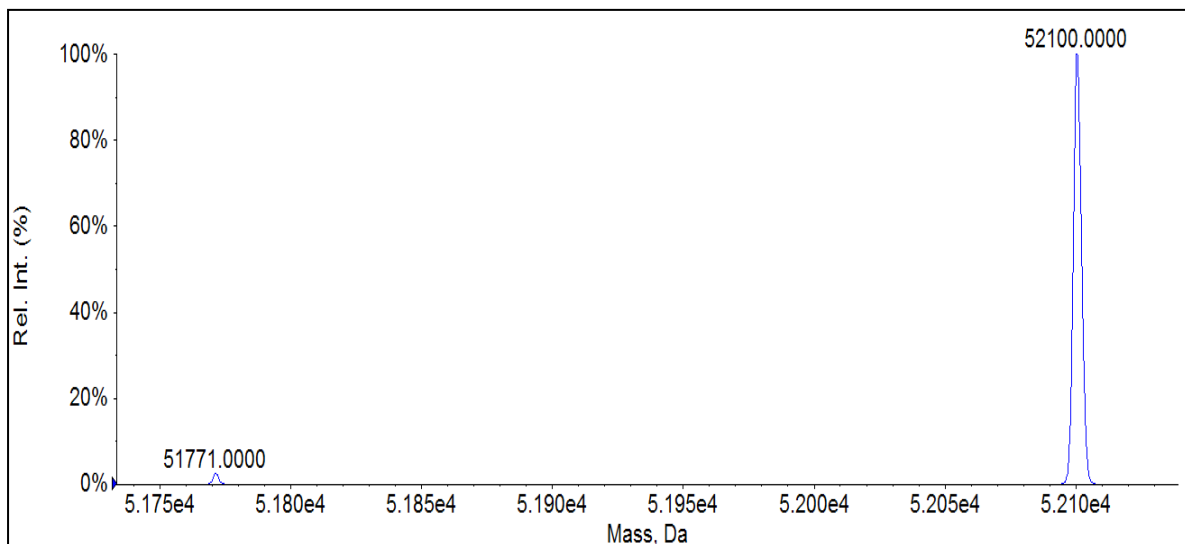

Figure 2.12: MS analysis of adenylylated *E.coli* GS had a calculated mass of 52,100.00 Da (theoretical mass = 52.1 kDa).
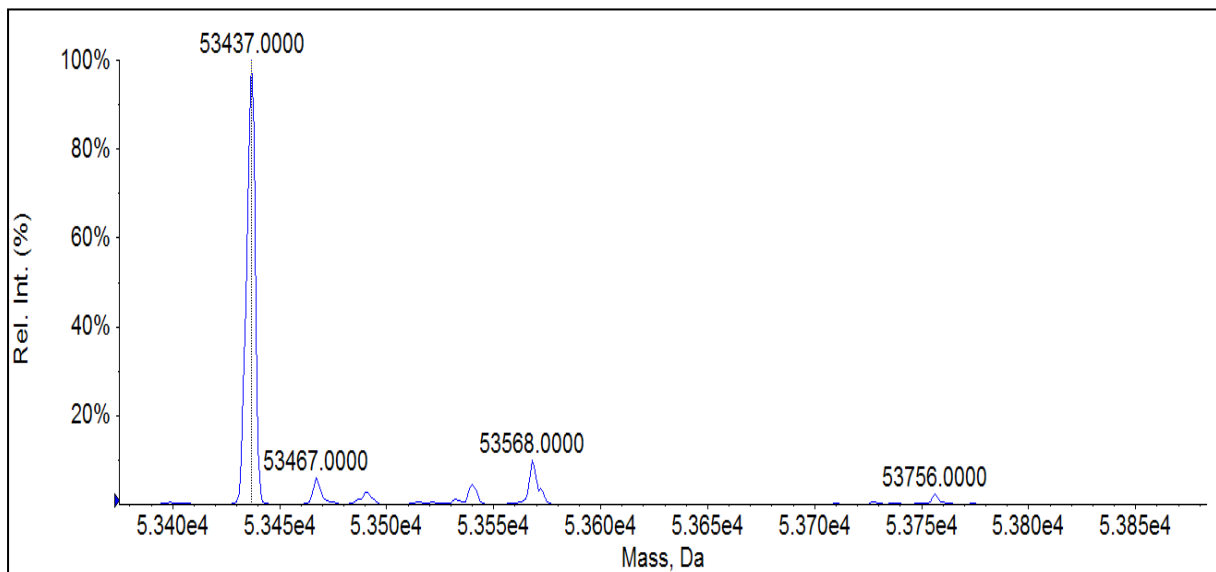
Figure 2.13: MS analysis of deadenylylated *M.tb* GS had a calculated mass of 53,437.00 Da (theoretical mass = 53.4 kDa)
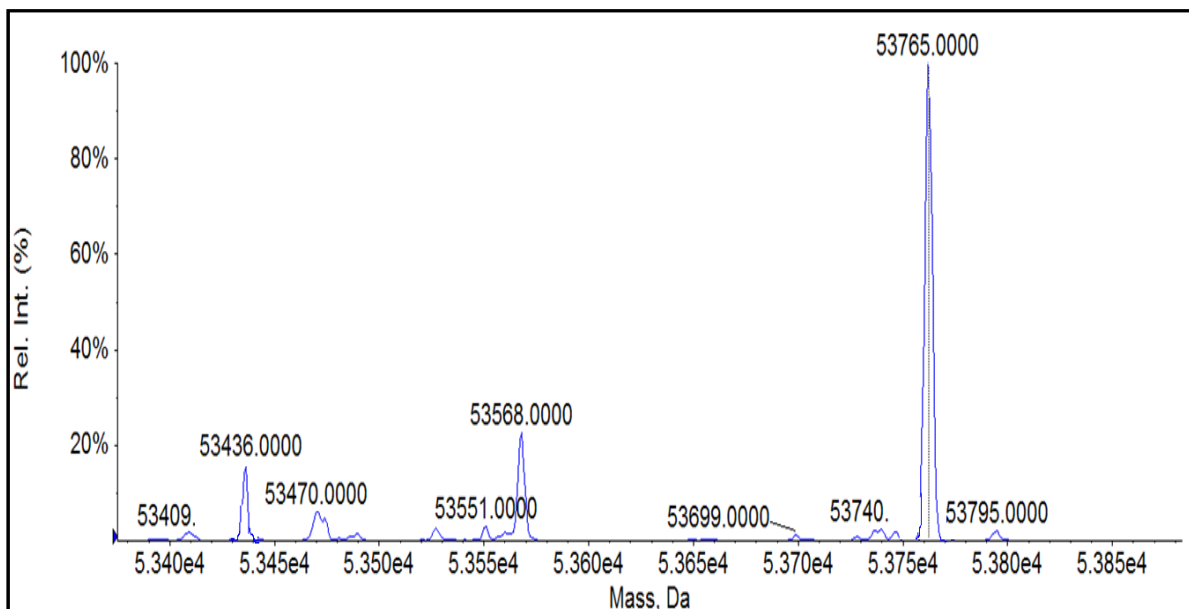
Figure 2.14: MS analysis of adenylylated *M.tb* GS had a calculated mass of 53,795.00 Da (theoretical mass = 53.7 kDa)

2.3.3.3 Enzyme Hydrolysis

The hydrolysis of GS for determination of phosphate content was carried out on the purified enzymes to confirm the degree of adenylylation (Figure 2.15). Each adenyl moiety contains 1 phosphate, and 1 µM of GS (containing 12 subunits) should contain 12 µM of phosphate, if each subunit is adenylylated. The result obtained for the adenylylated *M.tb* GS enzyme was the formation of 0.93 µM phosphate produced per µM GS active site, *i.e.* 94% adenylylated.   In the case of the deadenylylated enzyme there was no formation of phosphate.   The results obtained for *E. coli* GS were 0.95 µM and 0 µM for adenylylated and deadenylylated GS, respectively.

RBA buffer

HEPES buffer

E.coli Adenylylated GS

E.coli Deadenylylated GS

M.tb Adenylylated GS

M.tb Deadenylylated GS
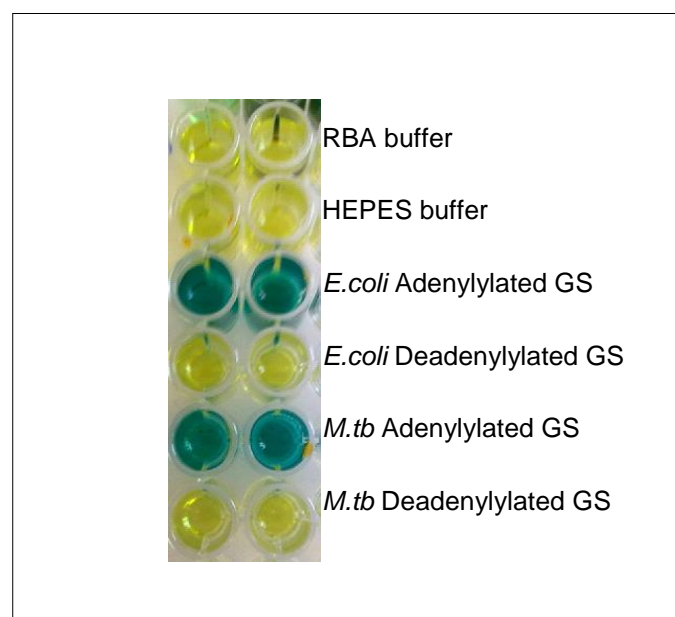
Figure 2.15: Hydrolysis of *M.tb* and *E.coli* GS purified protein (adenylylated and deadenylylated) for phosphate concentration determination. A blue colour indicates the presence of free phosphate.

Table 2.3 is a summary of the adenylylation states of both *M.tb* GS and *E.coli* GS determined by different methods including mass spectrometry, hydrolysis and phosphate concentration, and γ-glutamyl transferase assay.

Table 2.3: Summary of adenylylation states of *M.tb* GS and *E.coli* GS determined by different methods: (1) mass spectrometry, (2) hydrolysis and phosphate concentration, and (3) γ-glutamyl transferase assay.

Quality control assays	*M.tb GS*		*E.coli*	
	Deadenylylated	**Adenylylated**	**Deadenylylated**	**Adenylylated**
MS	0%	85$\pm$ 1%	7%	100$\pm$ 0%
Phosphate concentration	0 µM	0.93 $\pm$ 2µM	0 µM	0.95 $\pm$ 1µM
γ-Glutamyl transferase	3 $\pm$ 2%	68 $\pm$ 4%	0%	87 $\pm$ 3%

2.4 Discussion

M.tb GS is a potentially valuable therapeutic target for tackling the problem of tuberculosis disease. Its regulation via adenylylation of a tyrosine residue on each subunit makes it distinct from the human form of the enzyme. Previous reports of heterologous expression of *M.tb* GS in *E.coli* have shown that the endogenous ATase activity of *E.coli* does not adenylylate *M.tb* GS sufficiently, with only 25% of the *M.tb* GS subunits produced displaying adenylylation (Laemlli, 1970). The use of this expression system was therefore not considered optimal for the expression of adenylylated *M.tb* GS for further study.

Here we have described an *E.coli* production system lacking endogenous GS and ATase activity, which utilises the co-expression of the *M.tb* ATase with *M.tb* GS. Each gene was provided on a separate plasmid, the *glnA* gene on a pBluescript SKII$^+$ plasmid with the ColE1 origin of replication, and the *glnE* gene on a CDFDuet-1 plasmid containing a CloDF13 replicon. These replicons are compatible, and the two plasmids can be stably co-maintained, provided the relevant antibiotic selective pressure is exerted: ampicillin for pBluescript SKII$^+$ and streptomycin for pDFDuet-1 (Held *et al.,* 2003). Mehta and co-workers expressed *M.tb* GS in *E.coli* host strains that were deficient in chromosomal GS (*glnA*). They found that the *E.coli* ATase was inefficient in adenylylating the heterologous *M.tb* GS, with only ~25% of subunits being modified (Mehta *et al.,* 2004). By co-expressing *M.tb* ATase and *M.tb* GS we improved the percentage of subunits modified (or adenylylated) with ± 60-70% to ± 85-94%. In this way, we have produced recombinant *M.tb* GS that has a better adenylylation state than any previously reported.

The *E.coli* enzymes were produced recombinantly from pBluescript SKII$^+$ in *E.coli* strains lacking endogenous GS (for deadenylylated enzyme) or both GS and uridylyl transferase (adenylylated enzyme). The *E.coli* GS enzymes were only cloned, expressed and purified to be used as a model and for comparison with *M.tb* GS.

Three methods were used to assess the degree of adenylylation of adenylylated and deadenylylated *M.tb* GS, and *E.coli* GS. The first assay used, termed the γ-glutamyl transferase enzyme assay, is a variation of the reverse of the reaction that GS catalyses:

$$\text{Glutamate} + NH_4^+ + ATP \rightarrow \text{glutamine} + ADP + P_i + H^+$$
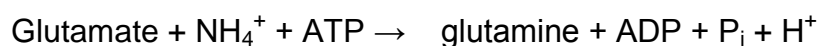
In this reverse reaction; hydroxylamine and glutamine react to form γ-glutamylhydroxamate and free ammonia in the presence of ADP, arsenate and manganese or magnesium (EP2008210 A1, 2008; Shapiro and Stadtman, 1970). This forms the basis of an assay for GS activity. At the correct pH, this is derived from determining the isoelectric point of the enzyme, the transferase activities of both the adenylylated and deadenylylated forms of GS are the same. The two forms can, however, be distinguished because at the isoelectric point, fully adenylylated GS is completely inhibited by 60mM Mg^{2+}, whereas the deadenylylated enzyme is unaffected (Bender *et al.,* 1977). Based on the data from the γ-glutamyl transferase assay, the adenylylation state of adenylylated *M.tb* GS expressed in this novel system is at least 68% compared to the 25% obtained from Mehta and co-workers.

The second assay used is the determination of the inorganic phosphate concentration after the hydrolysis of both adenylylated and deadenylylated *Mtb* GS. After the hydrolysis of the enzymes in the case of the deadenylylated enzyme there was no formation of phosphate. For the adenylylated *Mtb* GS each adenyl moiety contains 1 phosphate, and 1 µM of GS (containing 12 subunits) should contain 12 µM of phosphate, if each subunit is adenylylated. The result obtained for the adenylylated *M.tb* GS enzyme was the formation of 0.93 µM phosphate produced per µM GS active site, *i.e.* 94% adenylylated compared to the 25% obtained from Mehta and co-workers.

The third method used to assess the adenylylation is mass spectrometry. MS spectra showed distinct peaks for adenylylated and deadenylylated enzymes, with calculated masses agreeing with the theoretical values. Based on this data, it can be concluded that the adenylylation state of adenylylated *M.tb* GS expressed in this novel system is at least 85% from the MS spectra obtained.

In addition, the rate of conversion of ATP, glutamate and ammonia to glutamine and ADP was assessed using HPLC. This is termed the 'forward' or 'biosynthetic" reaction and is assayed in two different assays; one which measures the ability of glutamine synthetase to convert glutamate to glutamine in the presence of ATP, and the second determines the conversion of ATP to ADP and AMP in the same assay mixture. These assays will be discussed in Chapter 3.

Chapter 3

Differential inhibition of adenylylated and deadenylylated forms of *M.tb* glutamine synthetase in *E.coli* by ATP scaffold-based inhibitors

3.1 Introduction

GS was explored as a candidate new target for the development of innovative anti-TB drugs. In particular, whether post-translation mechanisms (i.e. adenylylation) of GS regulation could provide a possible clue to the development of anti-microbial compounds that would be safe and effective against TB, and possibly presenting cydal activity for latent or resistant form of the *M.tb*. The rationale of the project can be summarised as follows:

GS is an essential enzyme in bacterial metabolism, and previous studies have shown that inhibition/deletion of this enzyme can result in a static effect for pathogenic *M.tb.* GS belongs to the glutamine synthetase 1-β group of enzymes that are regulated via adenylylation of a single tyrosine residue (Kenyon *et.al.,* 2011). The adenylylation mechanism of GS is specific to bacterial forms of the enzyme and induces significant modifications in the active site and ion requirements for the catalytic activity of GS. The novel reaction mechanism and catalytic site elucidated by CSIR researchers and protected in two PCT patents could be used for the design and selection of candidate inhibitor molecules that could afford a specific activity against bacterial GS and could be considered as promising hits for the development of novel TB agents. As the adenylylated GS and the deadenylylated GS utilise different divalent metal ions in the reaction, it is believed that the overall structure and conformation of the ATP in the active site as well as the coordinating amino acid residues are significantly different, allowing for the selection of distinct classes of compounds specifically inhibitory to either adenylylated or deadenylylated forms of the enzyme (Kenyon *et. al.,* 2011).

A collection of 213 compounds will be tested against the adenylylated and deadenylylated forms of both *M.tb* GS and *E.coli* GS at a concentration of 10 μM.

The rational design and selection of these inhibitors were based on the typical ATP binding site since GS utilize ATP. The test compounds were designed and synthesized at CSIR Biosciences. Three sets of inhibitors were synthesized for testing: namely the 5 000, 10 000 and 12 000 series. The 5 000 series is the substituted pyrimidine series, the 10 000 series is the aminated imidazopyridenes series and the 12 000 series is related to the aminated imidazopyridenes.

3.1.2 Study Objectives

- Objective 1: To examine the inhibitory effect of a library of ATP scaffold-based inhibitors and the identification of possible adenylylated and deadenylylated *M.tb* GS inhibitors.

- Objective 2: To demonstrate differential inhibition of adenylylated and deadenylylated *M.tb* GS and using adenylylated *E.coli* GS, deadenylylated *E.coli* GS and mammalian GS enzymes as controls.

- Objective 3: Validation of assays: The HPLC based assay, Molybdate colorimetric phosphate assay and the colorimetric Kit based phosphate assay. The determination of the following parameters: intra-plate reproducibility, inter-plate reproducibility and the Z' factor determination.

- Objective 4: Determination of IC_{50} of hit compounds and the HeLa cell cytotoxicity assay of these hit compounds.

- Objective 5: Testing of compounds against *M.tb* strains in a Bactec 460 TB™ assay.

- Objective 6: Testing of compounds in a macrophage assays.

- Objective 7: LogD and Caco-2 permeability determination of the hit compounds.

3.2 Methods

3.2.1 Test compounds

The test compounds were designed and synthesized at CSIR Biosciences. Essentially three different sets of inhibitors were synthesized for testing: namely the 5 000, 10 000 and 12 000 series. The 5 000 series is the substituted pyrimidine series (Figure 3.2A). In the 5 000 series, the hydrogen bonding pattern is retained with varying steric components in the imidazole/sugar region of ATP. The 10 000 series is the aminated imidazopyridenes series (Figure 3.2B), where a hydrogen bonding network is retained with the placing of substituents in different areas of 3D space. The 12 000 series is related to the aminated imidazopyridenes (Figure 3.2B), where a hydrogen bonding network is retained and the compounds are spatially related to guanosines.
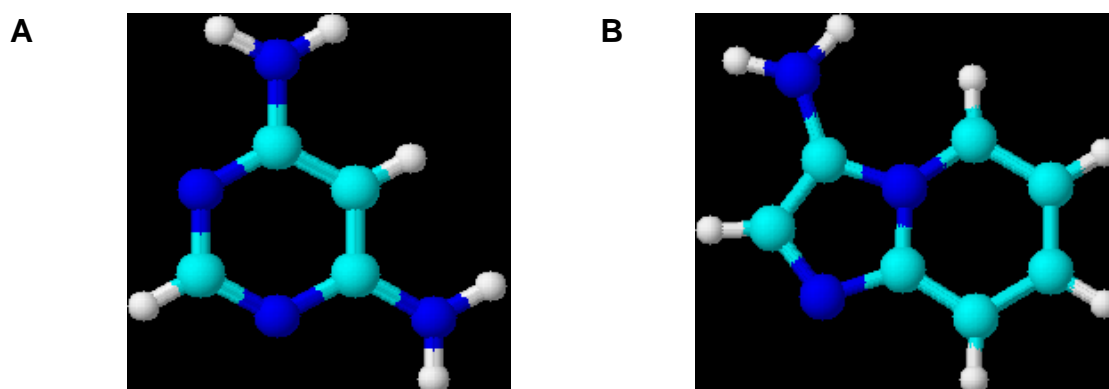
A   **B**

Figure 3.2: Classes of inhibitors: **A**, the pyrimidine series. **B**, the imidazo-pyridine series.

3.2.2 HPLC-based analysis

3.2.2.1 Standard assay

Concentrations of substrates used in the final assay were based on their *Km* values determined by Kenyon *et al.,* (2011) and set at approximately 3-times the *Km* value. For the 10 µM fixed concentration screens, 20 µL of 0.1 mM compound stocks in dimethyl sulfoxide (DMSO) were added to duplicate microtitre plate wells. Each well then received 180 µL of an enzyme/substrate/buffer master stock to achieve a final concentration of 50 mM HEPES (pH 7.15), 4 mM sodium glutamate, 4 mM NH_4Cl, 1.8 mM $MgCl_2$, 0.8 mM ATP and 5 µg/mL deadenylylated *M.tb* GS in 10% DMSO. For adenylylated *M.tb* GS the same conditions were used, except that 50 mM HEPES (pH 6.95) and 1.8 mM $MnCl_2$ was used. Enzyme and ATP was added to the

master stock immediately before distribution onto the plates. The reactions were incubated at 37ºC for 2 hours (hrs), before being terminated by the addition of 1 μL 50% trichloroacetic acid (TCA) to each well. Blank wells (no enzyme) were also prepared for each individual compound. In addition, each plate contained control wells (10% DMSO without inhibitor) and blank control wells (10% DMSO, no inhibitor, no enzyme). After termination of the reactions, ADP levels in each well were determined by HPLC. The samples were analysed on an Agilent series 1100 HPLC fitted with a Phenomenex Luna 5μ C18 column. Each sample was automatically injected (2 μL) and separated with a mobile phase containing 51 mM KH_2PO_4, PIC A Low UV Reagent (Waters Cooperation), 25% (v/v) acetonitrile. The flow rate of the mobile phase was 1 ml/min with UV detection (295nm). An AMP, ADP and ATP standard was used to calibrate the HPLC and the concentration of ADP in each sample was determined by the area under the curve using Agilent ChemStation (Revision B.02.01) software. The ADP values in the blank wells were subtracted from enzyme-containing wells, and percentage enzyme activity in each well calculated relative to the average net ADP values of the control wells without inhibitor.

3.2.2.2 Pre-incubation assays

After adding 20 μL 0.1 mM compound stock to each well, the wells received 164 μL adenylylated or deadenylylated *M.tb* GS in 50 mM HEPES (pH 6.95 or pH 7.15 respectively), 4 mM NH_4Cl, 1.8 mM $MnCl_2$ or $MgCl_2$. The plates were incubated at 37ºC for 2 hrs, after which the reactions were initiated by adding sodium glutamate and ATP to final concentrations of 4 mM and 0.8 mM respectively and a final reaction volume of 200 μL. After further 2 hr incubation, the reactions were terminated and ADP levels measured as described above.

3.2.3 Dose-response assays

These were carried out using the pre-incubation protocol described in section 3.2.2.2. Serial 4-fold dilutions of compounds were prepared in DMSO. For test compounds, the highest starting concentration for the dilution series was 1 mM for the first assay and 2 mM for the second. Eight dilutions were performed in DMSO to produce a concentration range of 1 mM to 61 nM or 2 mM to 122 nM. Twenty μL of each dilution was distributed into duplicate wells of the reaction plate, before adding

enzyme in HEPES/ammonium chloride/MnCl$_2$ or MgCl$_2$ and proceeding with the pre-incubation procedure as described in section 3.2.2.2.

3.2.4 *E.coli* and mammalian GS assays

The *E.coli* GS screen was carried out as described in section 3.2.2.1 for the *M.tb* GS standard assay, except that the adenylylated and deadenylylated *M.tb* GS enzymes were replaced by their *E.coli* counterparts. The mammalian GS assay was carried out using the pre-incubation protocol described in section 3.2.2.2 for *M.tb* GS, using the purified bovine enzyme (MSc. Thesis of Lutendo Mathomu, 2011, UNISA) and buffer composition as described for the deadenylylated form of the *M.tb* enzyme.

3.2.5 Determination of inorganic phosphate

3.2.5.1 Molybdate colorimetric phosphate assay

The assay was carried out according to the standard *M.tb* GS protocol (described in section 3.2.2.1), except that reactions were terminated by the addition of 180 µL molybdate colorimetric reagent (prepared fresh daily) containing 1.2 N sulphuric acid, 0.5% ammonium molybdate, 2% ascorbic acid. After 15 min at 37$^{\text{o}}$C, absorbance was measured at 620 nm with a multiwell plate reader.

3.2.5.2 Colorimetric kit phosphate assay

The assay was carried out using the BioVision™ phosphate assay kit (BioVision™ Research Products, CA). Enzyme/inhibitor reactions were prepared in a 96-well plate exactly as described in the standard *M.tb* GS protocol (see section 3.2.2.1). At the end of the incubation, reaction mixes were diluted 5x in water by transferring 40 µL from each well to a second plate containing 160 µL water per well. Subsequently, 30 µL of the phosphate reagent supplied with the kit (proprietary composition) was added to each well and the absorbance was read at 620 nm using a multiwell spectrophotometer after a 5 minute incubation.

3.2.6 HeLa cell cytotoxicity assay

HeLa cells (Human Negroid cervix epitheloid adenocarcinoma, ECACC) were routinely maintained as monolayer cell cultures in Eagle's minimal essential medium (EMEM) containing 5% fetal bovine serum, 2 mM L-glutamine and 50 µg/ml gentamicin at 37ºC in a 5% CO$_2$ incubator. To perform the cytotoxicity assay, the

cells (3 - 19 passages) were used to inoculate 96-well microtiter plates at plating densities of 7000 cells/well. After incubating for 24 hrs, the culture medium was replaced with medium containing serial dilutions of the experimental compounds. Each dilution series consisted of 8 x 3-fold serial dilutions, spanning the final concentration range 100 - 0.05 µM. Triplicate wells were used for each concentration point (n = 3). The dilutions were prepared from compound stocks of 10 mM in DMSO, thus the final DMSO content in the highest compound concentration wells was 1%. Control wells consisted of cells incubated in medium with 1% DMSO, while blank wells contained medium without cells. Emetine was used as a positive control drug standard. The plates were incubated for 48 hrs after addition of the compounds. The cellular protein present after the incubation period was fixed to the bottom of each well with cold 50% TCA, washed in tap water and stained with 0.4% sulforhodamine B (SRB) in 1% acetic acid. Unbound dye was removed by washing with 1% acetic acid, after which protein-bound dye was solubilised with 10 mM Tris base and transferred to a duplicate 96-well plate. Optical density was measured at 540 nm using a Tecan Infinite F500 multiwell spectrophotometer. OD_{540} values of the blank wells were subtracted from the readings obtained for all the other wells, and percentage cell viability at each test compound concentration calculated relative to the untreated (DMSO alone) control wells. Percentage viability was plotted against Log (compound concentration) and the IC_{50} for each compound calculated from fitted non-linear regression dose-response curves using GraphPad Prism software.

3.2.7 Testing of compound against *M.tb* strains in a BACTEC 460TB™ assay.
3.2.7.1 Bacterial strains

All *M.tb* strains used were from a strain bank kept in the Division Molecular Biology and Human Genetics of the University of Stellenbosch. *M.tb* H37Rv reference strain (ATCC 25618) and a clinical isolate of *M.tb* were used to evaluate compounds for anti-tuberculosis activity. Both strains were sensitive to the breakpoint concentrations (aproximately 10x higher than their minimal inhibitory concentrations (MIC)) of isoniazid (0.25ug/ml), ethambutol (9.4ug/ml), and rifampicin (2.0ug/ml) (Collin *et al.,* 1997). These sensitivity values were determined before and logged into a TB strain database.

3.2.7.2 Test Compounds

The compounds identified using the methodology stipulated in section 3.2.1 to 3.2.5 were used in the BACTEC 460TB™ assay (Siddiqi *et al.,* 1993). The identified compounds were dissolved and diluted with 100% DMSO.

3.2.7.3 Bacterial selection

All mycobacterial colonies were cultured and selected from Lowenstein-Jensen slant (Kenneth *et al.,* 2005) cultures followed by culture in Middlebrook 7H9 mycobacterial growth medium supplemented with OADC (0.005% v/v oleic acid (Merck), 0.5% w/v BSA Fraction V, 0.2% v/v glucose, 0.02% v/v catalase (Merck), w/v 0.085% NaCl). Cultures were stained by acid-fast staining (Ziehl-Neelsen staining) to control for contamination. This is a selective staining method for the mycolic acids found in the mycobacterial cell wall. An aliquot of the mycobacterial culture was immobilized onto a glass slide by heating for 20 min at 65 °C. The slide was covered completely with 0.3% carbol-fuchsin (Becton Dickenson, USA) and heated until steaming. The carbol-fuchsin was rinsed off with water after incubation of 5 min at room temperature. The slide was destained by flooding the slide with 5% alcohol at room temperature for 2 min. The slide was rinsed with water and stained with 0.3% methelyne blue counter stain (Becton Dickenson, USA) and left at room temperature for 2 min. The slide was analysed with a light microscope after the slide was rinsed with water and left to air dry. The mycobacterial cells were stained pink (mycobacterial cells are acid-fast) while non-mycobacterial cells were stained blue (non-acid fast bacteria) and thus be an indication of contamination.

3.2.7.4 BACTEC 460TB™ system determination of mycobacterial growth

All work was carried out in the BSL3 laboratory of the Division of Molecular Biology and Human Genetics of the University of Stellenbosch. The BACTEC 460TB™ system has been devised to monitor mycobacterial growth of the slow growing species. The bacteria are grown on a radioactive substrate and the radioactive carbon dioxide produced is directly proportional to the mycobacterial growth rate. Read-out values are expressed as growth index (GI). *M.tb* reference strain H37Rv was cultured in 7H9 mycobacterial medium (Difco) enriched with ADC (0.5% w/v BSA Fraction V, 0.2% v/v glucose, 0.015% v/v catalase (Merck)) with continuous stirring at 37 °C. When cultures reached a density of approximately 0.16 at OD_{600}

(one McFarland), 0.1 ml was inoculated into a BACTEC 12B medium vial. These primary cultures were incubated at 37 °C until a growth index of 500 (± 50) was reached. These primary cultures were used for drug testing of known and unknown compounds. The above protocol was also followed to generate a primary culture from the clinical isolate of *M.tb*. Unknown compounds, supplied in DMSO, were sterilized through a 13 mm organic solvent resistant syringe filter with 0.22 micron pore size (Millex-LG). Undiluted and sequentially diluted samples were tested for growth inhibitory activity. One hundred microliters of primary culture and 0.1 ml drug compound were added to a BACTEC 460TB™ vial, the vials incubated at 37ºC, and the growth monitored every 24 hrs. Controls included cultures with and without compound solvent. GI readings were continued until the controls reached the maximum GI value of or below 999. Control GI values between 50 and 800 are normally used to evaluate the efficacy of compounds with possible anti-tuberculosis activity.

3.2.8 Testing of screening hits against *M.tb* in a macrophage assay

3.2.8.1 *M.tb* cultures

M.tb H37Rv reference strain and clinical MDR strain (Beijing220) were cultured in 7H9 broth supplemented with 10% oleic acid-albumin-dextrose catalase (OADC, Difco, BD Biosciences, Mountain View, CA, USA) and 2% glycerol and 0.05% Tween 80 (Glickman et. al., 2000). Liquid cultures were grown for up to 3 weeks and stored at -80°C in 1ml aliquots with 15% glycerol. Clumps were eliminated by 30 passages through a needle (26-gauge 3/8; 0.45 x 10 for intradermal injection; BD Biosciences, USA). Before infection, viability of mycobacteria was evaluated by the propidium iodide exclusion method to ensure >90% viability. Contamination was checked by the Ziehl-Neelsen stain (ZN) see section 3.2.7.3. The required amount of mycobacteria was spun down at 16 300 g for 5 min. The supernatant was removed and the bacteria resuspended in PBS (phosphate buffered saline) and passaged again 20 times and then used for macrophage infection.

3.2.8.2 Manipulation of mouse bone marrow-derived macrophages (MBMM*)*

All animal studies were carried out under the Stellenbosch University Animal Ethics application number (11GH_PIE01). Bone marrow cells were obtained from femurs of 6-8 week-old C57BL/6 female mice and seeded into 24-well tissue culture plates. The culture medium was RPMI-1640 (Sigma, USA) supplemented with 10% heat-inactivated fetal bovine serum (Gibco), 10% L-929 cell conditioned medium (a source of colony stimulating factor-1) with no antibiotics. Incubation was performed at 37°C, 5% CO_2. At 5 days after seeding, adherent cells were washed twice with RPMI and re-fed with complete medium. Medium was then renewed every second day.

3.2.8.3 Macrophage infection and harvesting of TB

Frozen aliquots of *M.tb* (H37Rv/Beijing220) were removed from the -80°C freezer where they were kept for long-term storage and thawed and processed as indicated above see section 3.2.8.1. Infection of the 7-Day old MBMM in 24-well plates was performed in triplicate with 100 µl of bacterial suspension relative to a multiplicity of infection of 2 (2 MOI), and incubated for 4 hrs at 37°C , 5% CO_2. After the 4 hrs incubation period, non-ingested *M.tb* (H37Rv/Beijing220) was removed by washing 4 times with ice-cold PBS. Fresh RPMI medium (1 ml) was added and again on day 2. At day 4 post infection the test compounds were added at the desired concentrations between 10 µM and 100 µM. Included were uninfected, infected (no drug) and isoniazid drug controls. On days 1, 2 or 3 post drug intervention the macrophages were washed 3 times with cold PBS (4°C) and then the bacteria harvested by adding 1 ml 0.025% SDS for 5 min to lyse the adherent macrophages. The contents of each well were placed into separate Eppendorf tubes and the bacteria were pelleted at 13000 rpm for 5 min. The bacteria was resuspended in 100 µl 7H9 Middlebrook medium and then inoculated into BACTEC 460TB™ vials. Growth was monitored over time until the BACTEC 460TB™ readings of the infected (no drug) control reached about 500. The percentage growth inhibition for each drug compound was determined by relating the linear growth unit readings to the infected (no drug) control.

3.3 Results

3.3.1 Assay Characteristics - Linearity/Incubation time

To evaluate the comparative enzyme inhibitory activity of compounds in an end-point assay, it is preferable that the assay is terminated when product formation over time is linear. In addition, incubation time may significantly affect signal vs. background values and thus the optimal assay window. Consequently, an experiment was carried out where time-dependent ADP product formation by adenylylated *M.tb* GS was measured. The standard assay method (see section 3.2.1.1) was carried out, except that the reaction was terminated at 30 min intervals from 0 - 270 min by the addition of 1 µL 100% TCA to the reaction wells. The amount of ADP formed at the different time-points was determined by HPLC. Blank wells contained no enzyme.

The ADP HPLC (area under the curve) levels obtained for the blanks (no enzyme) at each time-point were subtracted from ADP values obtained for the corresponding time-point reactions containing adenylylated *M.tb* GS. The resulting net ADP levels, as well as the blank ADP levels, were plotted against time (Figure 3.3).
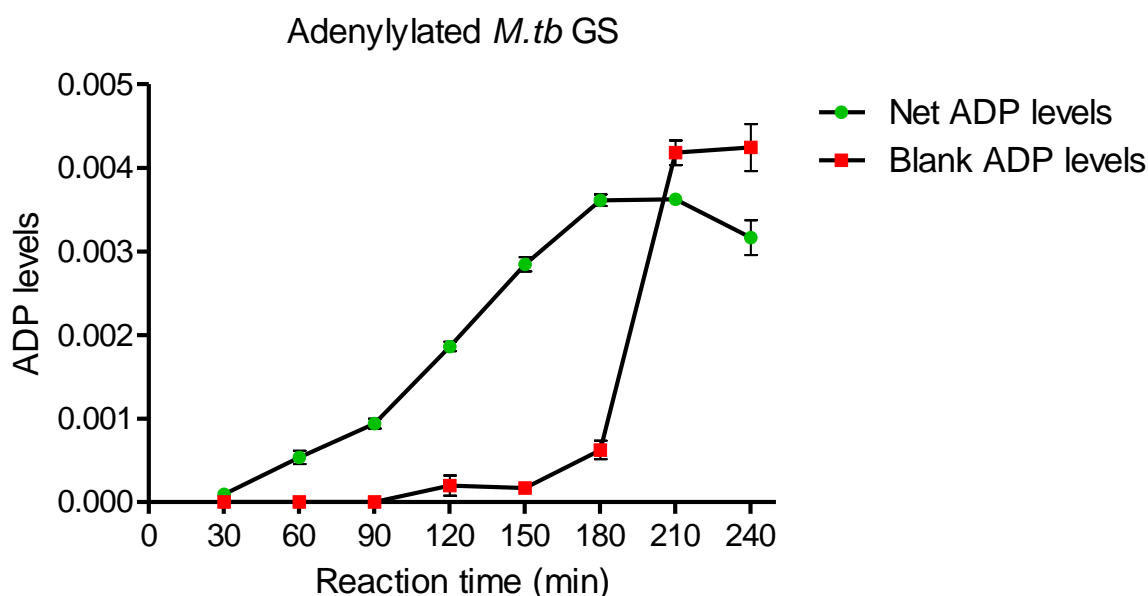

Figure 3.3: Standard *M.tb* GS assay – linearity/incubation time. Where not shown, error bars fall within symbols.

The net ADP levels increased linearly with incubation time from approx. 90 - 150 min. However, the net ADP levels decreased precipitously after 180 min. This was

due to an increase in blank ADP levels. The results indicate that ATP is labile under the reaction conditions, resulting in the non-enzymatic production of ADP at longer incubation times. The results suggest that enzyme incubations should be restricted to 2 - 2.5 hrs to ensure optimal enzyme activity and signal vs. background windows.

3.3.2 *E.coli* GS screen

For comparison purposes, adenylylated and deadenylylated *E.coli* GS was also heterologously expressed, purified and used in the inhibitor studies.

To determine if the panel of 213 compounds including the two standard inhibitors methionine sulfoximine (MSO) and phosphinothricin (PhosT) GS inhibitors inhibits adenylylated and deadenylylated *E.coli* GS, the compounds were incubated at a final concentration of 10 μM with purified adenylylated and deadenylylated *E.coli* GS. After incubation, ADP levels were determined by HPLC to derive the residual percentage enzyme activity for each inhibitor relative to untreated controls. The screen results obtained for the adenylylated and deadenylylated forms of the *E.coli* GS enzyme are shown in Figure 3.4 A and B.
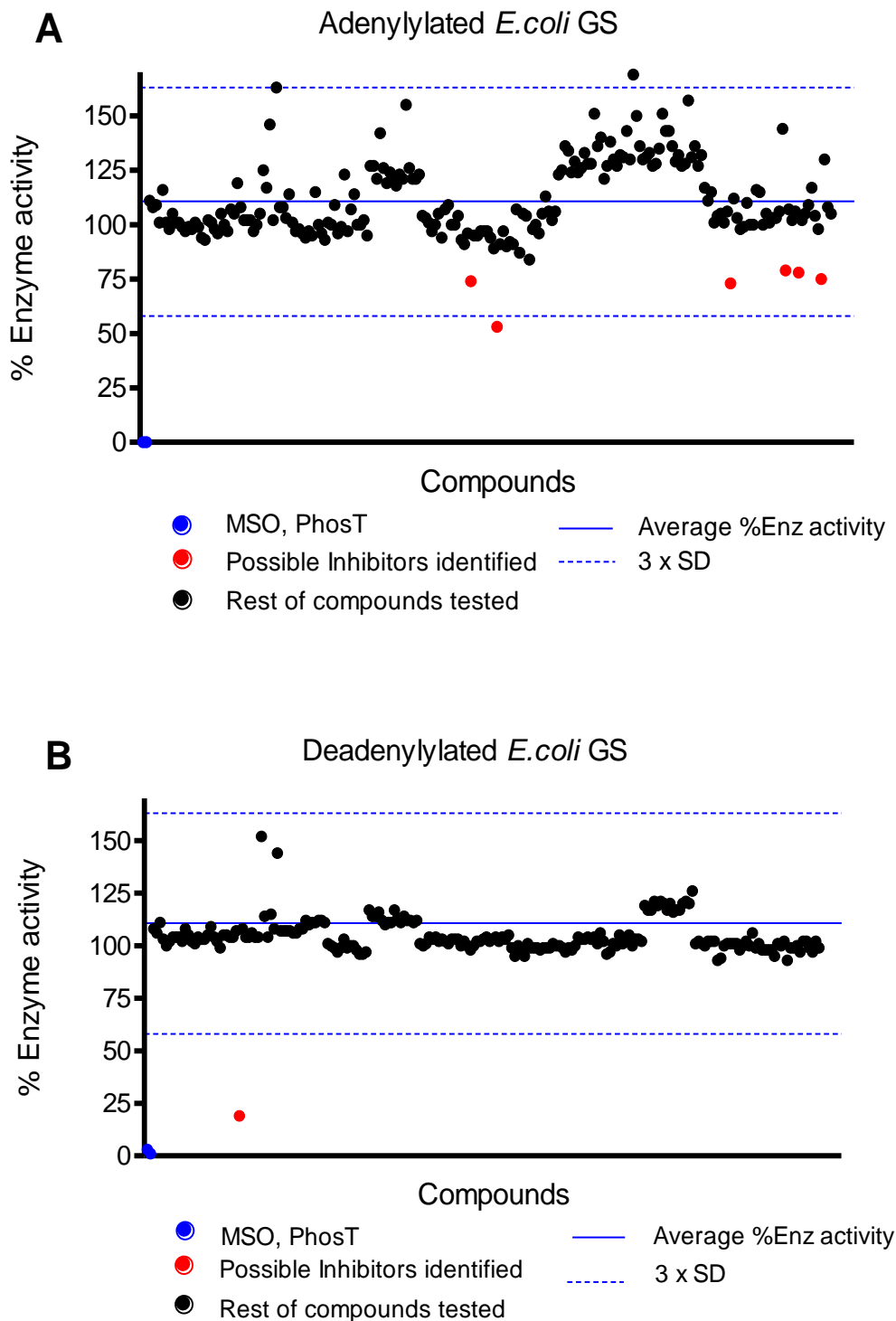
Figure 3.4: *E.coli* GS enzyme screen. The residual percentage adenylylated **(A)** and deadenylylated **(B)** GS enzyme activities after incubation with 10 µM of the individual compounds is shown, along with horizontal lines depicting the average % enzyme activity obtained with all compounds, as well as an indication of the confidence interval of the results, expressed as the average activity ± 3 x standard deviation (SD). Percentage activity obtained with MSO and PhosT is shown in blue, and candidate inhibitors in red.

With the exception of one compound (10067) and the MSO and PhosT standards, none of the compounds inhibited the deadenylylated form of *E.coli* GS (Figure 3.4 B). In the case of the adenylylated form of the enzyme, activities in the presence of the compounds were scattered more widely around the mean, as demonstrated by the wider ± 3 x SD window (Figure 3.4 A). Nonetheless, 5 compounds (indicated in red in Figure 3.4 A) caused a discernible inhibition of the enzyme. Inhibitory activities of the compounds obtained in the screens are summarized in Table 3.1.

Table 3.1: Candidate inhibitors of adenylylated and deanylylated *E.coli* GS.

Compound	% *E.coli* GS Inhibition	
	Adenylylated	Deadenylylated
1 (PhosT)	100	97
2 (MSO)	100	99
5032	26	0
5041	53	0
10029	27	6
10047	79	5
10054	22	7
10063	25	1
10067	0	81

3.3.3 *M.tb* GS screen

Following the promising results obtained in the *E.coli* GS screen which suggested that compounds may be able to discriminately inhibit the adenylylated and deadenylylated forms of the enzyme, the 213 compounds were re-screened at 10 µM against the recombinantly expressed and purified adenylylated and deadenylylated *M.tb* GS enzymes. The first screen was carried out with the deadenylylated form of the *M.tb* enzyme. As a read-out for enzyme activity, a more rapid kit-based phosphate assay was used instead of ADP quantitation by HPLC. As shown in Figure 3.5 A, the results produced a significant scatter around the average percentage enzyme activity, which precluded a confident identification of inhibitors. No compounds inhibited deadenylylated GS activity by >40%, compared to the 75% and 85% inhibition obtained for the standards MSO and PhosT respectively (indicated in blue in Figure 3.5 A). The screen was repeated with adenylylated

enzyme, using ADP HPLC quantitation as a measure of GS activity (Figure 3.5 B). On this occasion, 4 compounds (indicated in red in Figure 3.5 B) demonstrated clear inhibition of 35% - 46% of the enzyme compared to the rest of the compounds with an average inhibition of 2%, in addition to the 60% inhibition obtained with the MSO and PhosT standards. The inhibitory activities of the candidate inhibitors identified in the adenylylated GS screen are summarized in Table 3.2, along with the results obtained for the MSO and PhosT standards.

Of note is the fact that compound 10057 was the most inhibitory test compound in both the adenylylated and deadenylylated screens (the red data point to the far right in Figure 3.5 A and B).
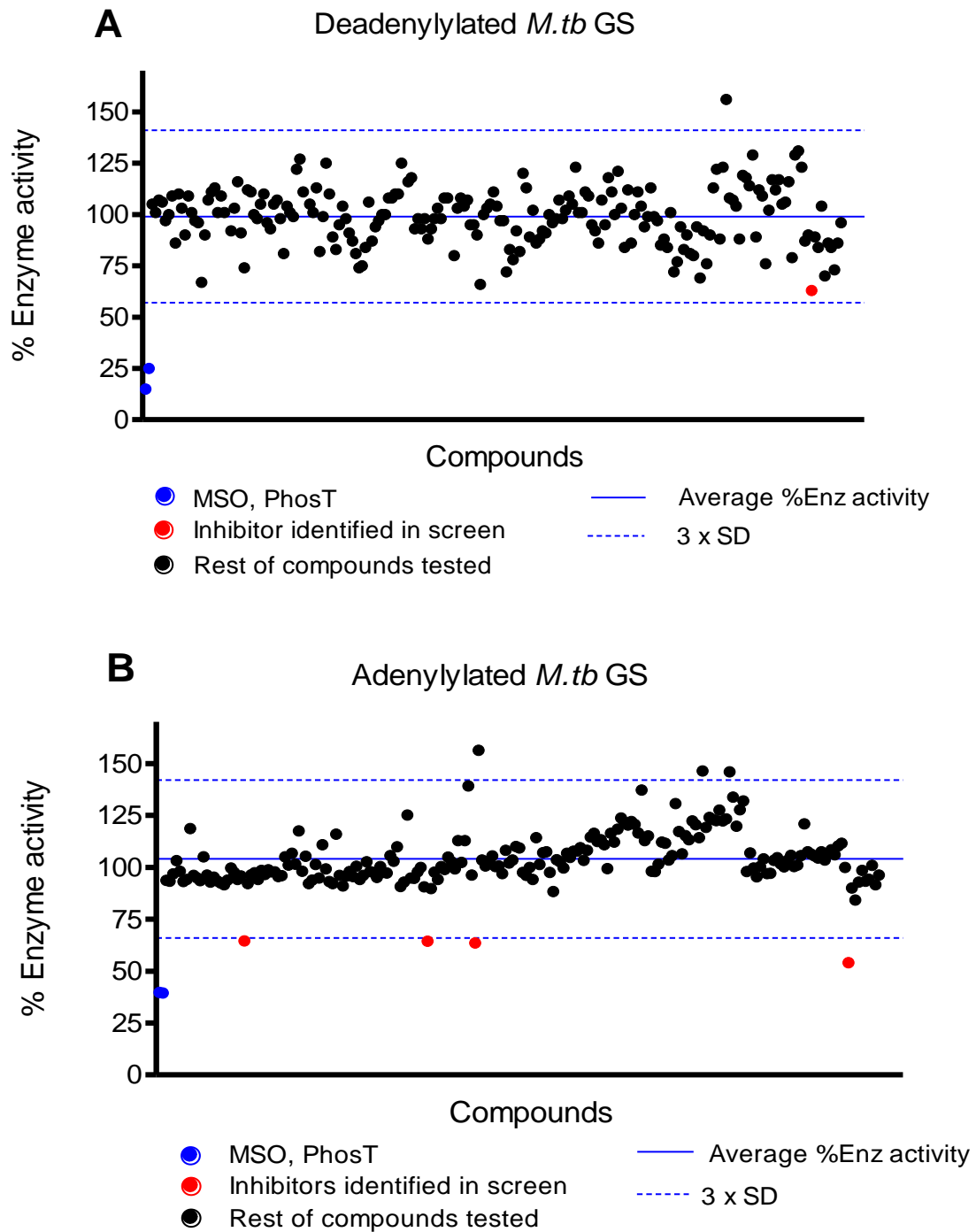
Figure 3.5: *M.tb* GS enzyme screen. The residual percentage adenylylated **(A)** and deadenylylated **(B)** GS enzyme activities after incubation with 10 µM of the individual compounds are shown, along with horizontal lines depicting the average percentage enzyme activity obtained with all compounds, as well as an indication of the confidence interval of the results, expressed as the average activity ±3 x SD. Percentage activity obtained with MSO and PhosT is shown in blue. Candidate inhibitors identified in the adenylylated GS screen are shown in red in **B**. For comparative purposes, the latter inhibitors are also indicated in red in the deadenylylated enzyme screening results **(A)**.

Table 3.2: Candidate inhibitors of adenylylated and deanylylated *M.tb* GS

Compound	% *M.tb* GS Inhibition	
	Adenylylated	**Deadenylylated**
1 (PhosT)	60 ±3%	85 ±1%
2 (MSO)	61 ±4%	75 ±2%
12004	35 ±2%	22 ±3%
5009	36 ±2%	0 ±0%
5024	36 ±3%	0 ±0%
10057	46 ±2%	37 ±2%

3.3.4 Pre-incubation *M.tb* GS assay

Subsequent to the *M.tb* GS screens reported above (Figure 3.5), *M.tb* GS assays using the standard inhibitors MSO and PhosT at a fixed 10 µM concentration often yielded GS inhibitory activities that varied from one experiment to the next, as well as intra-experimentally (plate-to-plate variability). In addition, attempts to determine the IC_{50} of these standard compounds produced highly erratic results. In an attempt to improve the reproducibility of inhibitor activity data, we explored pre-incubating the GS enzymes with the test compounds for two hours, prior to initiating the enzyme reaction by adding substrate for an additional 2 hrs. This was in contrast to the hitherto approach of adding test compounds and substrate simultaneously.

To assess the pre-incubation approach, two experiments were carried out with deadenylylated *M.tb* GS and the 4 candidate inhibitors (5009, 5024, 10057 and 12004), as well as MSO and PhosT (Exp 1 in Figures 3.6 A and B). In the second experiment (Exp 2 in Figures 3.6 A and B), three additional compounds from the panel of 213 (5056, 10037 and 12005) that were found not to be active against the GS enzymes in the earlier screens were also included as controls. In the experiments, compounds 5009, 5024, 10057 and 12004 that yield only low inhibitory activity against deadenylylated *M.tb* GS using the normal approach (compounds, enzyme and substrate added concurrently; Figure 3.6 A, Table 3.3), were very inhibitory when they were pre-incubated with the enzyme prior to substrate addition (Figure 3.6 B, Table 3.3). The control compounds (5056, 10037 and 12005) remained poor inhibitors under pre-incubation conditions.

Table 3.3: Inhibitory activities of test compounds against deadenylylated *M.tb* GS using conditions in which the enzyme is pre-incubated with the compounds for 2 hours before adding substrate to initiate the GS reaction (Pre-incubation) vs. no pre-incubation (No – compounds, enzyme and substrate added concurrently).

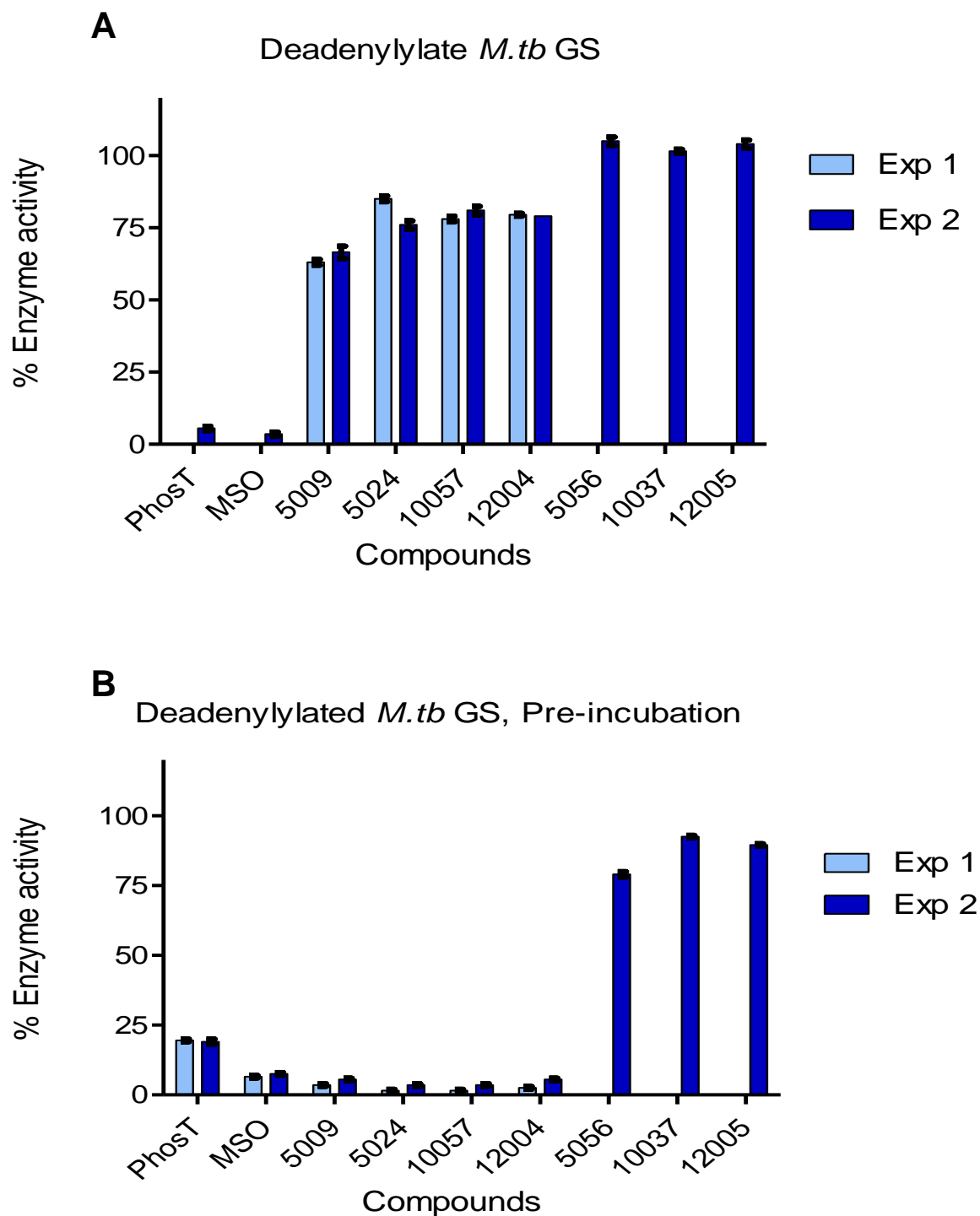| Compound	% *M.tb* GS inhibition			
	No Pre-incubation	**Pre-incubation**	**No Pre-incubation**	**Pre-incubation**
PhosT	100 ±0%	81 ±3%	95 ±1%	82 ±1%
MSO	100 ±0%	94 ±2%	96 ±1%	92 ±2%
5009	36 ±1%	97 ±1%	35 ±2%	95 ±2%
5024	14 ±2%	99 ±1%	23± 1%	97 ±2%
10057	23 ±1%	99 ±2%	20 ±2%	97 ±1%
12004	20 ±1%	98 ±2%	21 ±1%	95 ±3%
5056			0 ±0%	22 ±1%
10037			0 ±0%	8 ±2%
12005			0 ±0%	11± 3%

Figure 3.6: Inhibitory activities of test compounds against deadenylylated *M.tb* GS using conditions in which the enzyme is pre-incubated with the compounds for 2 hours before adding substrate to initiate the GS reaction **(B)** vs. no pre-incubation, i.e. compounds, substrate and enzyme added concurrently **(A)**. Where not shown, error bars fall within symbols. Exp 1: Consist of the 4 candidate inhibitors (5009, 5024, 10057 and 12004), as well as MSO and PhosT. Exp 2: Consist of the same as Exp 1 including three additional compounds from the panel of 213 (5056, 10037 and 12005).

3.3.5 Pre-incubation *M.tb* GS screens

Based on the markedly improved deadenylylated *M.tb* GS inhibitory activity of test compounds when they are pre-incubated with the enzyme prior to initializing the GS reaction, screens of the 213 compound panel against adenylylated and deadenylylated enzyme were repeated using the pre-incubation protocol, in the prospect of identifying candidate inhibitors additional to the 4 that were previously found. The results of the screens are shown in Figure 3.7.

With the deadenylylated enzyme, the 4 existing candidate inhibitors (5009, 5024, 10057 and 12004) again demonstrated significant GS inhibition using the pre-incubation protocol (Figure 3.7 A, red data points). Two additional compounds with promising inhibitory activity were also selected for further evaluation (5045, 10059 - green data points in Figure 3.7 A).
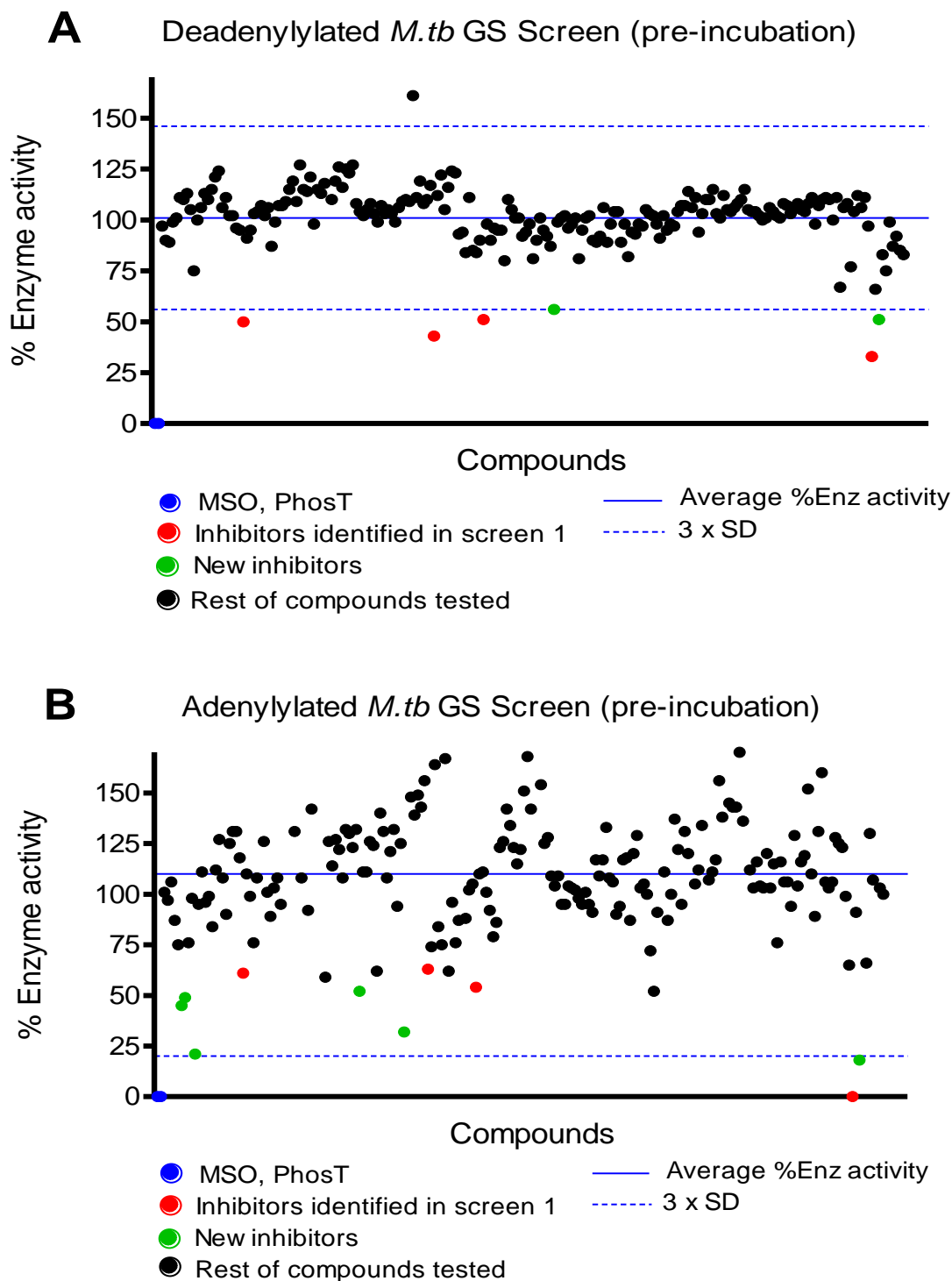
A   Deadenylylated *M.tb* GS Screen (pre-incubation)

B   Adenylylated *M.tb* GS Screen (pre-incubation)

Figure 3.7: *M.tb* GS enzyme screen using the pre-incubation protocol. The residual percentage adenylylated **(B)** and deadenylylated **(A)** GS enzyme activities after incubation with 10 µM of the individual compounds are shown, along with horizontal lines depicting the average % enzyme activity obtained with all compounds, as well as an indication of the confidence interval of the results, expressed as the average activity ± 3 x SD. Percentage activity obtained with MSO and PhosT is shown in blue. Candidate inhibitors previously identified in the adenylylated GS screen are shown as red data points. Additional compounds selected for further evaluation are shown as green data points.

With the adenylylated enzyme, the percentage enzyme activities in the presence of the individual compounds varied widely, producing a pronounced scatter of values around the mean and consequently a very wide confidence interval (Figure 3.7 B). This complicated the selection of candidate inhibitors. Nonetheless, the 4 existing inhibitors (red data points, Figure 3.7 B) were amongst the 14 most active compounds, with 10057 yielding an inhibition of 100%. Six additional compounds were selected as candidate inhibitors for further evaluation (5, 5002, 5012, 5016, 5029 and 10059 - green data points, Figure 3.7 B). Note that compound 10059 (the green data point furthest to the right in Figure 3.7 A and B) had also been identified in the deadenylylated enzyme screen. The percentage inhibition obtained for the existing and new inhibitors are displayed in Table 3.8 (the "Exp1" columns).

3.3.6 Assay Characteristics – Phosphate vs. HPLC assay

GS catalyses the reversible conversion of L-glutamic acid, ATP and ammonia to L-glutamine, ADP and inorganic phosphate via a γ-glutamyl phosphate intermediate. A standard assay therefore applied to measure GS activity is the HPLC quantification of ADP formed from ATP. However, this assay is reasonably labour- and resource-intensive and not ideally suited for medium-throughput inhibitor screens in a 96-well microtitre plate format. We therefore investigated a colorimetric assay based on the formation of the inorganic phosphate and the use of molybdate to create a chromophore measurable at 820 nm. As an alternative to the molybdate-based phosphate assay, the BioVision™ phosphate assay kit for colorimetric inorganic phosphate quantitation was also explored.

3.3.6.1 Data processing

For the molybdate phosphate assay, percentage GS enzyme activity was calculated as:

%GS activity = [mean OD_{820} (inhibitor) – mean OD_{820} (background control)] / [mean OD_{820} (+DMSO control) – mean OD_{820} (background control)] x 100.

For the colorimetric kit assay, percentage GS activity was calculated as above; using OD_{620} instead, while activity in the HPLC assay was calculated using ADP area under the curve as opposed to OD.

3.3.6.2 Correlation between colorimetric phosphate and HPLC ADP assays

To investigate the agreement between enzyme inhibition results obtained with the three assays, deadenylylated *M.tb* GS was incubated with a limited panel of 29 experimental GS inhibitors as well as reference standard inhibitors (PhosT - compound 1; MSO - compound 2) at a fixed single inhibitor concentration of 10 µM. The percentage residual enzyme activity obtained for each inhibitor was determined with the three assays in parallel and the results compared.

The bar graph in Figure 3.8 graphically depicts the percentage GS activity obtained with each inhibitor (inhibitor identity numbers are displayed on the X-axis) using the three parallel assays.
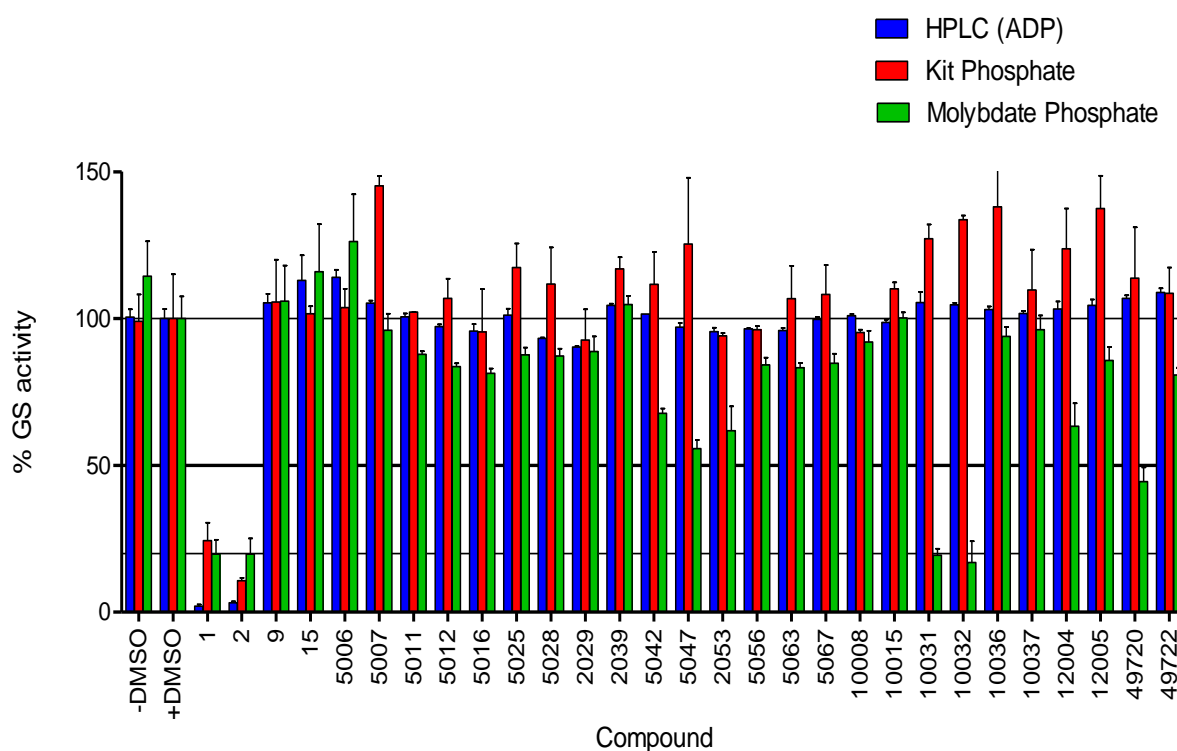

Figure 3.8: Correlation of deadenylylated *M.tb* GS inhibitory activities of 10 µM test compounds, as measured by the molybdate-based and kit-based inorganic phosphate assays, respectively, as well as the HPLC-based ADP assay. Where not shown, error bars fall within symbols.

The reference inhibitors 1 and 2 significantly inhibited GS activity by 76%-99% according to all three assays. However, some inconsistencies between the assays were found with the remaining experimental inhibitors, particularly with the molybdate-based phosphate assay (e.g. compounds 10031 and 10032). To better

illustrate the assay result correlations, percentage enzyme activity obtained with the HPLC ADP assay was compared with the respective colorimetric phosphate assays using X-Y plots, as shown in Figure 3.9 A and B.
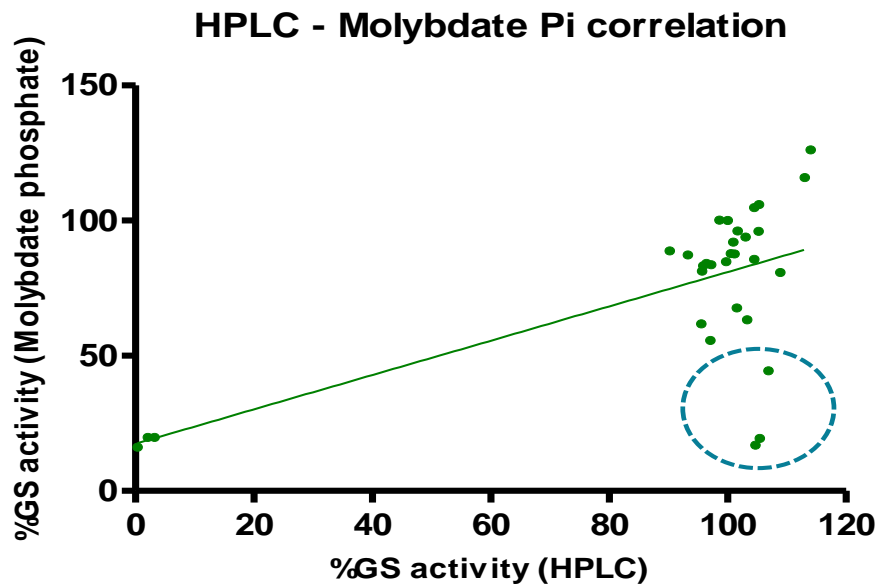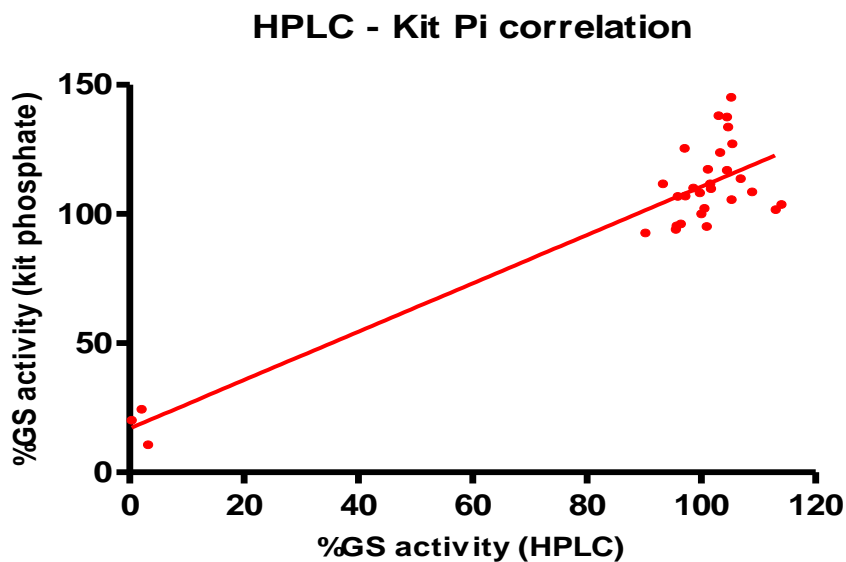
A

B

Figure 3.9: Correlation of deadenylylated *M.tb* GS enzyme activity in the presence of 10 µM test compounds, as measured by the HPLC-based ADP assay and the molybdate-based inorganic phosphate assays **(A)** and kit-based inorganic phosphate assay **(B)**.

As seen from the correlation graphs, the kit phosphate assay provides a better correlation of enzyme inhibitory activity with the HPLC assay than the molybdate phosphate assay. The latter appears to yield several false positives (denoted by the circled data points in Figure 3.9 A).

3.3.6.3 Further comparison of colorimetric phosphate and HPLC ADP assays for GS activity

Based on its better correlation with the HPLC assay compared to the molybdate assay, as discussed above, the BioVision™ phosphate assay kit was provisionally selected for multi-well plate screens of potential GS inhibitors. To further assess its utility as a GS activity screening method, additional parameters were explored. A screen of the entire panel of 213 compounds was carried out using deadenylylated and adenylylated *M.tb* GS. In parallel, GS activity in the presence of 10 µM compounds was measured by quantifying ADP levels by HPLC, or inorganic phosphate levels using the BioVision™ phosphate assay kit. Three parameters were investigated:

i)   Intra-plate reproducibility - an indication of the precision with which replicate measurements are made. The coefficient of variation (CV %) was calculated for 27 well replicates on the first plate of the individual assays as CV% = standard deviation/replicate mean x 100. The average of the 27 CV% values is presented in Table 3.3.

ii)   Inter-plate reproducibility - the mean ADP or phosphate levels obtained for the positive control wells (enzyme without inhibitor) on 5 different plates were averaged and the coefficient of variation determined as a percentage.

iii) The Z'-factor value was calculated for 5 plates from the respective assays, and the average value is presented in Table 1. The Z' is derived from the mean and standard deviations of the positive control wells (enzyme, no inhibitor) and blank wells (no enzyme, no inhibitor) on each plate: $Z' = 1-[3*(SD_{pos} + SD_{blank})/(Mean_{pos}-Mean_{blank})]$. Z'~1.0 indicates an ideal assay, while Z' ≥0.5 is indicative of a very good assay in terms of dynamic range (assay window between positive signals and background) and precision. Z' <0 is suspect.

Table 3.4: Reproducibility and precision of GS enzyme activity determinations in the presence of 10 µM test compounds, as measured by the HPLC-based ADP assay and the BioVision™ phosphate assay kit for the determination of inorganic phosphate.

Parameter	Deadenylylated *M.tb* GS		Adenylylated *M.tb* GS	
	Pi kit	HPLC ADP	Pi kit	HPLC ADP
Intra-plate CV% (n=27)	2.0	14.0	3.0	14.7
Inter-plate CV% (n=5)	3.4	12.7	6.9	17.5
Average Z' (n=5)	-0.07	0.78	0.28	0.76

The results presented in Table 3.4 suggest that both the HPLC and phosphate kit assays yield very precise and reproducible GS activity results, as judged from the low CV. In fact, the phosphate kit produces more reproducible well replicate and inter-plate readings. However, the kit assay produced very poor Z'-factor values, compared to the corresponding values for the HPLC assay. This is brought about by very high background absorbance readings obtained with the phosphate kit, which seriously reduces the assay window between positive and background signals. In fact, in follow-up assays, the window was often reduced even further, thus rendering the assay useless for expressing fractional inhibitory activities of test compounds. For this reason, the quantification of ADP by HPLC was adopted as the assay method for all subsequent compound screens.

3.3.7 Assay Characteristics - Pre-incubation assay

In the standard GS assay, compounds and substrates are mixed with the enzyme simultaneously immediately prior to incubation. However, it was later found that pre-incubation of the enzyme with compounds prior to substrate addition enhanced the inhibitory effect of compounds. The pre-incubation protocol was therefore used in several fixed concentration screens and dose-response assays. To further evaluate the reproducibility and precision of the assay, the data obtained from 3 assays was used to calculate intra-plate reproducibility (precision of ADP readings from replicate

wells), inter-plate reproducibility (reproducibility of ADP readings obtained for positive control wells in separate plates) and average Z' values (overall assay window and precision obtained per plate). The data from 5 separate assays was further used to calculate inter-assay reproducibility (the reproducibility of ADP readings for positive controls on the first plate of 5 assays carried out on separate occasions). The reproducibility parameters were expressed as CV, calculated as the standard deviation/mean x 100. Results are shown in Table 3.5.

Table 3.5: Reproducibility and precision of GS enzyme activity determinations, as measured by the HPLC-based ADP assay using the pre-incubation protocol.

Parameter		Deadenylylated *M.tb* GS			Adenylylated *M.tb* GS		
		Assay 1	Assay 2	Assay 3	Assay 1	Assay 2	Assay 3
CV %	Intra-plate (n=27*, 39**)	4.7	9.5	4.2	10.5	8.3	21.7
	Inter-plate (n=5*, 3**)	4.1	8.2	3.0	51.9	13.9	20.4
	Inter-assay (n=5)	53.7			22.8		
	Average Z' (n=5*, 3**)	0.97	0.75	0.83	0.75	0.56	0.49

 * Assay 1; ** Assay 2 and 3.

All parameters were calculated using the ADP area under the curve values obtained by HPLC. CV was calculated as standard deviation/mean x 100. Assay 1, 2 and 3 refer to the fixed concentration compound screen and two subsequent compound dose-response assays, respectively. To calculate inter-assay reproducibility, data from two additional dose-response assays carried out with MSO and PhosT was used. For inter-plate and inter-assay CV calculations, ADP values obtained in positive control wells of individual plates was used. For intra-plate CV calculations, ADP values obtained from replicate wells containing compounds was used.

In general, results obtained with the deadenylylated *M.tb* GS enzyme were more precise and reproducible than those obtained with adenylylated enzyme, as evidenced by the lower CV values. An exception is the inter-assay reproducibility, which produced a lower CV in the case of the adenylylated enzyme. Importantly, the inter-assay CV values suggest that the enzyme activities in separate assays were

reasonably comparable, despite the fact that different batches of enzyme were used in each case.

3.3.8 HeLa cytotoxicity assay

In the preceding screens with the *M.tb* GS enzyme (see sections 3.3.3 to 3.3.5), four inhibitors (5009, 5024, 10057 and 12004) showed promising inhibition of adenylylated GS. To assess the overt cytotoxicity and potential selectivity of the inhibitors, they were incubated with the human HeLa cell line and their effect on cell numbers determined. The standard GS inhibitors MSO and PhosT were also included, as well as a cytotoxic control compound, emetine. The amount of cells present after incubation was determined using the colorimetric protein-binding dye sulforhodamine B (see Methods, section 3.2.5) and expressed as percentage cell viability relative to untreated controls. To quantify cytotoxicity, dose-response plots of percentage cell viability vs. log compound concentration were prepared, in order to derive the 50% inhibitory concentrations (IC_{50}) of the individual compounds (Figure 3.10; Table 3.6)
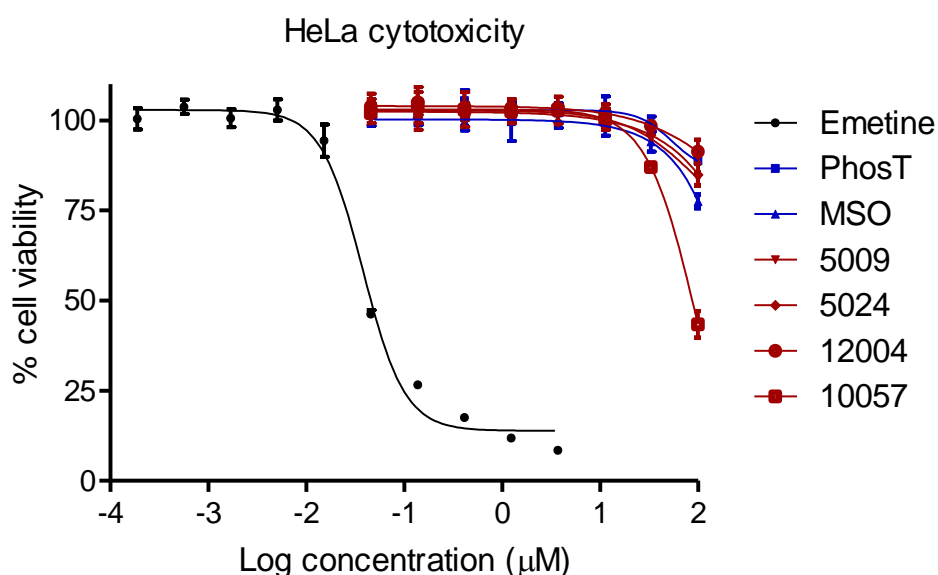

Figure 3.10: HeLa cell cytotoxicity determination. The percentage cell viability after incubation with serial dilutions of the individual test compounds vs. log compound concentration is shown. Lines were fitted by non-linear regression analysis using GraphPad Prism. Each data point is the mean of three replicate wells. Where not shown, error bars fall within symbols.

Table 3.6: HeLa cell cytotoxicity IC_{50} values. IC_{50}s were calculated by non-linear regression analysis using GraphPad Prism.

No.	Compound	IC_{50} (μM)	Estimated IC_{50} *
1	Emetine	0.04	
2	Phosphinotricin	>100	218.0
3	L-Methionine Sulfoximine	>100	235.5
4	5009	>100	321.2
5	5024	>100	323.4
6	12004	>100	239.9
7	10057	50 - 100	87.5

*The IC_{50}s are estimates based on the trends of the dose-response curves in Figure 3.6 accurate IC_{50}s could not be derived due to the incomplete sigmoidal dose-response plots.

The reference standard compound (emetine) yielded an IC_{50} of 0.040 μM, which is in close agreement with the average IC_{50} of 0.043 μM obtained for emetine in previous sulforhodamine B cytotoxicity assay experiments (Larsson *et al.,* 2012). By contrast, none of the experimental compounds significantly reduced cell numbers at the highest test concentration of 100 μM, and only one compound had an estimated IC_{50} below this concentration (10057 - 87.5 μM). The assay Z'-factor for the compounds ranged from 0.93 - 0.96, demonstrating excellent assay windows and accuracy. The results suggest that the compounds do not possess significant overt cytotoxicity.

3.3.9 Evaluation of LogD and Caco-2 permeability of hit compounds

LogD and Caco-2 permeability of the four candidate inhibitors of adenylylated *M.tb* GS identified in the earlier screen was assessed by an international service provider (Cerep). Results obtained are presented in Table 3.7.

LogD is a pH-dependent partitioning coefficient that is experimentally determined by quantitating the distribution of a compound between a water phase (buffered at pH 7.4) and an organic phase (n-octanol). As such, it is a measure of the lipophilicity of a compound at physiological pH, which in turn affects the solubility, permeability, protein binding, distribution, metabolism and general *in vivo* pharmacokinetic behaviour of the compound. Lipophilic compounds (LogD >5) tend to be subject to

more rapid metabolism and higher protein binding, coupled with poor solubility, which can lead to low bioavailability. Conversely, hydrophilic compounds (LogD <0) are highly soluble but their membrane permeability and oral absorption is compromised. To achieve a good balance between solubility and lipophilicity, a compound should thus have a LogD of 0-5. The results obtained from an international service provider (Cerep) (Table 3.7 A) indicate that compounds 5024, 12004 and 10057 have LogD values in the desired range (0.85, 0.89 and 4.21 respectively), while compound 5009 is more hydrophilic (-0.82).

Table 3.7: LogD **(A)** and Caco-2 permeability **(B)** results obtained from Cerep for the candidate *M.tb* GS inhibitors 5009, 5024, 10057 and 12004.

A

Assay (LogD, n-octanol PBS, pH7.4)	Inhibitor I.D.	Test Concentration(M)	Weighted Average of Three Replicates
Partition Coefficient	5009	0.0001	-0.82
Partition Coefficient	5024	0.0001	0.85
Partition Coefficient	10057	0.0001	4.21
Partition Coefficient	12004	0.0001	0.89

B

Compound Assay (TC7, pH6.5/7.4)		Permeability (10^{-6}cm/s)			Percent Recovery (%)		
		1st	2de	Mean Permeability	1st	2de	Mean Recovery
5009	A-B Permeability	0.01	0.01	<0.01	102	96	99
5024	A-B Permeability	58.30	54.93	56.6	111	109	110
10057	A-B Permeability	39.62	41.91	40.8	63	63	63
12004	A-B Permeability	0.10	0.10	<0.1	93	105	99

Caco-2 permeability is a measure of the ability of a compound to cross an intact intestinal epithelium cell monolayer and thus predicts the oral absorption of a compound. Compounds with a permeability of >20 x10^{-6} cm/s are regarded as highly

permeable, while values <2 x10^{-6} represent low permeability. The Cerep results (Table 3.7 B) show that compounds 10057 and 5024 yield high permeability values (40.8 x10^{-6} and 56.6 x10^{-6} cm/s respectively) and are thus predicted to be well absorbed from the intestinal tract. By contrast, compound 12004 has low permeability. As expected from the hydrophilicity of compound 5009 (LogD <0), it demonstrates very poor permeability in the Caco-2 system (<0.01 x10^{-6} cm/s).

3.3.10 Pre-incubation *M.tb* GS assay - further evaluation of candidate inhibitors

In total, 7 compounds were earmarked as new candidate *M.tb* GS inhibitors after the pre-incubation protocol screens, in addition to the 4 identified in the first screening round. The 11 inhibitors were subsequently subjected to three additional rounds of screening against adenylylated and deadenylylated *M.tb* GS using pre-incubation at 10 µM, in order to confirm their inhibitory activities, as well as to explore their selectivity's for one form of the enzyme vs. the other. The average percentage inhibition and corresponding standard deviation obtained for each compound over the 4 separate assays are shown in Table 3.8 and Figure 3.11. Based on the relative average inhibition of the adenylylated and deadenylylated enzymes, the compounds were provisionally categorized as selective for either of the two forms, or non-selective (Table 3.8). One compound (5045) displayed significant selectivity for the deadenylylated enzyme; while 4 compounds suggested specificity for adenylylated GS and 6 appeared relatively non-selective. The latter category included the two most active test compounds; 10057 and 10059.

Table 3.8: Fixed concentration evaluation of 11 candidate inhibitors in *M.tb* GS enzyme assays using the pre-incubation protocol. The percentage enzyme inhibition obtained with the compounds (10 µM final concentration) in 4 separate screens is shown, along with the average inhibition for each compound over the 4 screens and the corresponding SD. The colour coding of the highlighted table cells is clarified in the bottom legend.

Adenylylated *M.tb* GS (% inhibition)						Deadenylylated *M.tb* GS (% inhibition)					
Comp. (10µM)	Exp 1	Exp 2	Exp 3	Exp 4	AVG	SD	Exp1	Exp 2	Exp 3	Exp 4	AVG	SD
PhosT	100	95	97	100	98	2	100	98	100	100	100	1
MSO	100	100	96	100	99	2	100	100	99	100	100	1
5	48	33	40	29	38	8	0	0	6	0	2	3
5002	68	40	38	35	45	15	0	10	8	14	8	6
5009	37	50	50	22	40	13	57	41	44	44	47	7
5012	55	31	32	42	40	11	14	16	4	24	15	8
5016	51	43	46	30	43	9	7	19	3	13	11	7
5024	46	48	43	36	43	5	49	44	52	44	47	4
5029	79	46	56	60	60	14	5	8	7	9	7	2
5045	0	0	0	0	0	0	44	45	54	48	48	5
10057	100	99	98	100	99	1	67	62	47	58	59	9
10059	82	99	82	100	91	10	49	48	36	43	44	6
12004	39	32	33	30	34	4	50	43	38	38	42	6

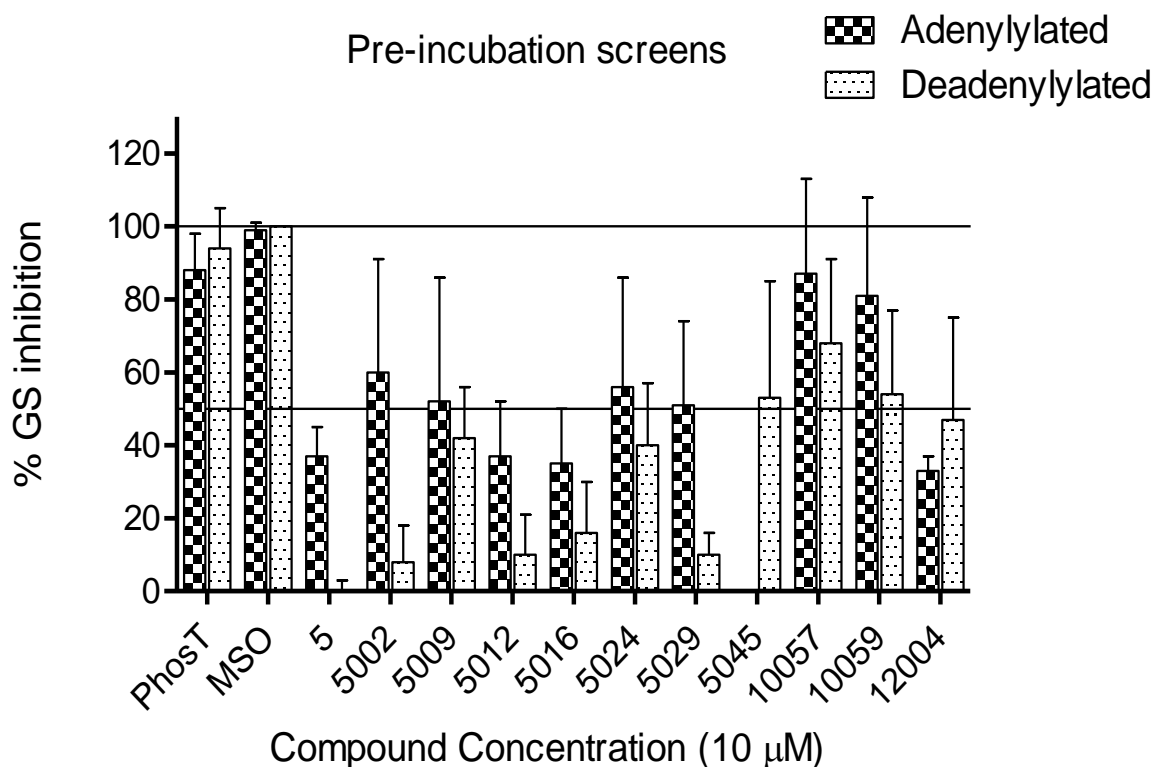|	
	Non-selective
	Adenylylated
	Deadenylylated

Figure 3.11: Fixed concentration evaluation of 11 candidate inhibitors in *M.tb* GS enzyme assays using the pre-incubation protocol. The average percentage GS inhibition obtained for each compound over the 4 independent screens against the deadenylylated and adenylylated forms of the enzyme is plotted. Error bars represent standard deviation. Where not shown, error bars fall within symbols.

3.3.11 Mammalian GS assay

To assess the species selectivity of the compounds and their potential for toxicity or side-effects, the 11 candidate inhibitors selected and evaluated using the pre-incubation *M.tb* GS assay protocol were further screened using the same approach against mammalian GS (mGS) isolated from bovine liver. Percentage inhibition of mGS by the compounds at a final concentration of 10 µM ranged from 0 - 40% (Figure 3.12, Table 3.9). The two standard GS inhibitors PhosT and MSO both inhibited the bovine enzyme by 100%. A concern is the fact that the two most potent *M.tb* GS inhibitors (10057 and 10059) also appeared to have the most effect on mGS activity, which could be a source of side-effects in further development. Based on the average inhibitory values obtained for the compounds against adenylylated *M.tb* GS (Table 3.8), 10057 displayed a 2.9-fold selectivity for the *M.tb* enzyme,

compared to 2-fold in case of 10059 (Table 3.9). The activity of 10057 against the bovine GS enzyme might be related to the fact that it displayed signs of some cytotoxicity in the HeLa cell assay (estimated IC_{50} = 87.5 µM; Table 3.5).
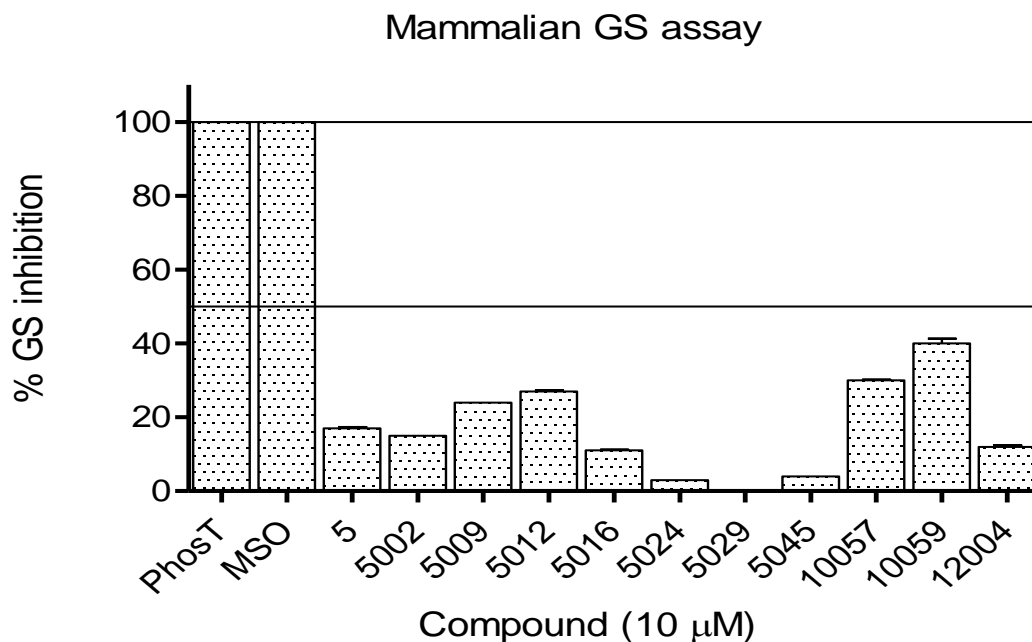

Figure 3.12: Fixed concentration evaluation of 11 candidate inhibitors in an mGS enzyme assay using the pre-incubation protocol. Where not shown, error bars fall within symbols.

Table 3.9: Fixed concentration evaluation of 11 candidate inhibitors in a mammalian GS (mGS) enzyme assay using the pre-incubation protocol. Results obtained against adenylylated *M.tb* GS are extracted from Table 3.7.

Compound	% mGS inhibition	SD	Average adenylylated *M.tb* GS inhibition %	-fold selectivity
PhosT	100	0.0	88	0.9
MSO	100	0.0	99	1.0
5	17	0.4	37	2.2
5002	15	0.0	60	4.0
5009	24	0.0	52	2.2
5012	27	0.4	37	1.4
5016	11	0.2	35	3.2
5024	3	0.0	56	18.7
5029	0	0.0	51	?
5045	4	0.0	0	0.0
10057	30	0.2	87	2.9
10059	40	1.3	81	2.0
12004	12	0.4	33	2.8

3.3.12 *M.tb* GS dose-response assays

To obtain a more accurate reflection of the activity and adenylylated vs. deadenylylated selectivity of the 11 candidate inhibitors, dose-response assays were performed on the 2 forms of the enzyme to derive compound IC_{50} (50% inhibitory concentration) values. Dose-response assays were initially performed using a pre-incubation protocol with the standard inhibitors PhosT and MSO. Based on the results, IC_{50} values derived from the dose-response curves suggested, firstly, that adenylylated *M.tb* GS is more sensitive to inhibition by the standards than the deadenylylated form of the enzyme and, secondly, that PhosT is a more potent inhibitor of the *M.tb* enzymes than MSO (Figure 3.13).
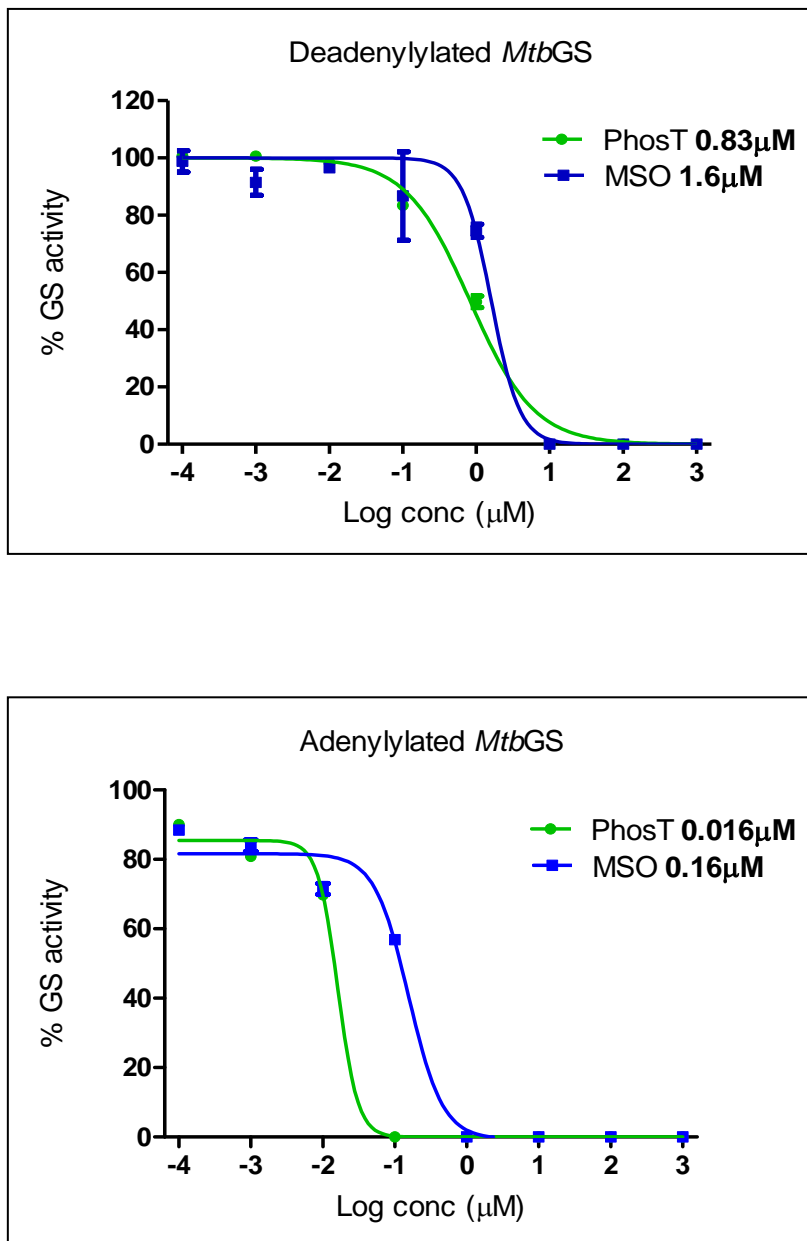
Figure 3.13: Dose-response assays for MSO and PhosT standard inhibitors. Percentage GS activity was plotted against log (compound concentration) and sigmoidal dose-response curves fitted to the data points using non-linear regression analysis. The curves were used to derive the IC_{50} values for the inhibitors (displayed in the top right legend). Where not shown, error bars fall within symbols.

Subsequently, the panel of 11 candidate inhibitors was subjected to two separate dose-response assays. In the first (Table 3.10, Assay 3), the highest final starting concentration for the serial compound dilutions was 100 µM, which was increased to 200 µM for the second assay (Table 3.10, Assay 4). Attempts to use higher starting

concentrations were thwarted by the appearance of visible precipitates in most of the compound wells. Table 3.10 summarizes the IC_{50} evaluations for the test compounds, as well as values obtained for PhosT and MSO in concurrent assays.

Table 3.10 Dose-response assays for MSO, PhosT and 11 candidate *M.tb* GS inhibitors. The latter were assayed on two separate occasions (Assay 3 and 4) using adenylylated and deadenylylated *M.tb* GS. Where relevant, IC_{50} values were derived from non-linear regression analysis of dose-response curves (Figure 3.10).

Compound	Adenylylated GS IC_{50} (µM)				Deadenylylated GS IC_{50} (µM)			
	Assay 4	Assay 3	Assay 2	Assay 1	Assay 4	Assay 3	Assay 2	Assay 1
1 (PhosT)	~0.001	0.37	0.016	0.016	0.11	0.33		0.83
2 (MSO)	0.07	3.42	0.16	0.14	0.44	2.76		1.6
5	>200	>100			>200	>100		
5002	>200	>100			>200	>100		
5009	>200	>100			>200	>100		
5012	>200	>100			>200	>100		
5016	>200	>100			>200	>100		
5024	>200	>100			>200	>100		
5029	>200	>100			>200	>100		
5045	>200	>100			>200	>100		
10057	3.51	15.6			13.2	17.3		
10059	3.56	31.2			17.1	19.2		
12004	>200	>100			>200	>100		

For reasons that are unclear, besides compounds 10057 and 10059, the candidate inhibitors failed to inhibit either form of the enzyme sufficiently to produce dose-response curves, resulting in predicted IC_{50}s above the highest starting concentrations of the compounds. This is in contrast to the fact that they repeatedly demonstrated inhibitory activity against either or both forms of *M.tb* GS at a fixed concentration of 10 µM. A possibility may be that the compounds form small aggregates invisible to the naked eye at high starting concentrations, resulting in serial dilutions that contain considerably less than the nominal concentration of active, monomeric compound. Nonetheless, compounds 10057 and 10059 produced dose-response graphs that were used to derive IC_{50} values for both (Figure 3.10).

The second assay (Assay 4) further suggests that the two compounds may be slightly more inhibitory (3.8 - 4.8 fold) towards the adenylylated form of *M.tb* GS.
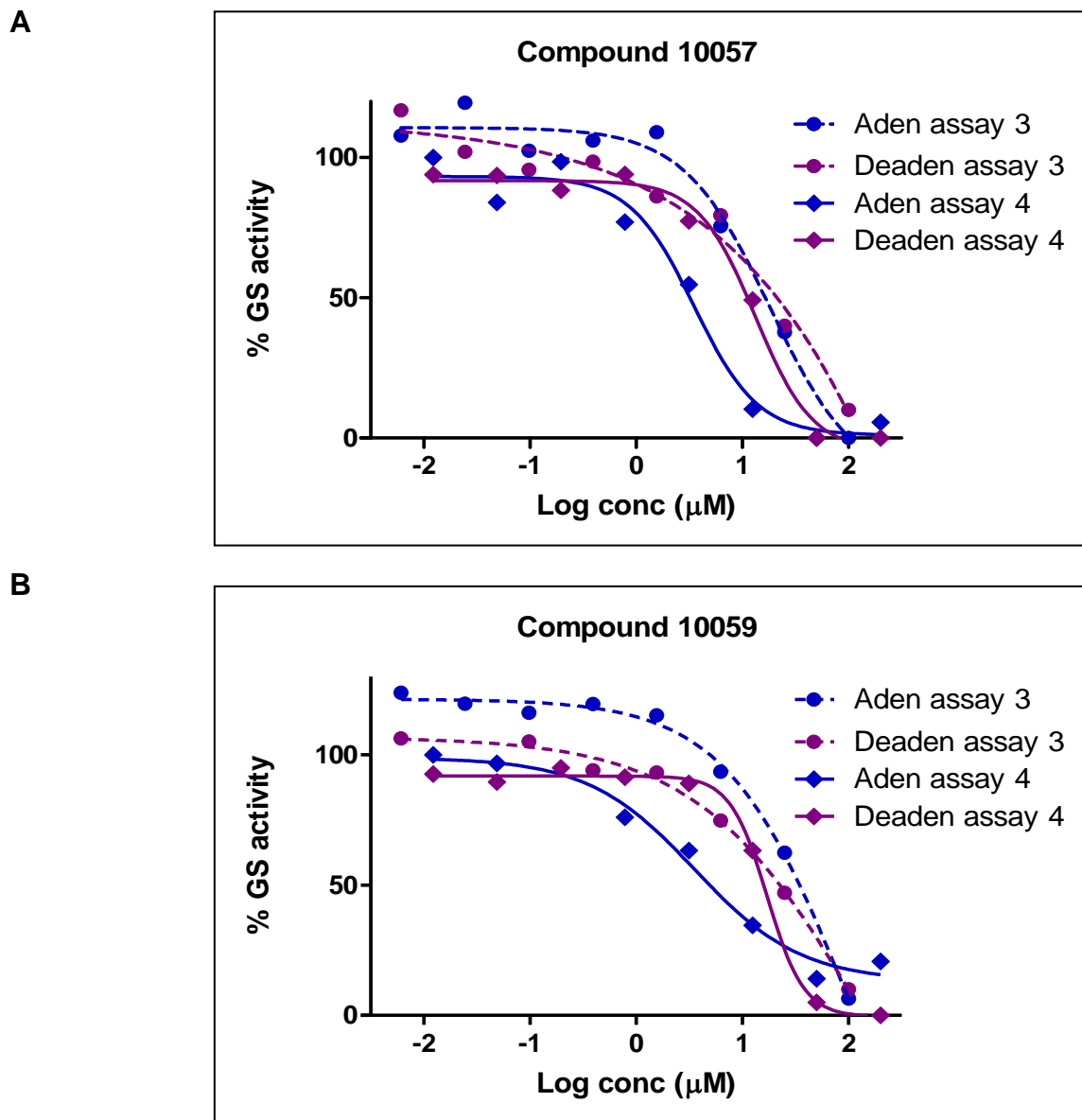
A

B

Figure 3.10: Dose-response assays for compounds 10057 and 10059, performed with adenylylated and deadenylylated *M.tb* GS in a pre-incubation protocol on two separate occasions (Assay 3 and 4). Percentage GS activity was plotted against log (compound concentration) and sigmoidal dose-response curves fitted to the data points using non-linear regression analysis. Where not shown, error bars fall within symbols.

A further concern is the variation in IC_{50} values obtained for the standard inhibitors MSO and PhosT using both forms of *M.tb* GS, but especially the adenylylated enzyme. The source of the variability is still unclear.

3.3.13 *M.tb* BACTEC 460TB™ assays

Compounds identified following the primary screening for enzymatic activity against adenylylated and deadenylylated *M.tb* GS were tested for antibacterial activity using a BACTEC 460TB™ assay with H37Rv reference strain. Compound 10057 showed approximately 50% growth inhibition at 100 µM on day 6 of incubation relative to the controls. However, the growth rate also increased over the period of incubation indicating that bacterial doubling is taking place although at a slower rate. All the other compounds and other concentrations showed no effect on mycobacterial growth rate (ΔGI) over the incubation period. Compounds 1 and 2 were MSO and PhosT and were included as controls in the study.

3.3.14 Intracellular drug testing in Mouse Bone Marrow-Derived Macrophages

Intracellular survival of *M.tb* (H37Hv/Beijing220) in mouse bone-marrow derived macrophages was monitored in response to compounds. A first batch of 6 compounds (10057, 5024, 12004 and 5009) were tested in the pilot test and compound 10057 showed activity at a concentration of 100 µM. The percentage killing exhibited by compound 10057 was about 93% as indicated in Figure 3.11.
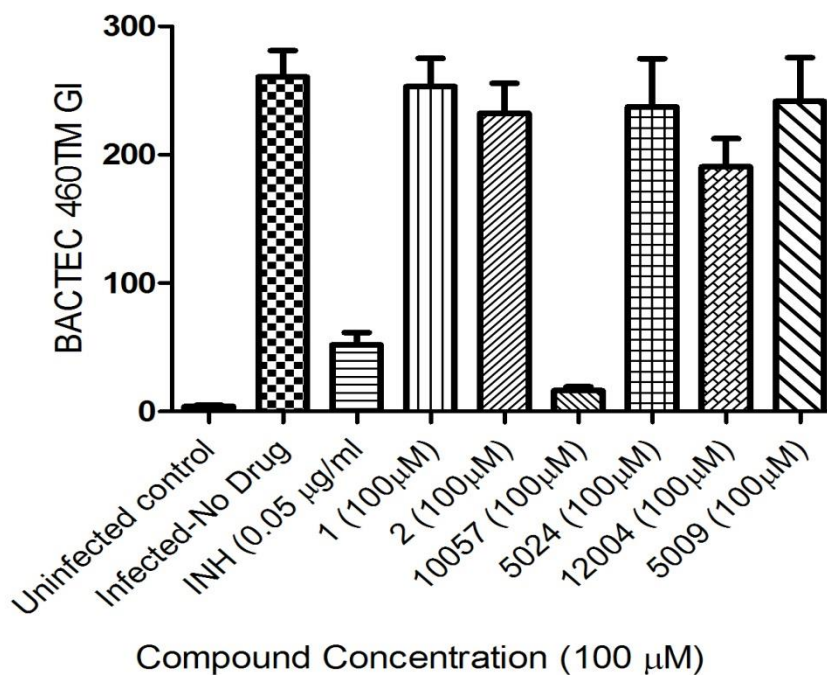
Figure 3.11: Intracellular survival of *M.tb* (H37Rv) in mouse bone-marrow derived macrophages after 5-day post-infection period followed by intervention on D5 PI with different compounds, MOI 2:1, 5 day incubation at 37°C, 5% CO_2. Cells were sacrificed on Day 2 Post Drug Intervention. Only Drug 10057 shows activity. But Drug 2 shows no activity in this initial screen, which may be due to the fact that Drug 2, was resuspended in DMSO instead of Water for this pilot test. Where not shown, error bars fall within symbols.

In the time course experiment (using the H37Rv lab strain) compound 2 was resuspended in water and showed activity on Day 2 post drug intervention. The percentage killing on Day 2 for compound 10057 was 73% at 100 µM and 27% at 50 µM.

The second batch of 7 compounds was provided for testing, namely (compounds 5, 5002, 5012, 5016, 5029, 5045 and 5059). In the pilot macrophage assay (using this time the clinical isolate Beijing220 MDR strain) only compounds 5029, 5045 and 5059 showed activity at a concentration of 100 µM (see Figure 3.12). The percentage killing exhibited by compounds 5029, 5045 and 5059 were 67%, 64% and 54% respectively at 100 µM. As a comparative control a new aliquot of compound 10057 was tested in the same assay. The percentage killing exhibited by compound 10057 at 100 µM in this assay was about 65%, which corresponds well with the result obtained in the time-course experiment (73%).
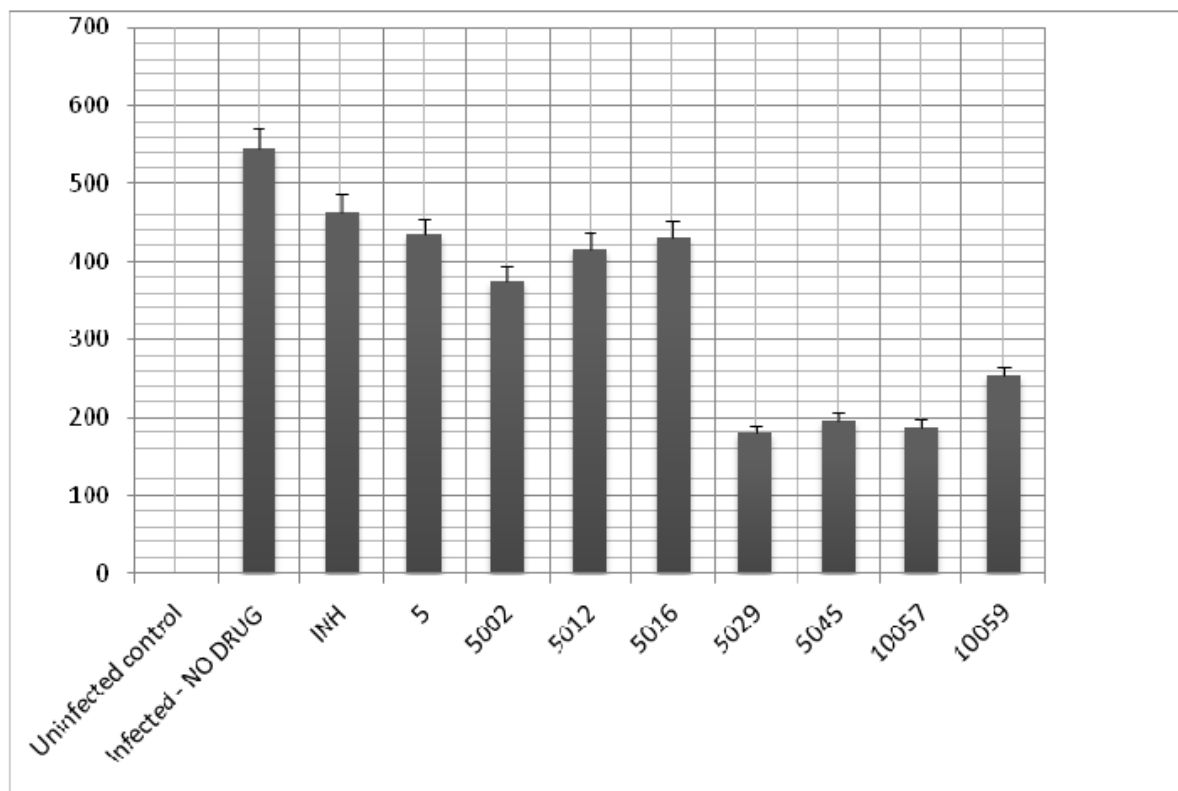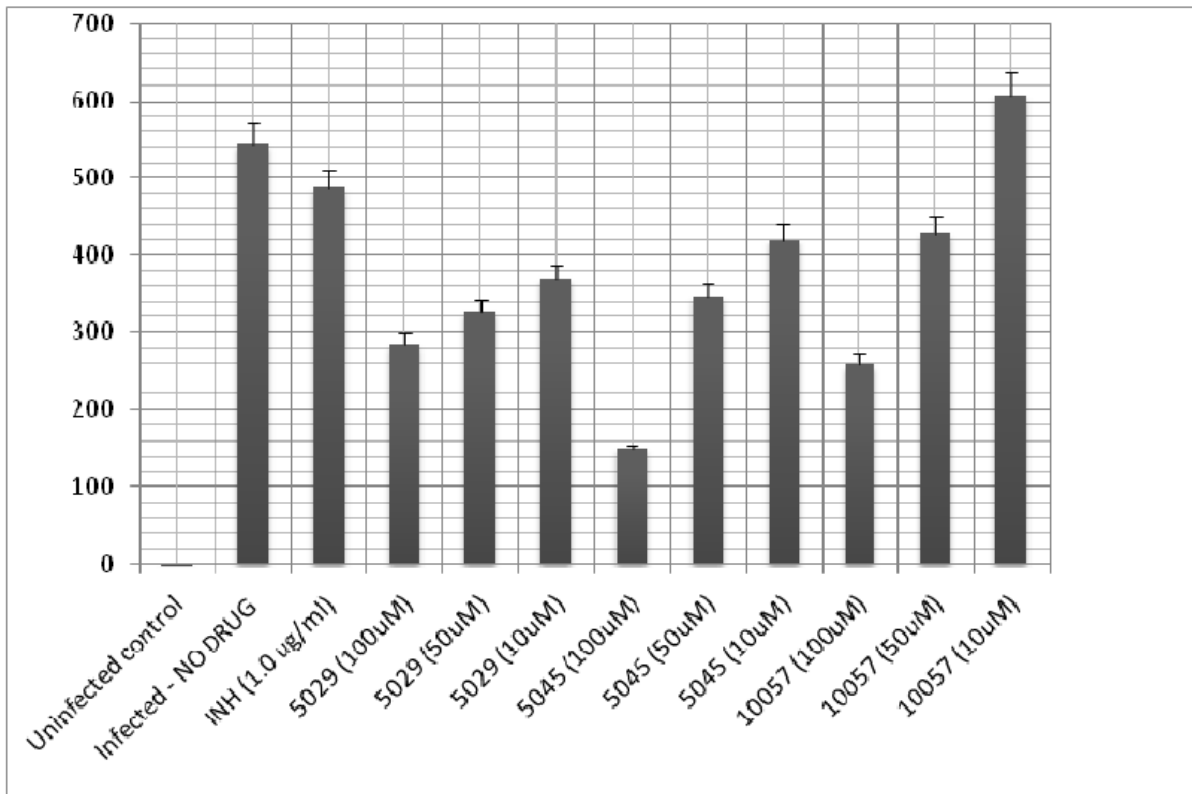
Figure 3.12: Intracellular survival of *M.tb* (H37Rv) in mouse bone-marrow derived macrophages after 5-day post-infection period followed by intervention on D5 PI with different compounds, MOI 2:1, 5 day incubation at $37^{\circ}C$, 5% CO_2. Cells were sacrificed on Day 2 Post Drug Intervention. Only Drugs 5029, 5045 and 10057 shows activity. Where not shown, error bars fall within symbols.

Compounds 5029, 5045 and 10057 were tested further at concentrations 10 µM, 50 µM and 100 µM for 3 days (see Figure 3.13). In this experiment drug 5045 showed the best activity (73% killing) at 100 µM which concurs with the results of the extracellular assay. However visually the mouse macrophages did appear more granular in the presence of drugs 5029 and 5045 at 100 µM, possibly indicates a toxic effect at this concentration.

Figure 3.13: Intracellular survival of *M.tb* (H37Rv) in mouse bone-marrow derived macrophages after 5-day post-infection period followed by intervention on D5 PI with different compounds, MOI 2:1, 5 day incubation at 37°C, 5% CO_2. Cells were sacrificed on Day 2 Post Drug Intervention. Drug 5045 showed the best activity (73% killing) at 100 µM. Where not shown, error bars fall within symbols.

3.4 Discussion

Several gaps exist in the TB drug development pipeline worldwide as very few new drugs or drug candidates are in the pipeline. Big pharmaceutical companies have not invested in TB drug development, as historically the disease did not pose a significant threat to the developed world. However, the threat of MDR-TB and the increased world demand for treatment of Latent TB Infection has prompted a number of global initiatives such as the Global Alliance for TB Drug Development and the Stop TB Partnership (WHO 2006); all aimed at ensuring a pipeline of new TB drug leads to ensure new more effective TB drugs enter clinical development.

The primary invention of this project relates to a biochemical pathway that yielded a new drug target that can be exploited to develop new therapies against *M.tb*. GS catalyses the conversion of glutamate to glutamine via a glutamyl phosphate intermediate, utilising ATP. ATP is utilized as either Mg-ATP or Mn-ATP, depending on the adenylylation state of the enzyme. The enzyme is regulated via adenylylation in bacteria containing the GS-1 form of the enzyme.

About 213 compounds were tested against the adenylylated and deadenylylated forms of both *M.tb* GS and *E.coli* GS at a concentration of 10 µM. The rational design and selection of these inhibitors were based on the typical ATP binding site.
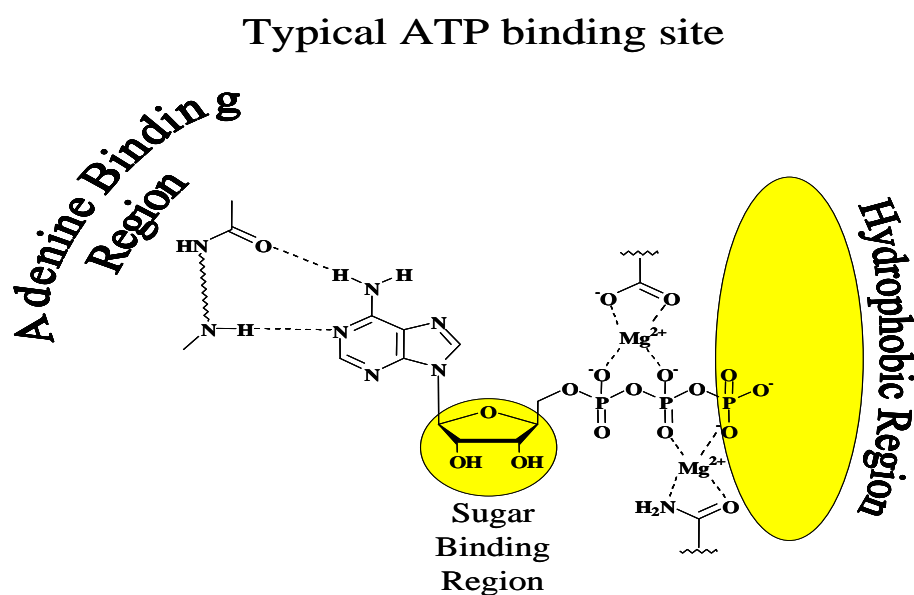

Figure 3.1: The basic structural characteristics of the ATP site (Traxler, 1996).

Approximately 213 compounds were tested for their ability to inhibit GS that had been synthesized and purified in both the adenylylated and deadenylylated forms. It has been shown that GS in the adenylylated form uses a novel histidine kinase-like reaction mechanism in the phosphorylation of the carboxyl of glutamate. The primary outcome of the project was the demonstration of the selective inhibition of adenylylated GS and the identification of specific compounds capable of inhibiting adenylylated GS.
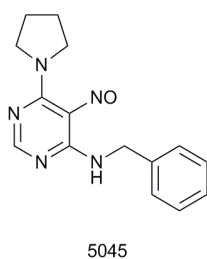
Compounds showing activity towards the adenylylated and/or deadenylylated forms of *E.coli* and *M.tb* GS enzymes at a single micromolar (µM) concentration were confirmed with repeated testing before being evaluated with full dose-responses to assess IC_{50} values and rank the order of potencies towards the adenylylated and deadenylylated forms of *E.coli* and *M.tb* GS. Compounds showing activity for the adenylylated or deadenylylated forms of the *M.tb* GS enzyme were further assessed for selectivity *vis-à-vis* the mammalian enzyme and for antibacterial action in a cellular model of *M.tb* infection. Any compound showing a selective activity for the adenylylated versus the deadenylylated and mammalian forms of the enzyme could be considered for further hit-to-lead and lead optimisation campaigns for the development of novel candidates for the treatment of TB.

The following inhibitors were identified as possible inhibitors of *M.tb* GS. The chemical structures and their selectivity are shown in Figure 5.

Non-selective:
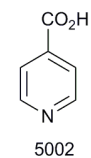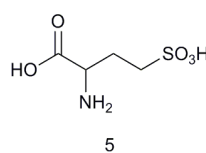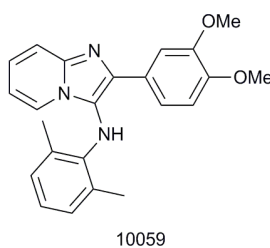

12004

5009

5024

Deadenylylated selective:

5045

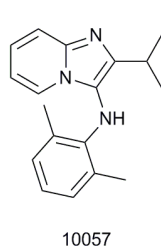Adenylylated selective:
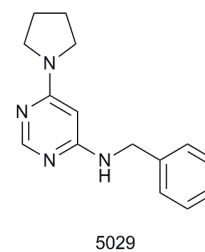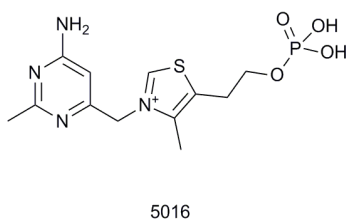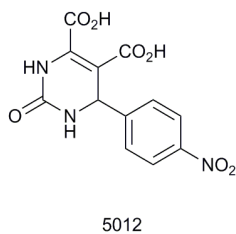

5012

5016

5029

10057

10059

5

5002
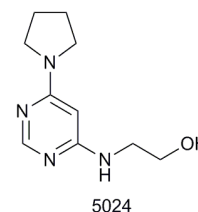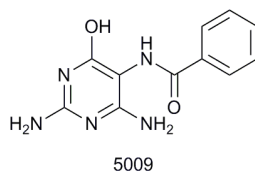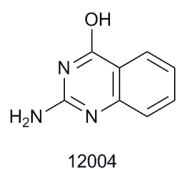
Figure 5: Chemical structures of the 11 synthesized ATP scaffold-based inhibitors which shown promising inhibition of *M.tb* GS enzymes. They are divided into three distinct groups non-selective, deadenylylated selective and the adenylylated selective.

Based on the dose-response assays, compounds 10057 and 10059 have emerged as the most promising anti-*M.tb* GS inhibitors with IC_{50} (µM) values of 9.6 µM and 17.4 µM respectively. They have regularly produced the most potent inhibitory activity against *M.tb* adenylylated GS enzyme in fixed concentration screens with 87% and 81% respectively. Compounds 10057 and 10059 are structurally very similar as indicated in Figure 6 below. In the case of 10057, preliminary ADME properties (LogD, permeability) are favourable with a value of 4.21. In further development, attention may be paid to improving the selectivity of the compounds *vis-à-vis* mammalian forms of GS, to reduce the possibility of side-effects as inhibitory activity of 30% and 40% respectively were observed. These compounds also showed selective inhibition of the adenylylated *M.tb* GS.

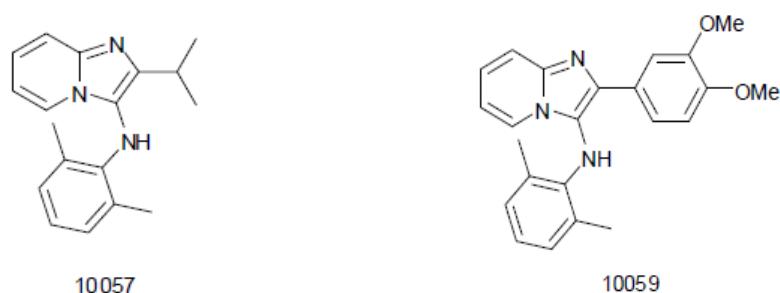**Figure 6:** Chemical structures of compounds 10057 and 10059 which have emerged as the most promising anti-*M*.tb GS inhibitors.

These two compounds that have been found to be inhibitory to *M.tb* GS may now be used as templates to synthesize additional target specific compounds as part of a lead optimisation programme and further optimised to yield a suitable drug candidate for clinical evaluation.

Chapter 4

The effect of deuterated ATP on *E.coli* and *M.tb* Glutamine synthetases regulation

4.1 Introduction

4.1.1 Enzyme Kinetics

Enzymes catalyse numerous reactions in nature, often causing spectacular accelerations in the catalysis rate. One aspect of understanding how enzymes achieve these feats is to explore how they use the limited set of residue side chains that form their 'catalytic toolkit'. Combinations of different residues form 'catalytic units' that are found repeatedly in different unrelated enzymes. Most catalytic units facilitate rapid catalysis in the enzyme active site either by providing charged groups to polarize substrates and to stabilize transition states, or by modifying the pKa values of other residues to provide more effective acids and bases. Given recent efforts to design novel enzymes, the rise of structural genomics and subsequent efforts to predict the function of enzymes from their structure, these units provide a simple framework to describe how nature uses the tools at her disposal, and might help to improve techniques for designing and predicting enzyme function.

4.1.2 Mechanisms of enzyme catalysis

Enzymes, and the principles by which they perform catalysis, have been the subject of intense study for over a hundred years, in which time the mechanisms of many different enzymes have been investigated in great detail. Serine proteases, for example, have been the focus of countless structural (Perona and Craik, 1997), kinetic (Hedstron, 2002) and theoretical (Topf *et al.,* 2002; Ishida and Kato, 2004) studies. Even now, however, when the general principles that govern enzyme catalysis seem to be well understood (Blow, 2000), new theories continue to be proposed to explain puzzling aspects of enzyme catalysis (Williams *et al.,* 2004), and novel resources are being developed (Porter *et al.,* 2004) to answer ongoing questions about the evolution and mechanism of enzymes. For instance, how do enzymes catalyse the diverse range of reactions found in a cell with only a small set of different chemical groups? Of the 20 naturally occurring amino acids, only the 11 polar and charged residues are generally observed to engage directly in catalysis

(Bartlett, 2002). These residues fall into seven different chemical groups: imidazole (histidine), guanidinium (arginine), amine (lysine), carboxylate (glutamate, aspartate), amide (glutamine, asparagine), hydroxyl (serine, threonine, and tyrosine) and thiol (cysteine). Of course, enzymes also use metal ions (Williams, 2003), cofactors (Mure, 2004; Murataliev 2004) and water molecules (Hernick and Fierke, 2005) to aid catalysis. However, a source of catalytic power that does not require additional groups stems from the ability of catalytic residues to interact with each other and thus to affect each other's chemical properties (Harris and Turner, 2002). But not all combinations of residues are useful: some might have no effect on or even reduce the power of their component residues. By reviewing the available structural and biochemical data, one can show which combinations of residues are used by enzymes and how their interactions affect enzyme properties. We also need to consider some important aspects of enzyme chemistry, such as the role of hydrophobic residues, metal ions, cofactors or water, quantum effects or the importance of factors such as entropy and binding energy.

This investigation was undertaken to ascertain the extent to which the adenyl group within ATP plays a direct role in the regulation of ATP binding and/or phosphoryl transfer within glutamine synthase and thus enzyme catalysis. To this end the role of the C8-H of ATP on the binding and/or phosphoryl transfer on the enzyme activity was elucidated in comparative enzyme activity assays using ATP and ATP deuterated (See section 4.1.3) at the C8 position.

4.1.3 The identification and functionality of deuterium

Deuterium was first identified by Harold Clayton Urey in the study of physics in 1933 then introduced to chemistry and biological chemistry. Molecular deuteration is the substitution of normal hydrogen (protium) by deuterium (heavy hydrogen) atom in a compound (Tung, 2010).

The deuterium atom is an isotope of hydrogen, differing from normal hydrogen by containing one neutron and one proton in its nucleus, this results in a change in atomic mass from 1(AMU) to 2(AMU) which doubles the atomic mass of a normal

hydrogen (protium). The nucleus of deuterium is called deuteron while the nucleus of protium consists of one proton and has an atomic mass of 1(AMU) (Tung 2010; Bateau *et al.,* 2009 and Limbach *et al.,* 1990). Deuterium was firstly discovered by Urey, Brickwedde and Murphy in 1933 in the study of water electrolysis (Limbach *et al.,* 1990 and Wade *et al.,* 1999).

Deuteration of a molecule is as a result of a change in covalent bond between a carbon to hydrogen (C-H) and the carbon to deuterium (C-D) bond (Wade *et al.,* 1999). The compound being deuterated only shows insignificant physical property changes. These property changes include hydrophobicity, chemical molecular mass and pKa (Tung, 2010). The C-D bond formed when a molecule is fully deuterated is much stronger than the C-H bond of a normal compound causing a reduced reaction rate when comparing these molecules. The rate of reaction ratio of a deuterated molecule when compared with the reaction rate of an undeuterated molecule is called the Kinetic Isotope Effect (KIE=V_H/V_D). In this study we focus on imidazole and purine compounds which are aromatic compounds.

4.1.4 Functionality of ATP

The study carried out by Fiske and Subbarow in 1929 was the first to define the ATP molecule, and was then followed by Lipmann in 1941 who elaborated on the function and structure of ATP in the cell (Novak *et al.,* 2011). The ATP molecule consists of two regions: the polar and nonpolar moiety (Figure 4.1). The polar region consists of a ribose sugar and three phosphates while the nonpolar region comprises the adenine moiety. ATP is the energy source for all living organisms. It is essential because it plays many roles from transporting many ions across the concentration gradient of the cellular membrane, to control function and signalling of numerous systems in all living organisms (Salisu *et al.,* 2011).

4.1.5 Deuteration of ATP

The ATP adenine base is a heterocyclic aromatic compound with nitrogen atoms in its ring structure (Figure 4.1 A). It consists of a six membered ring attached to a five membered ring where both rings fulfil their aromatic properties by contributing electrons which are located on the p-orbital, with a lone pair of electrons in the sp^2-orbital which is perpendicular the p-orbital. These electron characteristics cause these molecules to be less reactive than other aromatic compounds. In ATP the protons (Figure 4.1 B) at position 2 and 8 are the first to be substituted during deuteration. The deuteration of the proton at position 2 is depended on pH thus the deuteration of the proton at position 8 will be deuterated first.
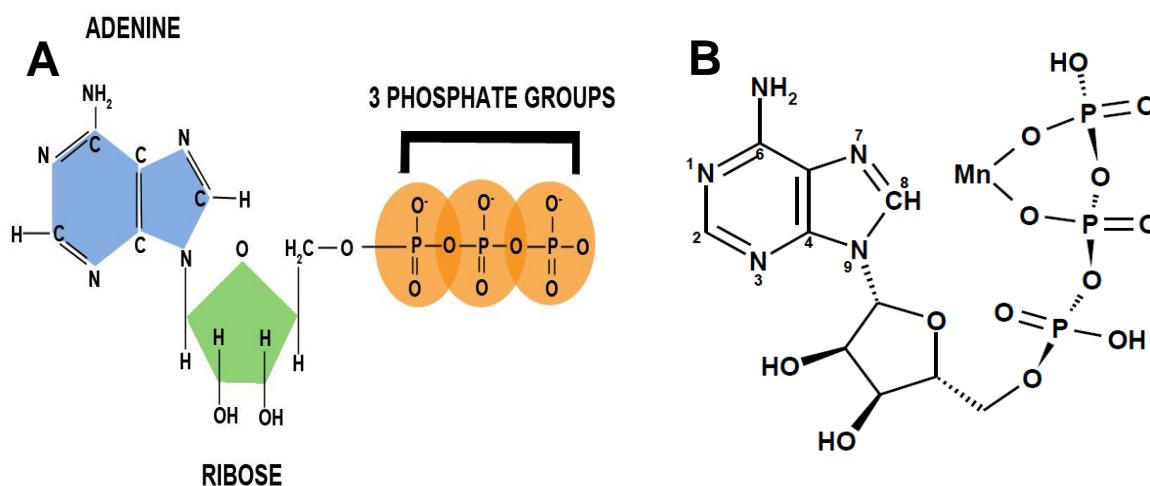
Figure 4.1: Schematic illustration of the structure of ATP: **A** ATP structure showing the nonpolar adenine moiety and the polar moiety consisting of the ribose sugar and phosphate moieties. **B** Atom numbering of the adenine moiety to show locations of the protons in the ATP structure to be substituted during deuteration.

Comparative assays were run to determine the effect of ATP and C8D-ATP on the specific activity of the enzymes investigated in Chapter 2 and 3, namely adenylylated and deadenylylated *E.coli* GS and adenylylated and deadenylylated *M.tb* GS.

4.1.6 Study Objectives

- Objective 1: To determine the specific activity of adenylylated and deadenylylated *E.coli* GS in the presence of ATP and C8D-ATP (deuterated ATP).

- Objective 2: To determine the specific activity of adenylylated and deadenylylated *M.tb* GS in the presence of ATP and C8D-ATP (deuterated ATP).

4.2 Methods

4.2.1 Construction, expression and purification of *E.coli* and *M.tb* GS

The construction, expression and purification of *E.coli* and *M.tb* GS is described and discussed in Chapter 2.

4.2.2 C8-D ATP synthesis

The synthesis of ATP deuterated at the C8 position (C8-D ATP) was carried out based on the method of Heller *et al.* (1968). A 20 mM solution of Na_2ATP in D_2O (Sigma) containing 60 mM triethylamine (TEA) was incubated at 60ºC for 144 hrs. The TEA was removed by twice passing the solution over a Dowex 20W ion exchange resin (Sigma) in the acid form. The pH of the solution was adjusted to pH 12 with NaOH prior to the second pass over the resin. The pH of the solution was adjusted to pH 6.3 prior to freeze drying. The extent of the deuteration at the C8 position was determined by ^{1}H NMR and mass spectroscopy. The ^{1}H NMR was carried out on a Varian VNMRS 600 MHz NMR in D_2O.

4.2.3 Steady-State kinetic analysis

4.2.3.1 Steady-State kinetic analysis of adenylylated and deadenylylate *E.coli* GS

The effect of the concentration of ATP and C8D-ATP on the specific activities of *E.coli* adenylylated and deadenylylated GS was determined at concentrations ranging from 150 to 3000 mM ATP and C8D-ATP in assays containing 4 mM sodium-glutamate, 4 mM NH_4Cl, 5.4 mM $NaHCO_3$ in 20 mM imidazole buffer. The deadenylylated *E.coli* GS assay was carried out at pH 7.4 (± pH 0.05), and at $MgCl_2$ concentrations equivalent to 3 times the ATP concentration. The adenylylated *E.coli* GS assay was carried out at pH 6.6 (± pH 0.05), and at $MnCl_2$ concentrations equivalent to 3 times the ATP concentration. The reaction was stopped by the addition of 100% trichloroacetic acis to give a pH of 2-3. The assay solutions were centrifuged prior to HPLC analysis. After termination of the reactions and centrifugation, ADP levels were determined by HPLC. The samples were analysed on an Agilent series 1100 HPLC fitted with a Phenomenex Luna 5μ C18 column. Each sample was automatically injected (0.2 μL) and separated with a mobile phase containing 51 mM KH_2PO_4, PIC A Low UV Reagent (Waters Cooperation), 25% (v/v)

acetonitrile. The flow rate of the mobile phase was 1 ml/min with UV detection. An AMP, ADP and ATP standard was used to calibrate the HPLC and the concentration of ADP in each sample was determined by the area under the curve using Agilent ChemStation (Revision B.02.01) software. All specific enzyme activities were expressed as moles ADP formed per minute per milligram protein and illustrated as graphs using GraphPad Prism 5 software.

4.2.3.2 Steady-State kinetic analysis of adenylylated and deadenylylate *M.tb* GS

The effect of the concentration of ATP and C8D-ATP on the specific activities of *M.tb* adenylylated and deadenylylated GS was determined at concentrations ranging from 150 to 3000 M ATP and C8D-ATP in assays containing 4 mM sodium-glutamate, 4 mM NH_4Cl in 50 mM HEPES buffer. The deadenylylated *M.tb* GS assay was carried out at pH 7.15 (± pH 0.05), and at $MgCl_2$ concentrations equivalent to 3 times the ATP concentration. The adenylylated *M.tb* GS assay was carried out at pH 6.6 (± pH 0.05), and at $MnCl_2$ concentrations equivalent to 3 times the ATP concentration. The reaction was stopped by the addition of 100% trichloroacetic acis to give a pH of 2-3. The assay solutions were centrifuged prior to HPLC analysis. After termination of the reactions and centrifugation, ADP levels were determined by HPLC. The samples were analysed on an Agilent series 1100 HPLC fitted with a Phenomenex Luna 5μ C18 column. Each sample was automatically injected (0.2 μL) and separated with a mobile phase containing 51 mM KH_2PO_4, PIC A Low UV Reagent (Waters Cooperation), 25% (v/v) acetonitrile. The flow rate of the mobile phase was 1 ml/min with UV detection. An AMP, ADP and ATP standard was used to calibrate the HPLC and the concentration of ADP in each sample was determined by the area under the curve using Agilent ChemStation (Revision B.02.01) software. All specific enzyme activities were expressed as moles ADP formed per minute per milligram protein and illustrated as graphs using GraphPad Prism 5 software.

4.3 Results

ATP was deuterated specifically at position C8 as outlined in the Experimental Procedures and the deuteration was assessed by ^{1}H NMR.

4.3.1 The effect of ATP and C8D-ATP on adenylylated and deadenylylate *E.coli* and *M.tb* GS

The effect of the ATP and C8D-ATP concentration on the specific activities of adenylylated and deadenylylated *E.coli* and *M.tb* GS were determined as indicated by Figures 4.2 to 4.5. The effect of the ATP and C8D-ATP on the specific activity of the enzyme was expressed over a concentration profile that included the ATP or C8D-ATP concentrations that would allow v_{max} to be calculated as well as an ATP or C8D-ATP concentration profile at low concentrations that would allow for the accurate determination of the KIE. The best-fit to the data was obtained for the specified kinetic model using the non-linear regression algorithms of the GraphPad Prism 5 software. As part of the software output a data-table is created containing 150 data-points defining the best kinetic fit for each enzyme's response to the presence of either ATP or C8D-ATP. These response curves were then used to define the KIE by the conventional estimation of KIE:

$$\text{KIE} = \frac{v_{\text{H}}}{v_{\text{D}}}$$

The KIE$_{\text{D}}$ was also determined using the following function:

$$\text{KIE}_{\text{D}} = \frac{v_{\text{D}}}{v_{\text{H}}}$$

Where v_{D} = specific activity in the presence of C8D-ATP

v_{H} = specific activity in the presence of ATP.

The calculation of KIE$_{\text{D}}$ was used as the data obtained is instructive in a putative role that the C8-H of ATP plays in the regulation of phosphoryl transfer.

The following parameters were defined from Figure 4.2 and Figure 4.3; the KIE was obtained in response to the presence of C8D-ATP as indicated on Figure 4.2 B and Figure 4.3 B. In both cases the KIE obtained was a primary KIE as extent of the KIE was two-fold or in excess of two-fold. Adenylylated *E.coli* GS and *M.tb* GS (Figure 4.2 A and Figure 4.3 A) use a similar mechanism with the KIE_D asymptoting to a level of 0.5 at V_{max} (KIE = 2). Adenylylated *E.coli* GS and *M.tb* GS are both dodecamers consisting of two stacked hexameric structures consisting of 12 identical subunits. The subunits probably interact allosterically on the binding of ATP.
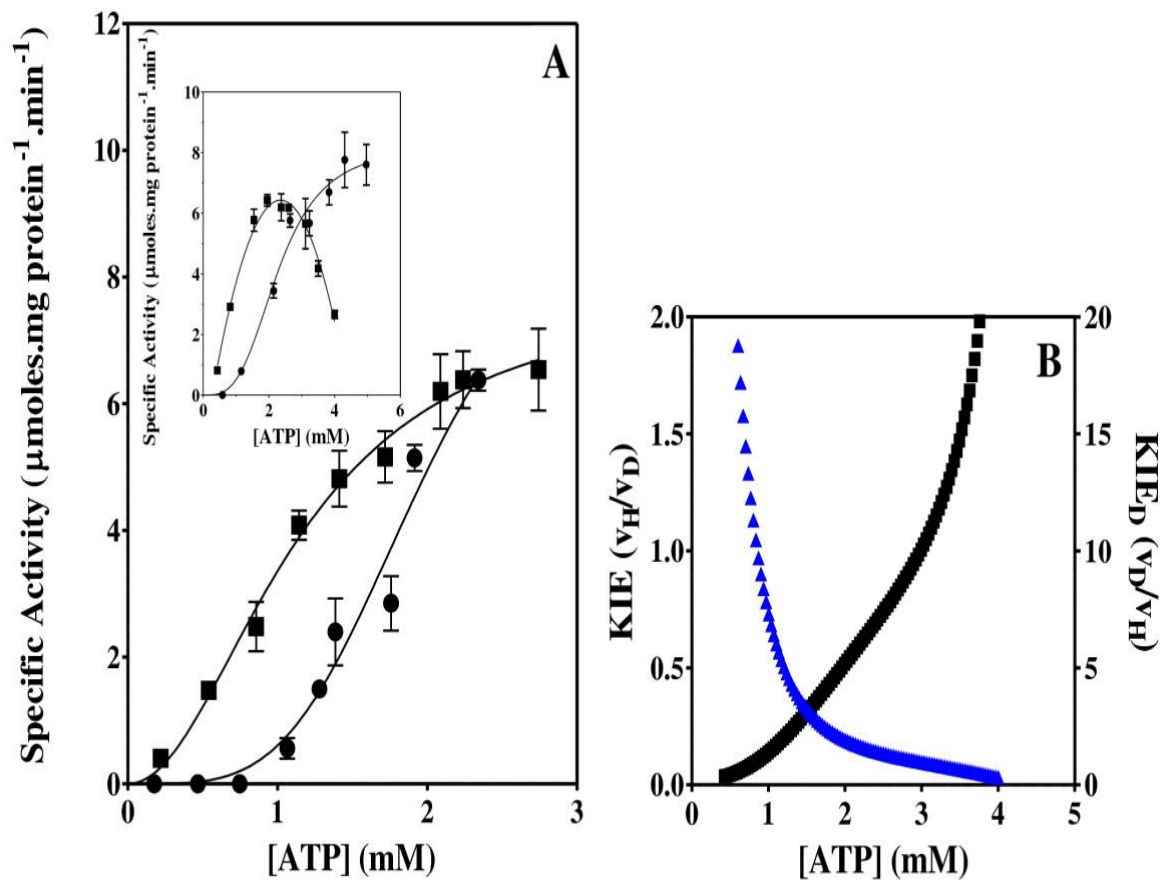

Figure 4.2: *E.coli* adenylylated glutamine synthetase activity and KIE: **A** Effect of the concentration of ATP (represented on the graph by the black circles) and C8D-ATP (represented on the graph by the black squares) on the specific activity of adenylylated *E.coli* GS. **B** Effect of the concentration of ATP (indicated by the black line on the graph) and C8D-ATP (indicated by the blue line on the graph) on the KIE of adenylylated *E.coli* GS.
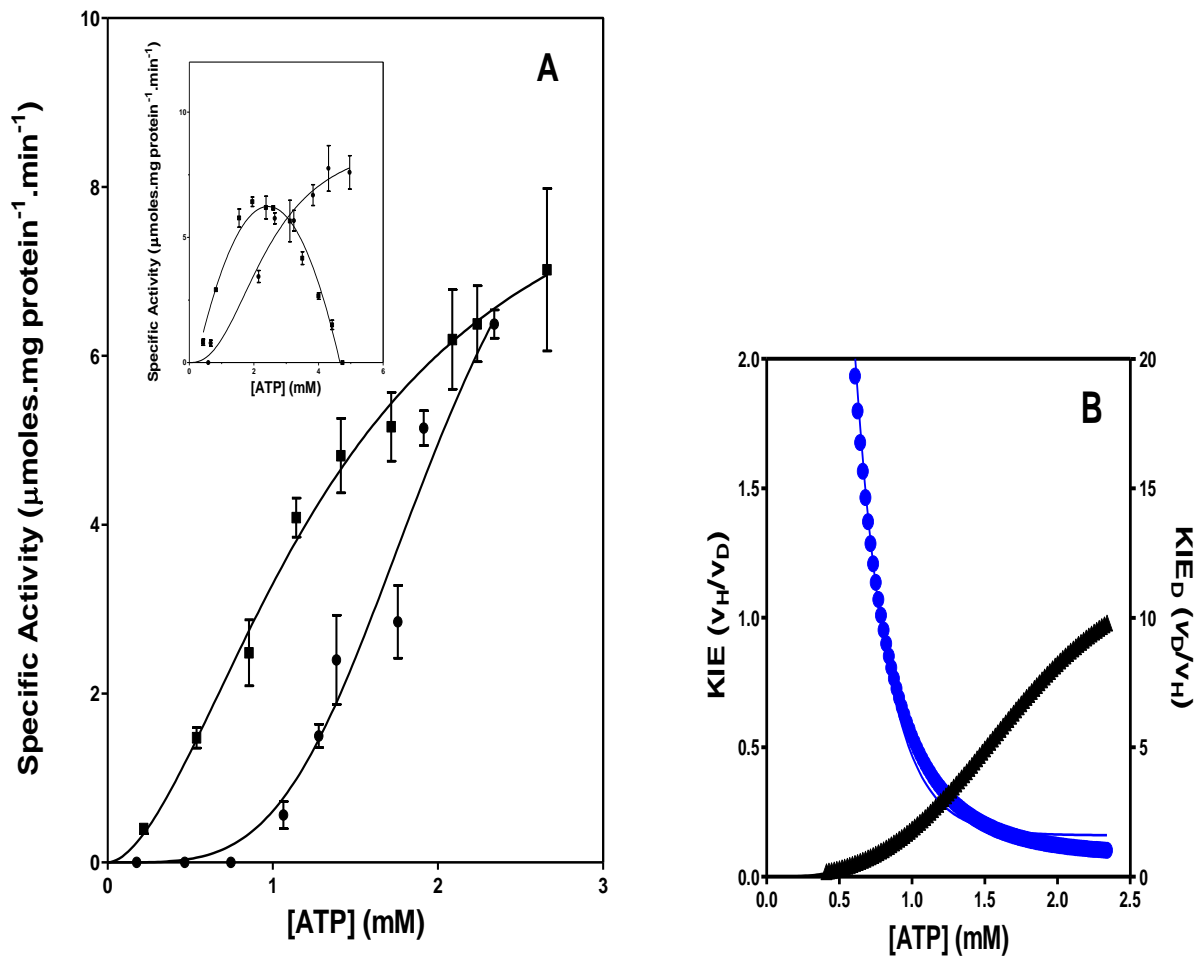
Figure 4.3: *M.tb* adenylylated glutamine synthetase activity and KIE: **A** Effect of the concentration of ATP (represented on the graph by the black circles) and C8D-ATP (represented on the graph by the black squares) on the specific activity of adenylylated *M.tb* GS. **B** Effect of the concentration of ATP (indicated by the black line on the graph) and C8D-ATP (indicated by the blue line on the graph) on the KIE of adenylylated *M.tb* GS.

The following parameters were defined from Figure 4.4 and Figure 4.5; the KIE was obtained in response to the presence of C8D-ATP as indicated on Figure 4.4 B and Figure 4.5 B. In both cases the KIE obtained was a primary KIE as extent of the KIE was two-fold or in excess of two-fold. Deadenylylated *E.coli* GS and *M.tb* GS (Figure 4.4 A and Figure 4.5 A) use the same mechanism for regulation. The KIE_D of the deadenylylated *E.coli* GS and *M.tb* GS negatively asymptote to 1 at V_{max} (Figure 4.4 B and Figure 4.5 B). Deadenylylated *E.coli* GS and *M.tb* GS are multimeric and allosteric regulation may occur via the interaction of subunits.

Figure 4.4: *E.coli* deadenylylated glutamine synthetase activity and KIE: **A** Effect of the concentration of ATP (represented on the graph by the black circles) and C8D-ATP (represented on the graph by the black squares) on the specific activity of deadenylylated *E.coli* GS. **B** Effect of the concentration of ATP (indicated by the black line on the graph) and C8D-ATP (indicated by the blue line on the graph) on the KIE of deadenylylated *E.coli* GS.
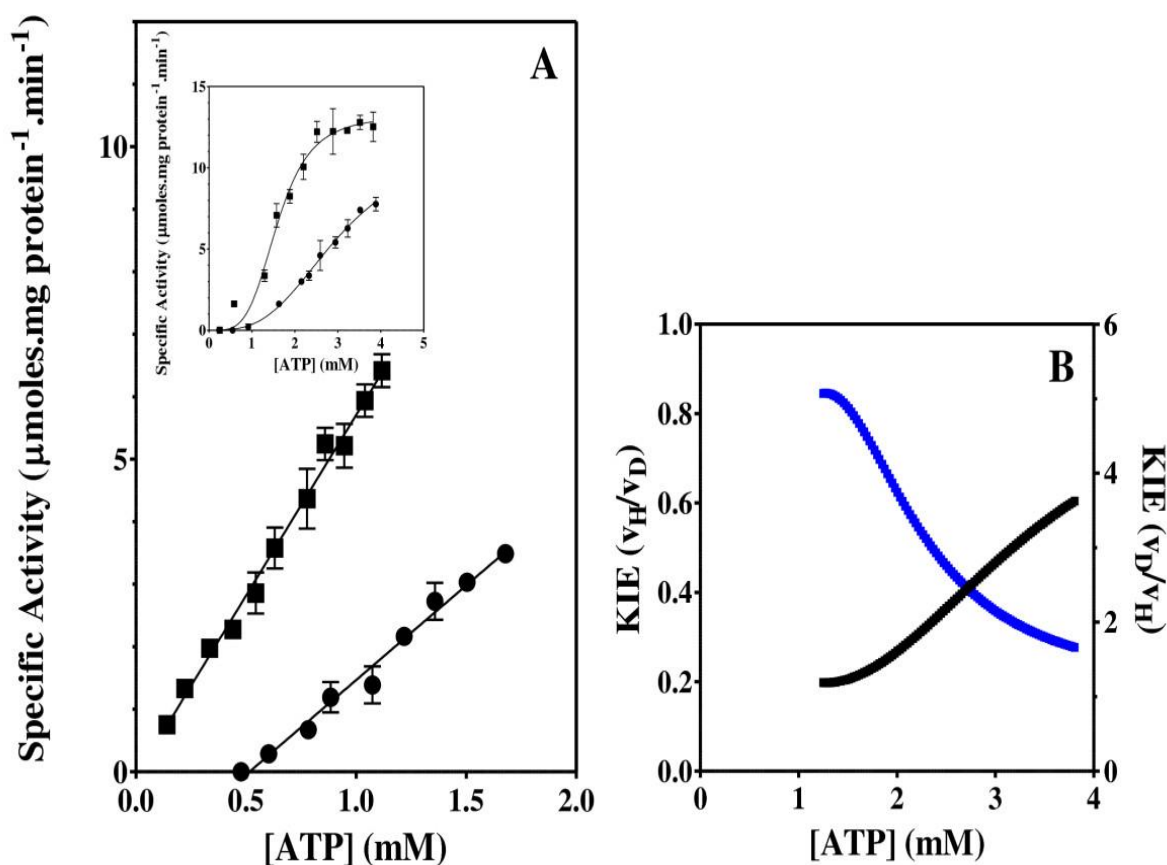
Figure 4.5: *M.tb* deadenylylated glutamine synthetase activity and KIE: **A** Effect of the concentration of ATP (represented on the graph by the black circles) and C8D-ATP (represented on the graph by the black squares) on the specific activity of deadenylylated *M.tb* GS. **B** Effect of the concentration of ATP (indicated by the black line on the graph) and C8D-ATP (indicated by the blue line on the graph) on the KIE of deadenylylated *M.tb* GS.
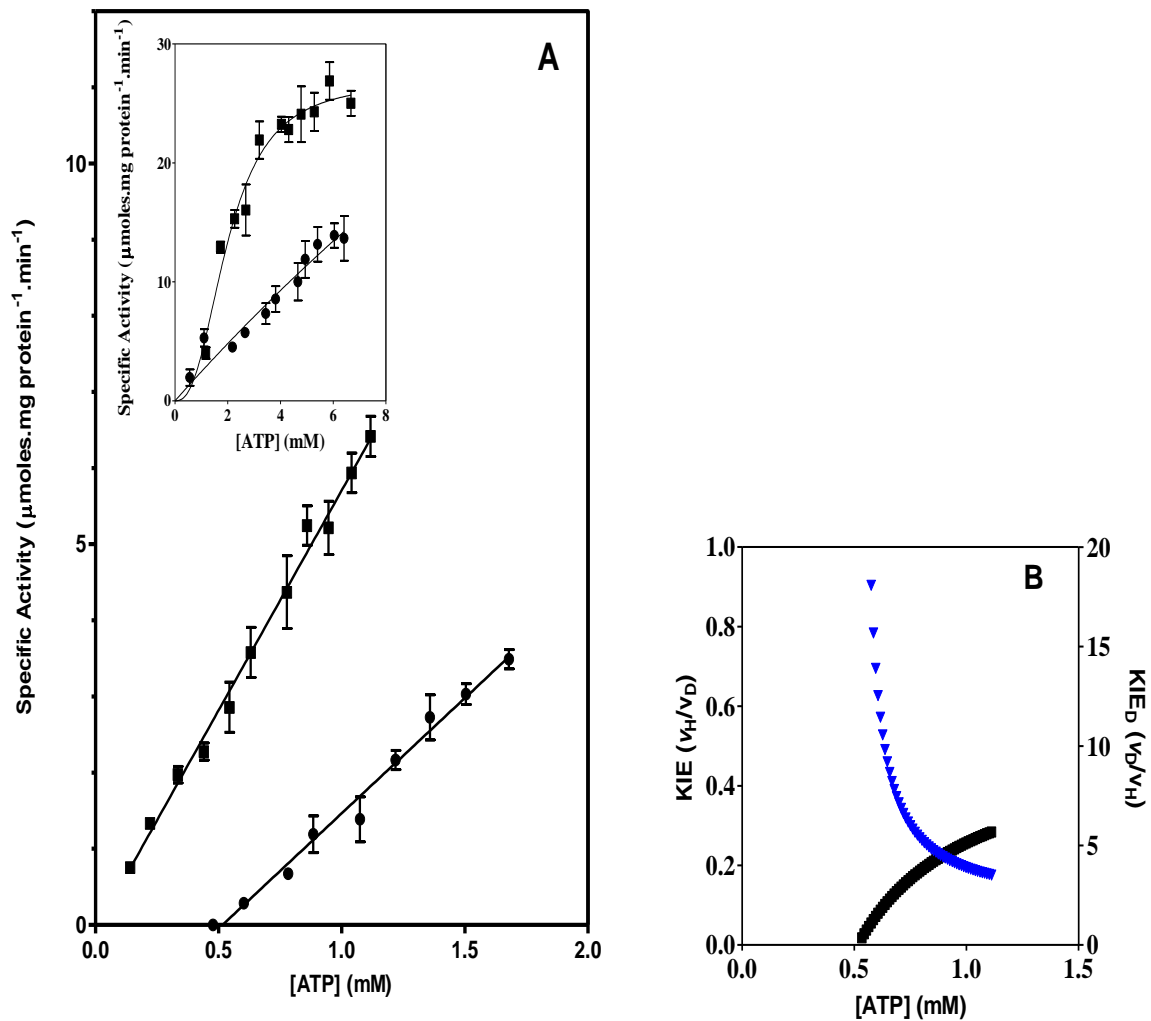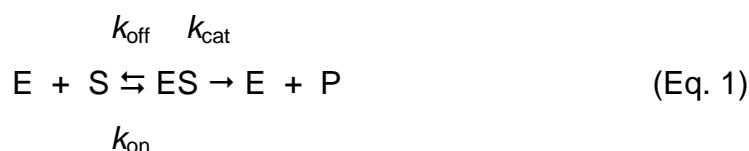
4.4 Discussion

The role of the KIE defining the kinetic models of the enzymes investigated has led to models for the regulation of the binding of ATP being proposed.

In classical steady-state kinetics as represented by the Briggs-Haldane modification of the Michaelis-Menton formulation (Equation 1),

$$E \; + \; S \; \underset{k_{on}}{\overset{k_{off}}{\rightleftarrows}} \; ES \; \xrightarrow{k_{cat}} \; E \; + \; P \qquad \text{(Eq. 1)}$$

with $k_{on} = k_1$, $k_{off} = k_{-1}$ and $k_{cat} = k_2$, $k_2 \gg k_{-1}$, and the Michaelis constant, K_M obtained from

$$\frac{[E][S]}{[ES]} = \frac{k_{-1} + k_2}{k_1} = K_M \qquad \text{(Eq. 2)}$$

It is proposed in enzymes such as Deadenylylated *E.coli* and *M.tb* GS that the enzyme kinetics follows classical Michaelis-Menton kinetics, where an equilibrium is set up between the enzyme concentration [E] and the substrate concentration [S] and binding of the second ATP is dependent on the conversion of the second active site into an ATP binding form by the release of ATP from the first active site, as defined by the coordinated half-sites mechanism. In enzymes using this mechanism of regulation, K_M is dependent on k_{-1} and k_2. The KIE obtained in these enzymes asymptotes to a value of 1. At low ATP concentrations the effect of the deuteration of C8 is to allow binding to occur for long enough to allow the reaction to occur and negate the effect of k_{-1}, thereby shifting the equilibrium to k_2. At high ATP concentrations the impact of the ATP concentration relative to the impact of ATP binding on the rate of reaction is significantly higher and as a result there is a concomitant decrease in the KIE. The impact of binding and the reaction rate, however, equilibrate to a KIE of 1. The maximum rate of binding can only ever be equivalent to the maximum rate at which the second ATP binding site is converted to the ATP binding form by the release of ATP from the first site. The classical impact

of deuteration on the KIE when the KIE is a primary effect, as determined by v_H/v_D, should yield a KIE of 2 or more (0.5 as determined by v_D/v_H as outlined above). As the regulation of the enzyme activity and ligand binding in these enzymes function in a coordinated half-the-sites mechanism binding in the second site only occurs on release of the ADP from the first site, it is therefore proposed that deuteration of the ATP improves the binding characteristics but does not impact on the catalysis of phosphoryl transfer. As the equilibrium shifts towards the binding of ATP with increasing ATP concentration the deuterated ATP binds effectively twice as efficiently as the non-deuterated ATP thereby negating the impact of the deuteration on the apparent enzyme activity at high ATP concentrations, yielding a KIE of 1.

 In enzymes where the second active site is made available to ATP binding by the conversion of ATP to ADP, in other words binding may occur to the second site prior to the release of the ATP from the first site; the K_M is dependent on k_1 and k_2. This occurs in the case of adenylylated *E.coli* and *M.tb* GS where the KIE becomes 2 at v_{max}. The impact of this binding is that at any point in time up to two reactions might be occurring simultaneously in two active sites. At high ATP concentrations, the deuterated ATP binds twice as efficiently as the non-deuterated ATP, allowing the KIE to asymptote to 2. At low concentrations, the deuteration has the same effect as occurs in the previous model, whereby binding occurs for a long enough period to negate the effect of k_{-1}. At high concentrations, the effect of deuteration is superseded by the concentration effect and as two or more active sites is able to function simultaneously; this allows the KIE to asymptote to 2 or more. It is conceivable that on adenylylation of GS the interaction between two subunits effectively creates a dimer of dimer interaction.

My making use of deuterated ATP we were able to show that the adenylylated and deadenylylated GS fundamentally differ in functionality. Proven that and also making use of the expression system to produce 95% adenylylated GS we clearly shown that adenylylated GS is active where it is shown in literature that the enzyme is basically inactive (Metha *et al*., 2004) and therefore making the adenylylated form of GS a potential new drag target. You can also go one step further and conclude that the deuteration of compounds may increase the "activity" of compounds leading to a lower IC_{50} values which will contribute significantly to the drug development process.

Chapter 5

Concluding Discussion

5.1 Concluding Discussion

Mycobacterium tuberculosis (M.tb) glutamine synthetase (GS) is a potentially valuable therapeutic target for tackling the problem of tuberculosis disease. Its regulation via the adenylylation of a tyrosine residue on each subunit makes it distinct from the human form of the enzyme. Previous reports of heterologous expression of *M.tb* GS in *Escherichia coli* (*E. coli)* have shown that the endogenous adenylyl transferase (ATase) activity of *E. coli* does not adenylylate *M.tb* GS sufficiently, with only 25% of the *M.tb* GS subunits produced displaying adenylylation (Mehta *et al.,* 2004). The use of this expression system was therefore not considered optimal for the expression of adenylylated *M.tb* GS for further study.

Here we have described an *E. coli* production system lacking endogenous GS and ATase activity, which utilises the co-expression of the *M.tb* ATase with *M.tb* GS. Each gene was provided on a separate plasmid, the *glnA* GS gene on a pBluescript SKII⁺ plasmid with the ColE1 origin of replication, and the *glnE* ATase gene on a CDFDuet-1 plasmid containing a CloDF13 replicon. These replicons are compatible, and the two plasmids can be stably co-maintained, provided the relevant antiobiotic selective pressure is exerted: ampicillin for pBluescript SKII⁺ and streptomycin for pDFDuet-1 (Held *et al.,* 2003). Mehta and co-workers (2004) expressed *M.tb* GS in *E. coli* host strains that were deficient in only chromosomal GS (*glnA*). They found that the *E. coli* ATase was inefficient in adenylylating the heterologous *M.tb* GS, with only ~25% of subunits being modified (Mehta *et al.,* 2004). By co-expressing *M.tb* ATase and *M.tb* GS we improved the percentage of subunits modified (or adenylylated) with ± 60-70% to ± 85-94%. In this way, we have produced recombinant *M.tb* GS that has a better adenylylation state than any previously reported.

The adenylylated and deadenylylated *E. coli* GS enzymes were also produced recombinantly, from pBluescript SKII⁺ in *E. coli* strains lacking endogenous GS (for deadenylylated enzyme) or both GS and uridylyl transferase (adenylylated enzyme). These *E. coli* GS enzymes were only cloned, expressed and purified to be used as a model and for comparison with *M.tb* GS.

Three methods were used to assess the degree of adenylylation of adenylylated and deadenylylated *M.tb* GS, and *E. coli* GS. The first assay used, termed the γ-glutamyl transferase enzyme assay, is a variation of the reverse of the reaction that GS catalyses:

$$\text{Glutamate} + NH_4^+ + ATP \rightarrow \text{glutamine} + ADP + P_i + H^+$$
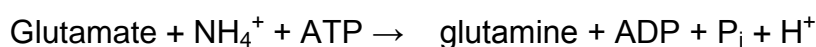
In this reverse reaction; hydroxylamine and glutamine react to form γ-glutamylhydroxamate and free ammonia in the presence of ADP, arsenate and manganese or magnesium (EP2008210 A1, 2008; Shapiro and Stadtman, 1970). This forms the basis of an assay for GS activity. At the correct pH (derived from determining the isoelectric point of the enzyme), the transferase activities of both the adenylylated and deadenylylated forms of GS are the same. The two forms can, however, be distinguished because at the isoelectric point, fully adenylylated GS is completely inhibited by 60 mM Mg^{2+}, whereas the deadenylylated enzyme is unaffected (Bender *et al.,* 1977). Based on the data from the γ-glutamyl transferase assay, the adenylylation state of adenylylated *M.tb* GS expressed in this novel system is at least 68% compared to the 25% obtained from Mehta and co-workers.

The second assay used is the determination of the inorganic phosphate concentration after the hydrolysis of both adenylylated and deadenylylated *Mtb* GS. In the case of the deadenylylated enzyme, there is no formation of phosphate after the hydrolysis. For the adenylylated *Mtb* GS, each adenyl moiety contains 1 phosphate, and 1 μM of GS (containing 12 subunits) should contain 12 μM of phosphate, if each subunit is adenylylated. The result obtained for the adenylylated *M.tb* GS enzyme was the formation of 0.93 μM phosphate produced per μM GS active site, *i.e.* 94% adenylylated compared to the 25% obtained from Mehta and co-workers.

The third method used to assess the adenylylation is mass spectrometry. MS spectra showed distinct peaks for adenylylated and deadenylylated enzymes, with calculated masses agreeing with the theoretical values. Based on this data, it can be concluded that the adenylylation state of adenylylated *M.tb* GS expressed in this novel system is at least 85% from the MS spectra obtained.

In addition, the rate of conversion of ATP, glutamate and ammonia to glutamine and ADP was assessed using HPLC. This is termed the 'forward' or 'biosynthetic" reaction and is assayed by HPLC to determine the conversion of ATP to ADP.

Several gaps exist in the TB drug development pipeline worldwide as very few new drugs or drug candidates are in the pipeline. Big pharmaceutical companies have not invested in TB drug development, as historically the disease did not pose a significant threat to the developed world. However, the threat of multi-drug resistant (MDR)-TB and the increased world demand for treatment of Latent TB Infection has prompted a number of global initiatives such as the Global Alliance for TB Drug Development and the Stop TB Partnership (WHO 2006); all aimed at ensuring a pipeline of new TB drug leads to ensure new more effective TB drugs enter clinical development.

The primary invention of this project relates to a biochemical pathway that yielded a new drug target that can be exploited to develop new therapies against *M.tb*. GS catalyses the conversion of glutamate to glutamine via a glutamyl phosphate intermediate, utilising ATP. ATP is utilized as either Mg-ATP or Mn-ATP, depending on the adenylylation state of the enzyme. The enzyme is regulated via adenylylation in bacteria containing the GS-I form of the enzyme, a mechanism not found in the GS-II in humans.

213 compounds were tested against the adenylylated and deadenylylated forms of both *M.tb* GS and *E. coli* GS at a concentration of 10 µM. The rational design and selection of these inhibitors were based on the typical ATP binding site. It has been shown that GS in the adenylylated form uses a novel histidine kinase-like reaction mechanism in the phosphorylation of the carboxyl of glutamate. The primary outcome of the project was the demonstration of the selective inhibition of adenylylated GS and the identification of specific compounds capable of inhibiting adenylylated GS.

Compounds showing activity towards the adenylylated and/or deadenylylated forms of *E. coli* and *M.tb* GS enzymes at a single micromolar (μM) concentration were confirmed with repeated testing before being evaluated with full dose-responses to assess IC_{50} values and rank the order of potencies towards the adenylylated and deadenylylated forms of *E. coli* and *M.tb* GS. Compounds showing activity for the adenylylated or deadenylylated forms of the *M.tb* GS enzyme were further assessed for selectivity *vis-à-vis* the mammalian enzyme and for antibacterial action in a cellular model of *M.tb* infection. Any compound showing a selective activity for the adenylylated versus the deadenylylated and mammalian forms of the enzyme could be considered for further hit-to-lead and lead optimisation campaigns for the development of novel candidates for the treatment of TB. Based on the dose-response assays, two compounds have emerged as the most promising anti-*M.tb* GS inhibitors with IC_{50} (μM) values of 9.6 μM and 17.4 μM respectively. They have regularly produced the most potent inhibitory activity against *M.tb* adenylylated GS enzyme in fixed concentration screens with 87% and 81% inhibition, respectively. These compounds, 10057 and 10059, are structurally very similar. These two compounds that have been found to be inhibitory to *M.tb* GS may now be used as templates to synthesize additional target specific compounds as part of a lead optimisation programme and further optimised to yield a suitable drug candidate for clinical evaluation.

In the study we also looked at the utilization of ATP by looking at the enzyme kinetics of both *M.tb* GS and *E. coli* GS as well as the kinetic isotope effect of these enzymes. It is proposed that for enzymes such as *M.tb* GS and *E. coli* GS, the enzyme kinetics follow the classical Michaelis-Menton kinetics where an equilibrium is set up between the enzyme concentration [E] and the substrate concentration [S] and binding of the second ATP is dependent on the conversion of the second active site into an ATP binding form by the release of ATP from the first active site, as defined by the coordinated half-sites mechanism. In enzymes using this mechanism of regulation, K_M is dependent on k_{-1} and k_2. The kinetic isotope effect (KIE) was determined using ATP and ATP deuterated at the C8-H of the adenyl moiety. The KIE is defined as v_H/v_D, where v_D = specific activity in the presence of C8D-ATP, and v_H = specific activity in the presence of ATP. The KIE obtained in these enzymes asymptotes to a value of 1. At low ATP concentrations the effect of the deuteration of

C8 is to allow binding to occur for long enough to allow the reaction to occur and negate the effect of k_{-1}, thereby shifting the equilibrium to k_2. At high ATP concentrations the impact of the ATP concentration relative to the impact of ATP binding on the on-rate of reaction is significantly higher and as a result there is a concomitant decrease in the KIE. The impact of binding and the reaction rate however equilibrate to a KIE of 1. The maximum rate of binding can only ever be equivalent to the maximum rate at which the second ATP binding site is converted to the ATP binding form by the release of ADP from the first site.

As the regulation of the enzyme activity and ligand binding in these enzymes function in a coordinated half-the-sites manner, and binding in the second site only occurs on release of the ADP from the first site, it is therefore proposed that deuteration of the ATP improves the binding characteristics but does not impact on the catalysis of phosphoryl transfer. As the equilibrium shifts towards the binding of ATP with increasing ATP concentration, the deuterated ATP effectively binds twice as efficiently as the non-deuterated ATP, thereby negating the impact of the deuteration on the apparent enzyme activity at high ATP concentrations, yielding a KIE of 1.

This work contributes to the field of mycobacterial drug discovery on a number of different levels firstly: a novel expression system has been developed for the expression and production of adenylylated GS. This system may be useful for the expression and production of other essential mycobacterial enzyme which also undergoes post-translation modifications like the adenylylation of GS is this case. Secondly as many drugs targeting the ATP binding site contain purine and imidazole moieties, the deuteration of ligands at the site equivalent to the C8 of the imidazole moiety of ATP, could lead to enhanced efficacy and ligand binding in a drug design programme. This project therefore has formed part of an ongoing programme of the chemical biology of the diversity of the ATP binding sites in biology and their potential use in drug design. It has been clearly demonstrated the adenylylation of bacterial GS creates sufficient diversity in the active site thereby allowing the design of selective inhibitors targeting either the adenylylated or the deadenylylated forms of the enzyme. In conclusion GS is an essential enzyme in bacterial metabolism, and previous studies by Kenyon and co-workers have shown that inhibition/deletion of this enzyme can result in a static effect for pathogenic *M.tb.* Since the adenylylation

mechanism is specific to the bacterial form of the enzyme and induces significant modifications in the active site and also the ion requirements for the catalytic activity of GS is novel this makes GS potential new drug target.

Reference list

Andrews J, Basu S, Scales D, Smith-Rohrberg D. XDR-TB in South Africa. *PLOS Medicine* 2007;**4**:770-771.

Backman K, Chen YM, Magasanik B. Physical and genetic characterization of the *glnA-glnG* region of the *Escherichia coli* chromosome. *Proc Natl Acad Sci USA* 1981;**78**:3743-3747.

Barry 3rd CE. New horizons in the treatment of tuberculosis. *Biochem Pharmacol* 1997;**54**:1165-1172.

Barry 3rd, CE, Boshoff HI, Dartois V, Dick T, Ehrt S, Flynn J, Schnappinger D, Wilkinson RJ, Young D. The spectrum of latent *tuberculsosis:* rethinking the biology and intervention strategies. *Nature Rev* 2009;**7**:845-855.

Bartlett G, Porter CT, Borkakoti N, Thornton JM. Analysis of catalytic residues in enzyme active sites. *J Mol Biol* 2002;**324**:105-121.

Bender RA, Janssen KA, Resnick AD, Blumenberg M, Foor F, Magasanik B. Biochemical parameters of glutamine synthetase from *Klebsiella aerogenes*. *J Bacteriol* 1977;**129**:1001-1009.

Bloom FR, Streicher SL, Tyler B. Regulation of enzyme synthesis by glutamine synthetase of *Salmonella typhimurium*: a factor in addition to glutamine synthetase is required for activation of enzyme formation. *J Bacteriol* 1977;**130**:983-990.

Blow D. So do we understand how enzymes work? *Struct Fold* 2000;**8**:77-81.

Brown JR, Masuchi Y, Robb FT, Doolittle WF. Evolutionary relationships of bacterial and archaeal glutamine synthetase genes. *J Mol Evol* 1994;**38**:566-576.

Buteau KC. Deuterated Drugs: Unexpectedly Nonobvious? *J High tech L* 2009;**10**:22-74.

Calver AD, Falmer AA, Murray M, Strauss OJ, Streicher EM, Hanekom M, Liversage T, Masibi M, van Helden PD, Warren RM, Victor TC. Emergnece of increased resistance and extensively drug-resistant tuberculosis despite treatment adherence, South Africa. *Emerg Infect Dis* 2010;**16**:264-271.

Cardona PJ. RUTI: A new chance to shorten the treatment of latent tuberculosis infection. *Tuberculosis* 2006;**86**:272-289.

Centers for Disease Control and Prevention. Guidelines for preventing the transmission of *Mycobacterium tuberculosis* in healthcare facilities. *MMWR* 1994;**43**:(RR-13).

Chandra H, Basir SF, Gupta M, Banerjee N. Glutamine synthetase encoded by *glnA-1* is necessary for cell wall resistance and pathogenicity of *Mycobacterium bovis. Microbiol* 2010;**156**:3669-3677.

Chopra P, Meena LS, Singh Y. New drug targets for *Mycobacterium tuberculosis*. *Indian J Med Res* 2003;**117**:1-9.

Cole ST, Riccardi G. New tuberculosis drugs on the horizon. *Curent Opinion in Microbiolog* 2011;**14**:570-576.

Collin LA, Franzblau SG*.* Microplate Alamar blue assay versus BACTEC 460 system for high- throughput screening of compounds against *Mycobacterium tuberculosis* and *Mycobacterium avium. Antimicrobial Agents and Chemotherapy* 1997;**41**:1004-1009.

Department of Health. The South African national tuberculosis control programme practical guidelines. 2004.

Drugbank (www.drugbank.ca).

Edwards D, Kirkpatrick CH. The immunology of mycobacterial diseases. *Am Rev Respir Dis* 1986;**134**:1062-1071.

Floor F, Janssen KA, Magasanik B. Regulation of synthesis of glutamine synthetase by adenylylated glutamine synthetase. *Proc Natl Acad Sci USA* 1975;**72**:4844-4848.

Gaillardin CM, Magasanik B. Involvement of the product of the *glnF* gene in the autogenous regulation of glutamine synthetase formation in *Klebsiella aerogenes. J Bacteriol* 1978;**133:**1329-1338.

Ginsberg A, Stadtman ER. Regulation of glutamine synthetase in *Escherichia coli.* In: Prusiner SR, Stadman ER, editors. *Enzymes of Glutamine Metabolism,* Academic Press, New York, 1973, p. 9-44.

Limbach H. Dynamic NMR Spectroscopy in the Presence of Kinetic Hydrogen/Deuterium Isotope Effects.1990.

Handbook of Anti-Tuberculosis Agents. *Tuberculosis* 2008;**88**:2.

Harper CJ, Hayward D, Kidd M, Wiid I, van Helden P. Glutamate dehydrogenase and glutamine synthetase are regulated in response to nitrogen availability in *Myocbacterium smegmatis. BMC Microbiology* 2010;**10**:138.

Harris T, Turner G. Structural basis of perturbed pKa values of catalytic groups in enzyme active sites. *IUBMB Life* 2002;**53**:85-98.

Harth G, Horwitz MA. An inhibitor of exported *Mycobacterium tuberculosis* glutamine synthetase selectively blocks the growth of pathogenic mycobacteria in axenic culture and in human monocytes: extracellular proteins as potential drug targets. *J Exp Med* 1999;**189**:1425-1435.

Harth G, Horwitz MA. Expression and efficient transport of enzymatically active *Mycobacterium tuberculosis* glutamine synthetase in *Mycobacterium smegmatis* and evidence that information for export is contained within the protein. *J Bio Chem* 1997;**272**:22728-22735.

Harth G, Horwitz MA. Inhibition of *Mycobacterium tuberculosis* glutamine synthetase as a novel antiobiotic strategy against tuberculosis: demonstration of efficacy *in vivo*. *Infect Immune* 2003;**71**:456-464.

Hasan S, Daugelat S, Rao PSS, Schreiber M. Prioritizing Genomic Drug Targets in Pathogens: Application to Mycobacterium tuberculosis. *PLOS Comput Biol* 2006;**6**:1371.

Hayward D, van Helden PD, Wiid I. Glutamine synthetase sequence evolution in the mycobacteria and their use as molecular markers for *Actinobacteria* speciation. *BMC Evolutionary Biology* 2009;**9**:48.

Hedstrom L. Serine protease mechanism and specificity, *Chem Rev* 2002;**102**:4501-4524.

Held D, Yaeger K, Novy R. New coexpression vectors for expanded compatibilities in *E. coli. Innovations* 2003;**18**:406.

Hernick M, Fierke C. Zinc hydrolases: the mechanisms of zinc-dependent deacetylases. *Arch Biochem Biophys* 2005;**433**:71-84.

Hirschfield GR, McNeil M, Brennan PJ. Peptidoglycan-associated polypeptides of *Mycobacterium tuberculosis*. *J Bacteriol* 1990;**172**:1005-1013.

Holzer H, Schutt H, Mašek Z, Mecke D. Regulation of two forms of glutamine synthetase in *Escherichia coli* by the ammonium content of the growth medium. *Proc Natl Acad Sci USA* 1968;**60**:721-724.

Horsburgh J. Tuberculosis without tubercles. *Tuberc Lung Dis* 1996;**77:**197-198.

Ishida T, Kato S. Role of Asp102 in the catalytic relay system of serine proteases: a theoretical study. *J Am Chem Soc* 2004;**126**:7111-7118.

Janssen KA, Magasanik B. Glutamine synthetase of *Klebsiella aerogenes*: genetic and physiological properties of mutants in the adenylylation system. *J Bacteriol* 1977;**129**:993-1000.

Jindani AE, Aber E, Edwards E, Mitchison D. The early bactericidal activity of drugs in patients with pulmonary tuberculosis. *AM Rev Respir Dis* 1980;**121**:939-949.

Kenyon CP, Steyn A, Roth RL, Steenkamp PA, Nkosi TC, Oldfield LC. The role of the C8 proton of ATP in the regulation of phosphoryl transfer within kinases and synthetases. *BMC Biochem* 2011;**12**:36.

Kingdon HS, Shapiro BM, Stadtman ER. Regulation of glutamine synthetase VIII. ATP: glutamine synthetase adenylyltransferase, an enzyme that catalyzes alterations in the regulatory properties of glutamine synthetase. *Proc Natl Acad Sci USA* 1967;**58**:1703-1710.

Korf J, Sroltz A, Verschoor JA, De Baetselier P, Grooten J. The *Mycobacterium Tuberculosis* cell wall component mycolic acid elicits pathogen-associated host innate immune responses. *Eur J Immunol* 2005;**35**:890-900.

Kumada Y, Benson DR, Hillemann TJ, Hosted DA, Rochefort CJ, Thompson W, Tetenovii T. Evolution of the glutamine synthetase gene, one of the oldest existing and functioning genes. *Proc Natl Acad Sci USA* 1993;**90**:3009-3013.

Kustu SG, McKereghan K. Mutations affecting glutamine synthetase activity in *Salmonella typhimurium*. *J Bacteriol* 1975;**122**:1006-1016.

Laemlli UK. Cleavage of structural proteins during the assembly of the head of bacteriophage T4. *Nature* 1970;**227**:680-685.

Ludden PW, Burris RH. Purification and properties of nitrogenase from *Rhodospirillum rubrum*, and evidence for phosphate, ribose and an adenine-like unit covalently bound to the iron protein. *Biochem J* 1978;**175**: 251-259.

McIlleron H, Meintjies G, Burman WJ, Maartens G. Complications of antiretroviral therapy in patients with tuberculosis: Drug interactions, toxicity, and immune reconstitution inflammatory syndrome. *J Ifect Dis* 2007;**196**:S63-75.

Mecke D, Wulff K, Liess K, Holzer H. Characterization of a glutamine synthetase inactivating enzyme from *Escherichia coli. Biochem Biophys Res Commun* 1966;**24**:452-458.

Merrick MJ, Edwards, RA. Nitrogen control in bacteria. *Microbiol Rev* 1995;**59**:604-622.

Metha R, Pearson JT, Mahajan S, Nath A, Hickey MJ, Sherman DR, Atkins WM. Adenylylation and catalytic properties of *Mycobacterium tuberculosis* glutamine synthetase expressed in *Escherichia coli* versus mycobacteria. *J Biol Chem* 2004;**279**:22477-22482.

Murataliev MB, Feyereisen R, Walker FA. Electron transfer by diflavin reductases. *Biochim Biophys Acta* 2004;**1698**:1-26.

Mure M. Tyrosine-derived quinone cofactors. *Acc Chem Res* 2004;**37**:131-139.

Murray J. Chapter 13: Defense mechanisms. *In* J.F. Murray, editor. The normal Lung: The Basis for Diagnosis and Treatment of Pulmonary Disease.
W.B. Saunders, Philadelphia, PA. 313-338.

Nardell EA. The Merck Manual Online. 2009, www.merck.com/mmpe/sec14/ch179/ch179b.html.

Novak I. Purinergic signalling in epithelial ion transport: regulation of secretion and absorption.*Acta physiologica (Oxford, England)* 2011;**202:**501-522.

Okano H, Hwa T, Lenz P, Yan D. Reversible adenylylation of glutamine synthetase is dynamically counterbalanced during steady state growth of *Escherichia coli*. *J Mol Biol* 2010;**404**: 522-536.

Parrish NM, Dick JD, Bishai WR. Mechanisms of latency in *Mycobacterium tuberculosis*. *Trends Microbiol* 1998;**6**:107-112.

Perona J, Craik C. Evolutionary divergence of substrate specificity within the chymotrypsin-like serine protease fold. *J Biol Chem* 1997;**272**:29987-29990.

Porter CT, Bartlett GJ, Thornton JM. The catalytic site atlas: a resource of catalytic sites and residues identified in enzymes using structural data. *Nucleic Acids Res* 2004;**32**:129-133.

PubChem (http://pubchem.ncbi.nlm.nih.gov/).

Rastogi N, Goh KS, Horgen L, Barrow WW. Synergistic activities of antituberculosis drugs with cerulenin and trans-cinnamic acid against *Mycobacterium tuberculosis. FEMS Immunol Med Microbiol* 1998;**21**:149-157.

Reitzer LJ, Magasanik B. Ammonia assimilation and the biosynthesis of glutamine, glutamate, aspartate, asparagine, l-alanine, and d-alanine. In: Neidart FC, Ingarhou JLL, Low KB, Magasanik B, Schaechter M Nunberger HE, editors. *Escherichia coli* and *Salmonella typhimurium*. Cellular and molecular biology, American Society for Microbiology, Washington DC, 1987, p. 302-320.

Reynaud C, Etienne G, Payron P, Lenelle MA, Daffe M. Extracellular enzyme activities potentially involved in the pathogeniticty of *Mycobacterium tuberculosis*. *Microbiol* 1998;**144**:577-587.

Riley R. Transmission and environmental control of tuberculosis. *In* Reichem L, Hershfield E, editors. Tuberculosis. Marcel Deckker, New York 1993.

Saleem A and Azher M. The next Pandemic – Tuberculosis: The oldest disease of mankind rising one more time. *Brit J of Medic Pract* 2013;**6**:615-622.

Salisu S, Kenyon CP, Kaye PT. Studies Towards the Synthesis of ATP Analogs as Potential Glutamine Synthetase Inhibitors. *Synth Commun* 2011;**41**:2216-2225.

Sassetti CM, Boyd DH, Rubin EJ. Genes required for mycobacterial growth defined by high density mutagenesis. *Mol Microbiol* 2003;**48**:77-84.

Senior PJ. Regulation of nitrogen metabolism in *Escherichia coli* and *Klebsiella aerogenes*: studies with the continuous-culture technique. *J Bacteriol* 1975;**123**:407-418.

Shapiro BM, Ginsburg A. Effects of specific divalent cations on some physical and chemical properties of glutamine synthetase from *Escherichia coli*. *Biochem* 1968;**7**:2153-2167.

Shapiro BM, Kingdon HS, Stadtman ER. Regulation of glutamine synthetase. VII. Adenylyl glutamine synthetase: a new form of the enzyme with altered regulatory and kinetic properties. *Proc Natl Acad Sci USA* 1967;**58**:642-649.

Shapiro BM, Stadman ER. The regulation of glutamine synthesis in microorganisms. *Ann Rev Microbiol* 1970;**24**:501-524.

Shapiro BM, Stadtman ER. Glutamine Synthetase (*Escherichia* coli). In: Hirs CHW, Timasheff SN, editors. *Methods in Enzymology 130*, Elsevier, 1970, p. 910-922.

Shapiro BM, Stadtman ER. 5'-adenylyl-*O*-tyrosine. The novel phosphodiester residue of adenylylated glutamine synthetase from *Escherichia coli. J Bio Chem* 1968;**243**:3769-3771.

Shinnick TM, Good RC. Mycobacterial taxonomy. *Eur J Clin Microbiol Infect Dis* 1994;**13**:884-901.

Siddiqi SH, Heifets LB, Cynamon MH, Hooper NM, Laszlo A, Libonati JP, Lindholm-Levy PJ, Pearson N. Rapid broth macrodilution method for determination of MICs for *Mycobacterium avium* isolates. J Clin Microbiol 1993;**31**:2332-2338.

Singh J, Joshi C, Bhatnagar R. Cloning and expression of mycobacterial glutamine synthetase gene in *Escherichia coli*. *Biochem Biophys Res Commun* 2004;**317**:634-638.

Sosnik A, Carcaboso AM, Glisoni RJ, Moretton MA, Chiappetta DA. New old challenges in tuberculosis: Potentially effective nanotechnologies in drug delivery. *Adv Drug Deliv Rev* 2009;**62**:547-559.

Thomson Pharma August 2013 (www.thomson-pharma.com).

Topf M, Vanai P, Richards WG. Ab *initio* qm/mm dynamics simulation of the tetrahedral intermediate of serine proteases: insights into the active site hydrogen-bonding network. *J Am Chem Soc* 2002;**124**:14780-14788.

Tuberculosis, *In Encyclopaedia Britannica.*2010, www.britannica.com/Ebchecked/topic/608235/tuberculosis/253299/Tuberculosis-through-history.

Tullius MV, Harth G, Horwitz MA. Glutamine synthetase GlnA1 is essential for growth of *Mycobacterium tuberculosis* in human THP-1 macrophages and guinea pigs. *Infect Immun* 2003;**71**:3927-3936.

Tung R. The Development of Deuterium-Containing Drugs. *Concert Pharma* 2005;**4**:4-7.

Tyler B. Regulation of the assimilation of nitrogen compounds. *Ann Rev Biochem* 1978;**47**:1127-1162.

Wade D. Deuterium isotope effects on noncovalent interactions between molecules. *Chemico-biological interactions* 1999;**117**:191-217.

WHO, Global tuberculosis control: epidemiology, strategy, financing: WHO report. WHO/HTM/TB/2009.

Wietzerbin J, Lederer F, Petit JF. Structural study of the poly-l-glutamic acid of the cell wall of *Mycobacterium tuberculosis* var *hominis*, strain Brevannes. *Biochem Biophys Res Commun* 1975;**62**:246-252.

Williams DH, Stephens E, O'Brien DP, Zhou M. Understanding noncovalent interactions: ligand binding energy and catalytic efficiency from ligand-induced reductions in motion within receptors and enzymes. *Angew Chem Int Ed Engl* 2004;**43**:6596-6616.

Williams R. Metallo-enzyme catalysis. *Chem Commun* 2003:1109-1113.

Wise J. Southern Africa is moving swiftly to combat the threat of XDR-TB. *Bull World Health Organ* 2006;**84**:924-925.

Wolhueter RM, Schutt H, Holzer H. Regulation of glutamine synthetase *in vivo* in *E. coli.* In: Prusiner SR, Stadman ER, editors. *Enzymes of Glutamine Metabolism,* Academic Press, New York, 1973, p. 45-61.
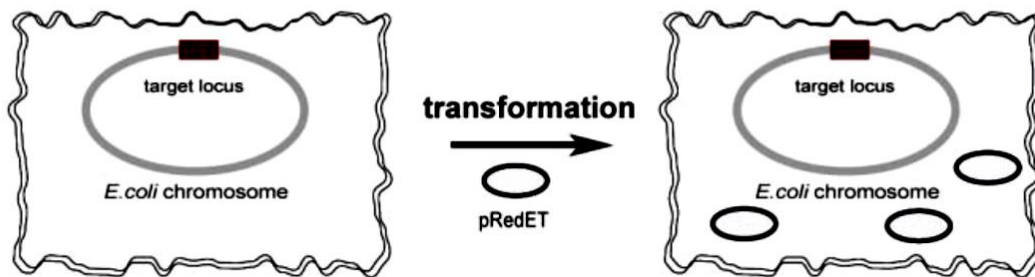
Woolfolk CA, Shapiro B, Stadtman ER. Regulation of glutamine synthetase I. Purification and properties of glutamine synthetase from *Escherichia coli*. *Arch Biochem Biophys* 1966;**116**:177-19
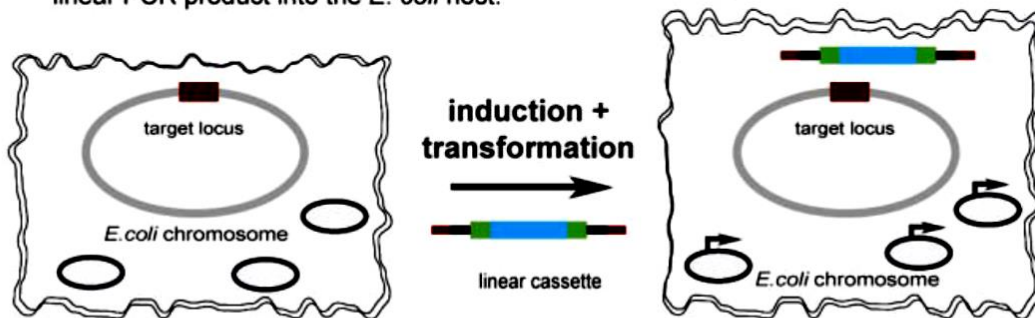
Appendix A

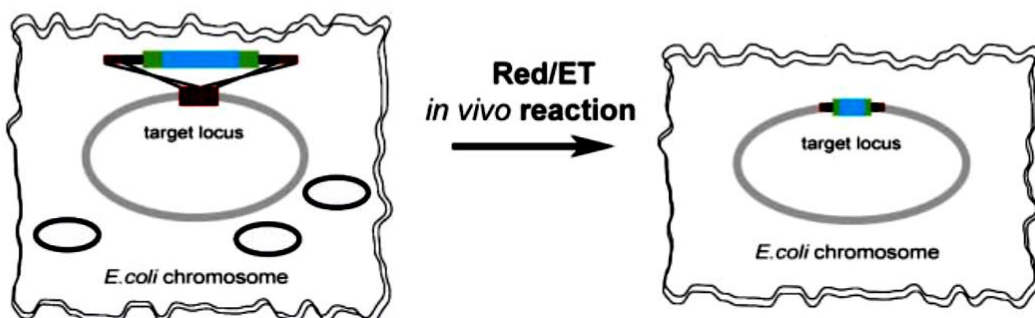**1. step:** Generation of a PCR product from the functional cassette flanked with homology arms

oligo up

PCR

oligo down

FRT-PGK-gb2-neo-FRT
template

functional cassette
flanked with homology arms + FRT sites
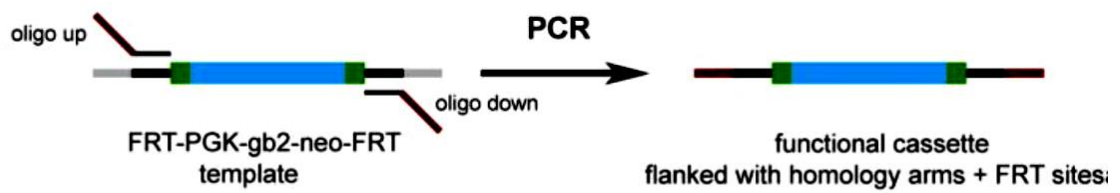
2. step: Transformation of pRedET into the *E. coli* host

target locus

E.coli chromosome
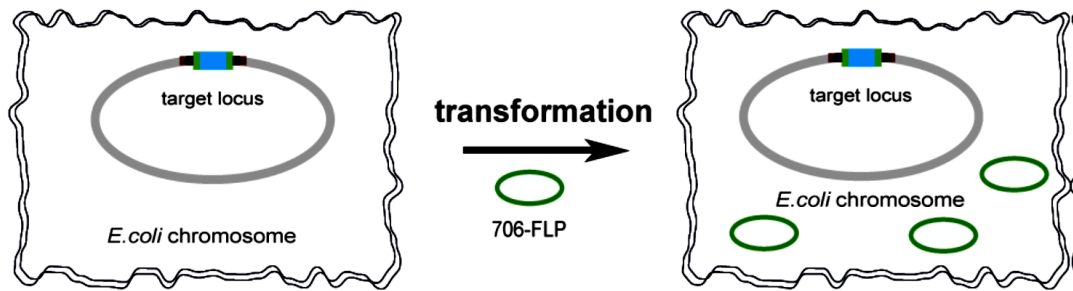
transformation

pRedET

target locus

E.coli chromosome

3. step: Induction of the Red/ET recombination genes and subsequent transformation of the linear PCR product into the *E. coli* host.

target locus

E.coli chromosome

**induction +
transformation**

linear cassette

target locus

E.coli chromosome

4. step: Red/ET recombination inserts the functional cassette into the target locus

target locus

E.coli chromosome

Red/ET
in vivo **reaction**

target locus

E.coli chromosome

127

5. step: Transformation of FLP-expression plasmid into the *E. coli* host (optional)

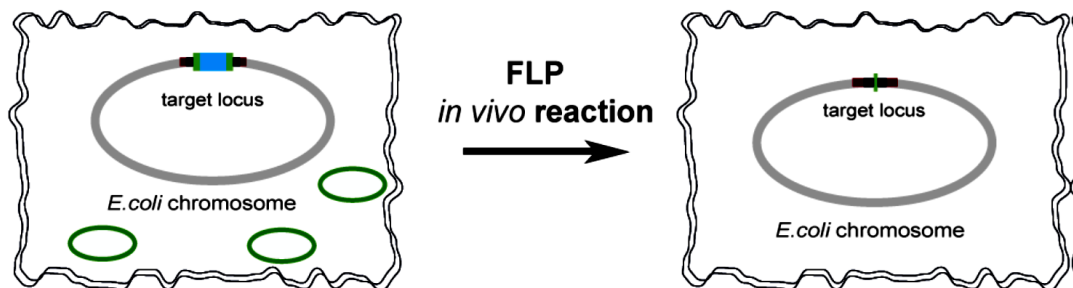6. step: Removal of the selection marker by FLP recombination (optional)

Figure A1: Flowchart of the experimental outline for the targeted disruption of genes on the *E. coli* chromosome.